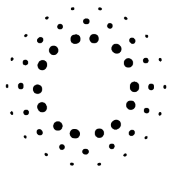

IFT - UNESP
INSTITUTO DE FÍSICA TEÓRICA

Master's Dissertation IFT–D.003/2023

The Evolution of Microbial Cooperation Under Chaotic Environmental Flows

João Pedro Valeriano Miranda

Supervisor

Ricardo Martínez-García

July 2023

Miranda, João Pedro Valeriano
M672e The evolution of microbial cooperation under chaotic environmental flows / João Pedro Valeriano Miranda. – São Paulo, 2023
94 f.

Dissertação (mestrado) – Universidade Estadual Paulista (Unesp), Instituto de Física Teórica (IFT), São Paulo
Orientador: Ricardo Martínez-García

1. Dinâmica populacional. 2. Ecologia microbiana. 3. Turbulencia. I. Título

Sistema de geração automática de fichas catalográficas da Unesp. Biblioteca do Instituto de Física Teórica (IFT), São Paulo. Dados fornecidos pelo autor(a).

Acknowledgements

I am extremely thankful to lots of people that supported me in different ways throughout my Master's degree.

Em primeiro lugar, gostaria de agradecer aos meus pais, Renata e Rogério, e ao meu irmão, Paulo, pelo apoio incondicional, pelo carinho, pelo companheirismo, pelo amor.

Second, I would like to thank Ricardo for being the best advisor I could ever ask for. Thank you for the numerous lessons, not only about physics and ecology, but also about critical scientific thinking, work ethics, among many other things. Thank you for giving me the freedom to explore things on my own and make mistakes, and for helping me get over those mistakes. Thank you for your honest interest in the success of all your students. If I am a better scientist today than two years ago, I owe a lot of that to you. And I can't forget your contribution to this text through multiple, very careful reviews.

I would also like to thank the rest of our research group at IFT, Benjamin, Daniel, Gabriel, Jesus, Pablo, Rafael and Vivian. Meeting with you and hearing you talk about your work was often the highlight of my week. It was a great pleasure to work and learn so much with all of you. Hope to see you all again soon.

Agradeço aos amigos que a Física me deu e que hoje, mesmo que às vezes longe, estão sempre por perto: Felipe, Lud, Vítor, Ranier, Leandro, Batata, Pedro, João Augusto, Graciele, Deborah, PP, Paulo, Vítor, Caio, Lettieri, Mari, Igor, Miguel, Lorena. Obrigado pelas incansáveis discussões científicas, mas especialmente pela camaradagem e pelo apoio mútuo. Fica um agradecimento especial ao Pedro, por ser a "má influência" necessária, que me lembra que a vida vai além a Física. E outro à Mariana, pelo carinho mútuo, pelo companheirismo, por sempre me ouvir e me apoiar. Aproveito para agradecer a outras amigas e amigos de longa data, Nathália, Leo, Julia, Sarah, Laura, Letícia, Matheus, Letícia e Igor, pela amizade apesar da infrequência dos nossos encontros. Agradeço também a Lucia, Susie e Beto, minha segunda família, por sempre me receberem de braços abertos, pelo apoio e pelo carinho.

I also want to thank the Foster Lab at the University of Oxford for hosting me during my BEPE project. Anna, Bella, Connor, Elisa, Erik, Frances, George, Holly, Jake, Martin, Megan, Lou, Louise, Sean, Vit and Kevin: thank you for receiving me so well and for teaching me so much, for guiding me through the world of microbial ecology and evolution. I also want to thank the Tsikas family, Tanya, Themos, Chris, George, and Olya, and all the other residents of Rosedale, Bashir, Brooke, Cristina, Duhita, Federico, Gareth, Jamieson, Sam, Sian and Shivaang, for welcoming us so warmly and making us feel at home in a new country.

I thank the Brazilian National Council for Scientific and Technological Development (CNPq) for funding this project through March 2021 with a Master scholarship (process 130507/2021-0). I also thank the São Paulo Research Foundation (FAPESP) for funding this research project from April 2021 to July 2023 through the Master Fellowship number 2020/14169-0 and also through the BEPE Fellowship number 2022/04976-1 (August 2022 to February 2023).

This research was supported by resources supplied by the Center for Scientific Computing (NCC/GridUNESP) of the São Paulo State University (UNESP).

Resumo

Comunidades microbianas exibem uma variedade de comportamentos sociais que podem melhorar o desempenho de múltiplas tarefas. Um desses comportamentos é a cooperação, que podemos definir amplamente como qualquer ação em que o executor assume um custo para gerar um benefício que é compartilhado com o restante da população. Como os subprodutos do comportamento cooperativo podem ser compartilhados com indivíduos que não contribuem para esse comportamento, os indivíduos cooperadores estão propensos à exploração por cepas "trapaceiras". Um exemplo paradigmático de cooperação no mundo microbiano é a síntese de bens públicos, exoprodutos produzidos a um custo, que proporcionam benefício a células nas proximidades do produtor, independentemente de estas contribuírem ou não para a sua produção.

De acordo com os modelos simples, os cooperadores são sempre extintos devido ao surgimento de mutações trapaceiras. No entanto, a cooperação ainda é um comportamento onipresente na natureza, o que motivou um desenvolvimento de pesquisa na área com o objetivo de desvendar os mecanismos capazes de tornar o comportamento cooperativo evolutivamente estável.

Espécies cooperativas podem desenvolver múltiplas características que funcionam como contramedidas diretas contra a sua exploração, como policiamento ou punição destes trapaceiros. Outras características podem fornecer benefícios indiretos aos cooperadores, como a agregação espacial.

Neste trabalho, estamos interessados em saber se – e até que ponto – o ambiente físico de uma comunidade microbiana pode ou não fornecer um mecanismo que facilite a sobrevivência dos cooperadores. As populações microbianas são frequentemente encontradas em habitats aquosos, onde os fluxos ambientais podem misturar os organismos para gerar estruturas espaciais muito diferentes daquelas formadas na ausência de fluxos externos.

Combinamos simulações numéricas e aproximações analíticas para investigar o efeito de fluxos ambientais caóticos na dinâmica de um sistema de duas cepas microbianas, uma que produz bens públicos e outra que não. Nossas simulações numéricas mostram que a mistura caótica dos organismos pode levar à coexistência estável das duas cepas, um resultado não previsto pela aproximação de campo médio que derivamos para nosso modelo de duas cepas.

Para melhor entender como a coexistência das cepas se torna estável, comparamos o cenário de fluxo caótico com um em que os organismos se difundem muito rapidamente. Comparando esses dois cenários, observamos que fluxos caóticos rápidos permitem a coexistência não por criar estruturas espaciais que separam cooperadores de trapaceiros, mas por enfraquecer as correlações espaciais criadas por eventos de reprodução. A quebra das correlações espaciais aproxima o sistema de um cenário com distribuição homogênea de indivíduos. No entanto, devido ao alcance finito das interações e à natureza estocástica do sistema, a vizinhança de cada produtor é diferente e muda constantemente devido ao fluxo externo. Concluímos que a combinação de mistura caótica, estocasticidade demográfica e interações de alcance finito permite a coexistência, pois a vizinhança de cada cooperador alterna continuamente entre os estados de presença e ausência de trapaceiros. Por fim, propomos direções para investigações futuras para melhor entender a coexistência no sistema estudado.

Palavras Chaves: Dinâmica populacional; Ecologia microbiana; Turbulência.

Áreas do conhecimento: Ecologia Teórica; Física Estatística Fora do Equílibrio.

Abstract

Microbial communities display a range of social behaviors that can enhance the performance of multiple tasks. One of these behaviors is cooperation, which we can broadly define as any action in which the executor assumes a cost to generate a benefit that is shared with the rest of the population. Because the byproducts of the cooperative behavior might be shared with individuals that do not contribute to this behavior, cooperating individuals are prone to exploitation by defecting strains. A paradigmatic example of cooperation in the microbial world is the synthesis of public goods (PG), exoproducts that are costly to produce and provide a benefit to cells in the vicinity of the producer, regardless of whether they contribute to its production or not.

According to basic models, cooperators are always driven to extinction due to the emergence of cheating mutations. However, cooperation is still a ubiquitous behavior in nature, which motivated the development of a large body of research aiming to uncover the mechanisms capable of making cooperative behavior evolutionarily stable.

Cooperating species can evolve multiple traits that work as direct countermeasures against exploitation by defectors, such as policing or punishment of defectors. Other traits can provide indirect benefits to cooperators, such as spatial aggregation.

In this work, we are interested in whether and to what extent the physical environment of a microbial community can or cannot provide a mechanism that facilitates the survival of cooperators. Microbial populations are often found in aqueous habitats, where environmental flows can mix the organisms to generate spatial structures very different from the ones formed in the absence of external flows.

We combine intensive numerical simulations and analytical approximations to investigate the effect of chaotic environmental flows on the dynamics of a system of two microbial strains, one that produces public goods and another that does not. Our numerical simulations show that fast chaotic mixing can lead to stable coexistence of the two strains, a result that was not predicted by the mean-field approximation we derived for our two-strain model.

To better understand how strain coexistence becomes stable, we compare the

chaotic-flow scenario to one in which organisms diffuse very fast. Comparing these two scenarios, we find that fast chaotic flows allow for coexistence not by creating spatial structures that segregate cooperators from defectors, but by breaking the spatial correlations created by reproduction events. The break of spatial correlations brings the system close to a well-mixed scenario. However, because of the finite range of interactions and the stochastic nature of the system, the neighborhood of each producer is different, and constantly changing due to the external flow. We conclude that the combination of chaotic mixing, demographic stochasticity, and finite-range interactions allows for coexistence as the neighborhood of each cooperator continuously switches between states of presence and absence of defectors. Finally, we propose routes for future investigation to better understand the coexistence in the studied system.

Keywords: Population dynamics; Microbial ecology; Turbulence.

Areas of knowledge: Theoretical Ecology; Out of Equilibrium Statistical Physics.

Contents

Chapter 1

Introduction

The evolution of cooperative behavior often poses a dilemma for evolutionary theory. Cooperation, which we will define as a costly behavior of one individual that provides fitness benefits to other individuals, is prone to exploitation by cheating individuals who do not behave cooperatively but gain benefits from cooperators [41]. Therefore, cooperation is not evolutionarily stable, at least under the assumptions of simple models [58].

In the last few decades, microbial communities were discovered to behave collectively to execute a range of tasks, such as foraging, dispersal, and biofilm or fruiting body formation. These tasks are frequently mediated by the secretion of different molecules to the extracellular medium. Some of these molecules can also establish different ecological interactions within the community (see Reviews [15, 51, 56]). This variety of behaviors, together with the fast evolution of microbes and their ease of manipulation in controlled laboratory conditions make microbial communities a rich experimental platform for studying the ecology and evolution of social behaviors.

One relevant example of cooperative behavior in microorganisms is the production of public goods (PGs). Microbial public goods are molecules that are produced and (at least partially) released into the environment of the producer individual. These molecules can often be used by other microbes in the environment, independent of being conspecific to the producer or not. There is a range of molecules that can act as public goods and provide different advantages to their recipients [56] (see the introduction of Chapter 4 for a more detailed discussion).

Public good production comes at an energetic cost for producer cells, and it can be exploited by non-producing individuals sharing the environment with producers. Because these non-producers do not pay this cost while benefitting from the behavior of cooperators, non-producers have a fitness advantage over producers. This pattern of exploitation can lead to a so-called tragedy of the commons, where the selfish behavior of cheaters drives the extinction of producers, and the population loses access to the public good [24, 43].

In this work, we theoretically investigate the dynamics of a system of two microbial strains, one that produces public goods, and another that does not. This problem has been extensively explored [3, 8, 12, 47], but we still lack a robust understanding of how the physical environment shapes interactions between the two strains and ultimately determines the long-term fate of the community. Uppal and Vural (2018) [53] have looked into the effect of laminar environmental flows, and showed that these flows enhance the survival of PG producers when combined with an additional long-range interaction that generates spatial aggregates of microbes. Motivated by this observation, we are interested in the effect of chaotic environmental flows which can enhance mixing, but can also generate transient coherent structures that segregate different species [32].

More specifically, our goal is to understand how chaotic environmental flows can shape the ecology of this two-strain system by changing the spatial distribution of the community and consequently the inter- and intrastrain encounter rates. We derive a master equation for the two-strain system departing from a set of individual-level stochastic reactions that define the population dynamics. We analyze this system through numerical simulations[1], which is the core of this work. We also consider the mean-field approximation for the system, which provides the necessary intuition to understand the numerical results. The chaotic environmental flow of choice for this work is a point-vortex flow, which consists of multiple vortices orbiting one another while generating chaotic flows. This flow model is very useful as it is computationally very cheap to simulate while reproducing interesting properties of turbulent flows.

The numerical simulations of the two-strain system show the possibility of stable coexistence of the two strains given that the chaotic flow is fast enough. This coexistence result has been observed before in a similar model in a regime of strong diffusion of microbes [4]. However, reaching this strong diffusion regime would require microbes moving at a very fast rate, which is very often beyond their physical limits. Environmental flows, on the contrary, are independent of the properties of the microbial species and thus provide a more feasible explanation for the coexistence of PG-producing and non-producing strains in natural systems.

[1]The implementations of all the simulations associated with this dissertation can be found in the GitHub following repository: https://github.com/joaovaleriano/Master-IFT_cooperation-and-flows

The dissertation is structured as follows:

In Chapter 2, we give an introduction to fluid dynamics. We derive basic equations for continuum mechanics and obtain the Euler equation, which describes ideal fluids with no viscosity and no energy exchange. From the Euler equation, we derive the point-vortex flow solution that will be used in our model for the two-strain system.

Chapter 3 introduces the master equation formalism, a generic tool to describe stochastic dynamics departing from basic reactions. We first introduce the non-spatial birth-death model, which we use as a study case to introduce different analytical techniques for the analysis of master equations. Second, we consider spatial processes and show how reactions associated with movement and non-local interactions enter into the master equation formalism. Lastly, joining demographic and movement reactions, derive and analyze a single-species spatial birth-death model in which organisms compete non-locally and move due to diffusion (caused by the Brownian motion of the organisms) and advection by an external flow.

Chapters 2 and 3 introduce the mathematical techniques necessary for the development of Chapter 4 and, therefore, can be skipped by the familiarized reader. However, section 3.5 can be useful to build some intuition about the effect of non-local interactions in the spatial structure of the population density, and about the effect of external flows in the shape of this spatial structure.

Chapter 4 contains the core of the present work. We derive a master equation for the two-strain system, in which we implement the public good dynamics through a spatial PG game that is an adaptation of the classical model used in economic theory. We perform numerical simulations of the master equation and show that the two strains can coexist under fast chaotic environmental flows. We argue that this coexistence is allowed by the fast mixing that nullifies spatial correlations generated by demographic processes. The analytical consideration of the mean-field approximation of the two-strain system provides some intuition for understanding these numerical results. However, the existence of a coexistence equilibrium point in the limit of strong mixing is not captured by the mean-field approximation we considered, and thus we propose a pair approximation analysis to try to obtain this coexistence solution.

Lastly, in Chapter 5 we summarize our work and make connections with the relevant published literature. We also propose further extensions to improve the presented work in the direction of (1) making our implementation of public goods more realistic and (2) developing a better theoretical understanding of how

mixing allows coexistence, also speculating on the effect of flows for more complex microbial communities.

Chapter 2

Introduction to Fluid Dynamics and the Point-Vortex Flow

In this chapter, we present a brief introduction to fluid dynamics. We will provide the necessary background to understand the derivation of point-vortex flow, clarifying the physical assumptions behind the derivation.

We start with the derivation of basic continuum mechanics equations: the continuity equation and the Cauchy momentum balance equation. From there, we can derive the Euler equation, a simplification of the Navier-Stokes, considering an inviscid (no viscosity) and adiabatic (no heat exchange) flow. Thus, we will not touch on Navier-Stokes equations in this text. The inviscid and adiabatic approximations in the flows described by the Euler equation may seem crude. However, the Euler equation can describe multiple flow scenarios with properties similar to real-world flows, laminar or turbulent.

We will focus on incompressible flows, for which we will obtain the point-vortex solutions in two different ways. First, we will follow the most common derivation: we present the associated stream function, which satisfies the incompressible Euler equation. Second, we show that the point-vortex is a particular case of the vortex-sheet solution for the Euler equation.

We choose to work with point-vortex flows in this project because they can produce rich behaviors, from periodic to chaotic, similar to what we expect from turbulent flows. The simulation of point-vortex flows is also much cheaper than numerically solving fluid dynamics equations.

The presentation given here is inspired by a few different sources I recommend. The book by Reddy [44] provides a good introduction to continuum mechanics. The first few chapters of the lecture notes by Lars Davidson [16] are useful in connecting general continuum mechanics and fluid dynamics and an introduction to potential flows. The classical books by Lamb [33] and Batchelor [2] are very rich. These two were good references for calculations on stream functions and vortex

flows. However, these sources go way beyond the scope of the present work in many directions. In this chapter, I will provide a good summary of these different references, focusing on what is relevant to this dissertation.

2.1 Introduction to Continuum Mechanics

We begin by considering the stresses on the surface of a small element of a three-dimensional continuous body. Suppose a rectangular element of sides δx_1, δx_2 and δx_3, aligned with the Cartesian axes $(\hat{\mathbf{x}}_1, \hat{\mathbf{x}}_2, \hat{\mathbf{x}}_3)$. On each of its six surfaces, we have three stress components. One is perpendicular to the surface, corresponding to pressure. The other two are parallel to the surface, corresponding to shear stresses. Analogous to the usual definition of pressure, we can define each of the stress components for a given surface of the element, and considering the limit of an infinitesimal element, we can define a stress vector $\boldsymbol{\tau}$ with components

$$\tau_i(\hat{\mathbf{n}}) = \lim_{\Delta S \to 0} \frac{\Delta F_i}{\Delta S}, \tag{2.1}$$

where ΔS is the element of surface area perpendicular to the normal vector $\hat{\mathbf{n}}$ – for instance, if $\hat{\mathbf{n}} = \hat{\mathbf{e}}_2$, $\Delta S = \delta x_1 \delta x_3$. F_i is the i-th component of the force exerted on the element. In this chapter, we will stick to the Einstein summation convention for denoting vector components and their operations. We will write summations only if needed for clarity.

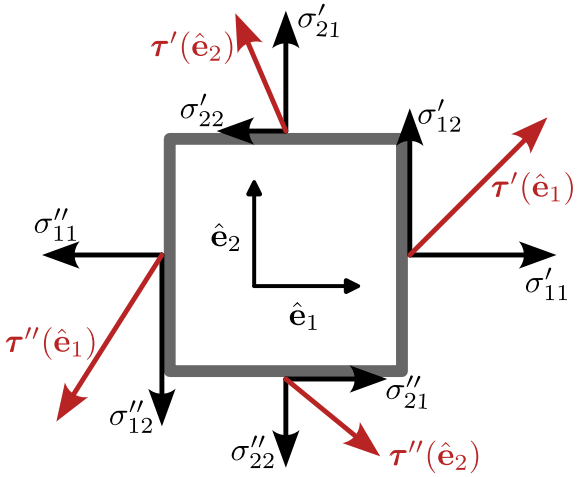

Figure 2.1: Stress tensor components over the surface of a material element.

We can simplify our notation by defining the stress tensor $\sigma_{i,j} = \tau_j(\hat{\mathbf{e}}_i)$, so

that $\sigma_{i,j}$ denotes the stress on the surface perpendicular to $\hat{\mathbf{e}}_i$, in the j-th direction. The components of the stress vector are recovered from the stress tensor as $\tau_j = n_i \sigma_{i,j}$, where n_i is the i-th component of the normal vector $\hat{\mathbf{n}}$. The stress tensor's components are drawn in the diagram in Figure 2.1. We present it in 2D for easy visualization, but the extension for three dimensions is straightforward. Notice that the stress vectors in opposite faces are not necessarily equal. Our stress tensor then is the difference between the components in opposite faces, $\sigma_{i,j} = \tau_j(\hat{\mathbf{e}}_i) = \tau'_j(\hat{\mathbf{e}}_i) + \tau''_j(\hat{\mathbf{e}}_i)$ (looking at Figure 2.1), evaluated at the center of mass of the material element. Here, the difference between stress components comes from the opposite sign of normal vectors in opposite faces.

When working with fluids, it is important to discern between the Eulerian and the Lagrangian descriptions of the flow. We will discuss this in the following section, 2.1.1. In section 2.1.2, we will derive the Reynolds' transport theorem, and then use it to write common physical conservation laws.

2.1.1 Eulerian and Lagrangian Descriptions of Fluid Flow

The Eulerian description of a flow velocity field is probably easier to understand for someone familiar with the concept of fields defined in space and time. In this description, the properties of the fluid are defined as fields, characterizing the fluid at every point in space, for all instants of time. With this description, when looking at a point $(\mathbf{x}, t)$ in spacetime, these coordinates are used to define the properties of any fluid element passing by the position $\mathbf{x}$ at time t. The velocity field in the Eulerian description is then given by a vector function $\mathbf{v}(\mathbf{x}, t)$.

On the other hand, the Lagrangian description does not focus on a single position $\mathbf{x}$, but on a single fluid element, or fluid "particle". We can tag each fluid particle based on its position $\mathbf{x}_0$ at a given time t_0. This way, the position $\mathbf{X}$ of the tagged particle at a later time will be $\mathbf{X}(\mathbf{x}_0, t)$. We can understand the Lagrangian description as a change to a reference frame moving along with the fluid particle, in contrast to the fixed frame used in the Eulerian description.

In a sense, the Lagrangian description is simpler. After choosing a fluid particle to keep track of, its properties are described as a function of time only. This can work very well if we are interested in a single fluid particle. However, to keep track of multiple particles, it would become unmanageable. This is where the Eulerian description shines. By defining fields to describe fluid properties everywhere in space, it becomes much simpler to track the variation of these properties along

large portions of fluid. This way, we can describe complex fluid systems more easily. For this reason, we will focus on the Eulerian description from now on.

Say we want to describe the variation through time of a property ϕ of a fluid, in the Eulerian description. The fluid moves according to an external velocity field $\mathbf{v}(x,t)$, that is, the position $\mathbf{x}$ of a fluid element changes with time according to

$$\frac{\mathrm{d}\mathbf{x}}{\mathrm{d}t} = \mathbf{v}(\mathbf{x},t)\,. \tag{2.2}$$

So, to calculate the total time derivative of a field $\phi(\mathbf{x},t)$, we need to take into account the spatial dependence of the field. Using the chain rule:

$$\begin{aligned}\frac{\mathrm{d}\phi(\mathbf{x},t)}{\mathrm{d}t} &= \frac{\partial\phi(\mathbf{x},t)}{\partial t} + \frac{\mathrm{d}x_i}{\mathrm{d}t}\frac{\partial\phi(\mathbf{x},t)}{\partial x_i} = \frac{\partial\phi(\mathbf{x},t)}{\partial t} + v_i\frac{\partial\phi(\mathbf{x},t)}{\partial x_i} \\ &= \frac{\partial\phi(\mathbf{x},t)}{\partial t} + \mathbf{v}\cdot\nabla\phi(\mathbf{x},t)\,.\end{aligned} \tag{2.3}$$

The operation in Equation (2.3) is called the material derivative of ϕ, to remind us that we are calculating the time derivative of a field describing a material element that belongs to a macroscopic body.

2.1.2 Reynolds' Transport Theorem

In order to write conservation laws over continuous bodies, we will need to integrate over material elements, but these elements are deformed as they move. In this section we will first describe these deformations and how they lead to changes in the volume of material elements. Then, we will use these results to prove Reynolds' transport theorem, which describes the derivative of quantities integrated over continuous bodies.

To understand the deformation of material elements, we start by considering a fluid particle with initial location $\mathbf{x}^*$. If the particle moves to a new position $\mathbf{x}$, we can define the displacement vector for this particle by $\mathbf{u} = \mathbf{x} - \mathbf{x}^*$. Let's see how this displacement leads to a change in element volume. In the limit of infinitesimal material elements, the volume of the element at location $\mathbf{x}$ is $\mathrm{d}\mathbf{x} = \mathrm{d}x_1\mathrm{d}x_2\mathrm{d}x_3$. Also, we can consider the deformation to be linear in this limit of infinitesimal distances, so that we can connect the volumes before and after displacement by the deformation gradient tensor $\mathbf{F}$:

$$\mathrm{d}x_i = F_{i,j}\mathrm{d}x_j^*, \tag{2.4}$$

which means the tensor $\mathbf{F}$ can be written as

$$F_{i,j} = \frac{\partial x_i}{\partial x_j^*} = \frac{\partial}{\partial x_j^*}(u_i + x_i^*) = \frac{\partial u_i}{\partial x_j^*} + \delta_{i,j}. \tag{2.5}$$

When investigating the conservation of a property ϕ, we look at the time derivative of its integral over a given volume V. However, this volume will change as the system evolves, so we can alternatively write the integral in terms of the volume at the initial time, V_0:

$$\int_V \phi \mathrm{d}\mathbf{x} = \int_{V_0} \phi J \mathrm{d}\mathbf{x}^*, \tag{2.6}$$

where J comes from the change of variables from $\mathbf{x}$ to $\mathbf{x}^*$. As this change is linear, according to Equation (2.4), we know that $J = \det(F)$.

To calculate the time derivative of the integral of ϕ (2.6), we will need the time derivative of J. Notice that we can write

$$\frac{\mathrm{d}J}{\mathrm{d}t} = \frac{\mathrm{d}}{\mathrm{d}t}\det(F) = \sum_{i,j} \frac{\partial \det(F)}{\partial F_{i,j}} \frac{\mathrm{d}F_{i,j}}{\mathrm{d}t}. \tag{2.7}$$

Let's focus on the first term inside the summation in equation (2.7). We can write the determinant of a matrix as a sum over one of its rows or columns multiplied by the respective cofactors. This is known as the Laplace formula:

$$\det(F) = \sum_j F_{i,j}\, \mathbf{C}\big(F_{i,j}\big)\,, \tag{2.8}$$

where the cofactor of cell $F_{i,j}$ is given by

$$\mathbf{C}\big(F_{i,j}\big) = (-1)^{i+j} \det\left(\mathbf{M}\big(F_{i,j}\big)\right), \tag{2.9}$$

where $\mathbf{M}(F_{i,j})$ is the submatrix obtained by removing the i-th row and the j-th column from matrix $\mathbf{F}$. Therefore, $\mathbf{C}(F_{i,j})$ is, by definition, independent of $F_{i,j}$. Another important result from linear algebra is that the inverse of a matrix is given by its adjugate matrix (transpose of the cofactor matrix), divided by its determinant:

$$\mathbf{F}^{-1} = \mathbf{C}(F)^{\mathrm{T}} \det(F)^{-1}, \text{ or } \mathbf{C}(F_{i,j}) = \det(F)\, F^{-1}_{j,i}. \tag{2.10}$$

Using this result (2.10) together with the Laplace formula (2.8), we can write the derivative of the determinant of the tensor $\mathbf{F}$ with respect to its elements $F_{i,j}$ as

$$\begin{aligned}\frac{\partial \det(F)}{\partial F_{i,j}} &= \frac{\partial}{\partial F_{i,j}} \sum_k F_{i,k}\mathbf{C}(F_{i,j}) = \sum_k \frac{\partial F_{i,k}}{\partial F_{i,j}} \det(F)\, F^{-1}_{j,i} \\ &= \sum_k \delta_{k,j} \det(F)\, F^{-1}_{j,i} \\ &= \det(F)\, F^{-1}_{j,i}.\end{aligned} \tag{2.11}$$

Now let's look at the second term inside the summation in equation (2.7), the time derivative of $F_{i,j}$. We can write

$$\frac{\mathrm{d}F_{i,j}}{\mathrm{d}t} = \frac{\mathrm{d}}{\mathrm{d}t}\frac{\partial x_i}{\partial x^*_j} = \frac{\partial}{\partial x^*_j}\frac{\mathrm{d}x_i}{\mathrm{d}t} = \frac{\partial}{\partial x^*_j} v_i(\mathbf{x}, t) = \frac{\partial v_i}{\partial x_k}\frac{\partial x_k}{\partial x^*_j} = \frac{\partial v_i}{\partial x_k} F_{k,j}. \tag{2.12}$$

Substituting equations (2.10) and (2.12) in equation (2.7), we get:

$$\frac{\mathrm{d}}{\mathrm{d}t}\det(F) = \sum_{i,j,k} \det(F)\, F^{-1}_{j,i}\frac{\partial v_i}{\partial x_k} F_{k,j}. \tag{2.13}$$

Notice that $\sum_j F_{k,j}F^{-1}_{j,i} = \delta_{i,k}$, so that we have

$$\frac{\mathrm{d}J}{\mathrm{d}t} = \frac{\mathrm{d}}{\mathrm{d}t}\det(F) = \det(F)\sum_i \frac{\partial v_i}{\partial x_i} = \det(F)\,\nabla\cdot\mathbf{v}. \tag{2.14}$$

Now we are ready to write the Reynolds' transport theorem for time change of a property ϕ:

$$\frac{\mathrm{d}}{\mathrm{d}t}\int_V \phi \mathrm{d}\mathbf{x} = \frac{\mathrm{d}}{\mathrm{d}t}\int_{V_0} \phi J \mathrm{d}\mathbf{x}^* = \int_{V_0}\left[\frac{\mathrm{d}\phi}{\mathrm{d}t}J + \phi\frac{\mathrm{d}J}{\mathrm{d}t}\right]\mathrm{d}\mathbf{x}^*$$
$$= \int_{V_0}\left[\frac{\mathrm{d}\phi}{\mathrm{d}t} + \phi\nabla\cdot\mathbf{v}\right]J\mathrm{d}\mathbf{x}^*. \tag{2.15}$$

Changing variables back from $\mathbf{x}^*$ to $\mathbf{x}$, we obtain the Reynolds' transport theorem:

$$\frac{\mathrm{d}}{\mathrm{d}t}\int_V \phi \mathrm{d}\mathbf{x} = \int_V\left[\frac{\mathrm{d}\phi}{\mathrm{d}t} + \phi\nabla\cdot\mathbf{v}\right]\mathrm{d}\mathbf{x}. \tag{2.16}$$

With this result (2.16), we can write the conservation laws for continuous bodies, which will lead us to the Euler equation.

2.1.3 Conservation Laws: Continuity and Momentum Equations

In this subsection, we are going to describe the implications of some conservation laws for the mechanics of continuous bodies. From the conservation of mass, we will derive the continuity equation. We will also see that the conservation of angular momentum implies the symmetry of the stress tensor, $\sigma_{i,j} = \sigma_{j,i}$. The conservation of linear momentum will lead to the Cauchy momentum balance equation, which describes a very general problem for the time evolution of a velocity field over a material body. The Euler equation is a special case of the Cauchy momentum balance equation, as we will see in the next section 2.2.

Conservation of mass

We can write the total mass M of a body occupying a region V as

$$M = \int_V \rho\,\mathrm{d}\mathbf{x}, \tag{2.17}$$

where ρ is our density field, which can depend on space and time. Imposing mass conservation, we obtain:

$$\frac{\mathrm{d}}{\mathrm{d}t}M = \frac{\mathrm{d}}{\mathrm{d}t}\int\limits_V \rho \mathrm{d}\mathbf{x} = \int\limits_V \left[\frac{\mathrm{d}\rho}{\mathrm{d}t} + \rho\nabla\cdot\mathbf{v}\right]\mathrm{d}\mathbf{x} = 0, \tag{2.18}$$

where we just used the Reynolds' transport theorem. We can expect this result to be valid for any choice of volume V. Therefore, the integrand should be identically null, which leads to the well-known continuity equation:

$$\frac{\mathrm{d}\rho}{\mathrm{d}t} + \rho\nabla\cdot\mathbf{v} = 0. \tag{2.19}$$

Conservation of Linear Momentum

We can write the momentum P as

$$\mathbf{P} = \int\limits_V \rho\mathbf{v}\,\mathrm{d}\mathbf{x}. \tag{2.20}$$

Its time derivative is given by the Reynolds transport theorem:

$$\frac{\mathrm{d}\mathbf{P}}{\mathrm{d}t} = \int\limits_V \left[\frac{\mathrm{d}\rho\mathbf{v}}{\mathrm{d}t} + \rho\mathbf{v}\nabla\cdot\mathbf{v}\right]\mathrm{d}\mathbf{x} = \int\limits_V \left[\frac{\mathrm{d}\rho}{\mathrm{d}t}\mathbf{v} + \rho\frac{\mathrm{d}\mathbf{v}}{\mathrm{d}t} + \rho\mathbf{v}\nabla\cdot\mathbf{v}\right]\mathrm{d}\mathbf{x}. \tag{2.21}$$

Using the continuity equation (2.19), the result reduces to

$$\frac{\mathrm{d}\mathbf{P}}{\mathrm{d}t} = \int\limits_V \rho\frac{\mathrm{d}\mathbf{v}}{\mathrm{d}t}\mathrm{d}\mathbf{x} \tag{2.22}$$

Momentum conservation implies its time derivative should match the applied force F, which we can write as

$$\mathbf{F} = \int\limits_V \rho\mathbf{f}\,\mathrm{d}\mathbf{x} + \oint\limits_S \boldsymbol{\tau}\mathrm{d}s, \tag{2.23}$$

where $\mathbf{f}$ is a density of force by unit mass and $\boldsymbol{\tau}$ is the stress vector, which has units of force by area, as one may recall. S is the surface surrounding the volume V, and

ds is the corresponding element of area. Rewriting the stress vector in terms of the tensor σ and using Stokes' theorem, we have the stress components

$$\oint_S \tau_i \mathrm{d}s = \oint_S \sigma_{j,i} n_j \mathrm{d}s = \int_V \frac{\partial \sigma_{j,i}}{\partial x_j} \mathrm{d}\mathbf{x} \tag{2.24}$$

It is interesting to notice that we could also derive this relation by analyzing the difference between stresses in opposite faces of the material element in Figure 2.1, taking the limit of an infinitesimal material element.

Going back to the momentum conservation, we can combine equations (2.22) and (2.23), substituting equation (2.24) to obtain:

$$\frac{\mathrm{d}P_i}{\mathrm{d}t} - F_i = \int_V \left[\rho \frac{\mathrm{d}v_i}{\mathrm{d}t} - \rho f_i - \frac{\partial \sigma_{j,i}}{\partial x_j} \right] \mathrm{d}\mathbf{x} = 0, \tag{2.25}$$

which, using the argument of validity independent of the volume V, leads to the Cauchy momentum balance equation:

$$\rho \frac{\mathrm{d}v_i}{\mathrm{d}t} - \rho f_i - \frac{\partial \sigma_{j,i}}{\partial x_j} = 0. \tag{2.26}$$

Equation (2.26) describes the evolution of a velocity field over a material body given the external forces f_i and the spatial derivatives of the stress tensor $\boldsymbol{\sigma}$

Conservation of Angular Momentum

To prove that the stress tensor σ is symmetric, that is, $\sigma_{j,i} = \sigma_{i,j}$, we will look into the conservation of angular momentum. The angular momentum components are given by

$$L_i = \int_V \varepsilon_{ijk}\, x_j\, \rho v_k \mathrm{d}\mathbf{x}, \tag{2.27}$$

where ε_{ijk} is the Levi-Civita pseudotensor, defined as +1 if (i, j, k) is an even permutation of $(1, 2, 3)$, -1 if (i, j, k) is an odd permutation, or 0 if at least two indices have the same value. In this notation, we are representing a component of

the cross-product between position and momentum, as expected for the definition of angular momentum.

Similarly to the case of linear momentum, we can use the continuity equation to cancel terms inside the integral for angular momentum $\mathbf{L}$, so that we can write:

$$\frac{\mathrm{d}L_i}{\mathrm{d}t} = \int_V \rho \varepsilon_{ijk} \left[v_j v_k + x_j \frac{\mathrm{d}v_k}{\mathrm{d}t} \right] \mathrm{d}\mathbf{x}. \tag{2.28}$$

The first term inside brackets is zero, as it is a component of the cross-product of $\mathbf{v}$ with itself – seen another way, it is a product between a symmetric tensor, $v_j v_k$, and an antisymmetric one, ε_{ijk} (considering j and k indices), which is identically null.

The time derivative of the angular momentum $\mathbf{L}$ is equal to the torque T, which can be calculated as the cross product of position and force. Using equation (2.23), we can write:

$$\begin{aligned} T &= \int_V \varepsilon_{ijk} \left[x_j \rho f_k + \frac{\partial x_j \sigma_{m,k}}{\partial x_m} \right] \mathrm{d}\mathbf{x} \\ &= \int_V \varepsilon_{ijk} \left[x_j \rho f_k + \delta_{j,m} \sigma_{m,k} + x_j \frac{\partial \sigma_{m,k}}{\partial x_m} \right] \mathrm{d}\mathbf{x} \\ &= \int_V \varepsilon_{ijk} \left[x_j \rho f_k + \sigma_{j,k} + x_j \frac{\partial \sigma_{m,k}}{\partial x_m} \right] \mathrm{d}\mathbf{x}. \end{aligned} \tag{2.29}$$

Writing the angular momentum conservation:

$$\frac{\mathrm{d}L}{\mathrm{d}t} - T = \int_V \varepsilon_{ijk} \left[x_j \left(\rho \frac{\mathrm{d}v_k}{\mathrm{d}t} - \rho f_k - \frac{\partial \sigma_{m,k}}{\partial x_m} \right) - \sigma_{j,k} \right] \mathrm{d}\mathbf{x} = 0. \tag{2.30}$$

The term in parentheses in equation (2.30) is null due to the conservation of the linear momentum (equation (2.26)), so we are left with

$$\varepsilon_{ijk} \sigma_{j,k} = 0 \Rightarrow \sigma_{j,k} = \sigma_{k,j}, \text{ for any } i, \tag{2.31}$$

as swapping j and k values is an odd permutation, so that for any i we have

$\sigma_{j,k} - \sigma_{k,j} = 0$.

We will not discuss energy conservation in this presentation as we will not consider flows with energy exchange.

2.2 Euler Equation

Provided the conservation laws derived in the last section, we are almost ready to write the Euler equation as a particular case of the Cauchy momentum balance equation (2.26).

We want to consider flows free from external forces, adiabatic and inviscid. It is simple to set external forces to zero in equation (2.26). Adiabatic flows must not exchange energy, which we can already take for granted because we do not consider the effects of energy conservation in our equations. If the flow is inviscid, i.e., has no viscosity, we should expect no shear stresses. This will be encoded in the stress tensor, which we have considered very generally until now.

If there are no shear stresses, the off-diagonal terms of the stress tensor should be null, and the diagonal terms will only depend on the thermodynamic pressure p. Thus, we have

$$\sigma_{i,j} = -p\delta_{i,j}. \tag{2.32}$$

Substituting equation (2.32) in the Cauchy momentum balance equation (2.26), we obtain the Euler equation:

$$\rho \frac{\mathrm{d}v_i}{\mathrm{d}t} = \rho f_i - \frac{\partial p}{\partial x_i}. \tag{2.33}$$

Together with the continuity equation (2.19), equation (2.33) fully describes the dynamics of the fluid. If we consider incompressible flows, the fluid density must be constant, $\rho(\mathbf{x}, t) = \rho$. In this case, the continuity equation (2.19) implies the well-known condition for an incompressible flow:

$$\nabla \cdot \mathbf{v} = 0. \tag{2.34}$$

We can also write the Euler equation in a different form, alternative to the usual

equation (2.33). Instead of describing the flow in terms of the time evolution of the velocity field, we can look at the evolution of the vorticity, defined as the curl of the velocity field:

$$\boldsymbol{\omega} = \nabla \times \mathbf{v}. \tag{2.35}$$

This alternative approach to the Euler equation (2.33) will be especially useful in our analysis because we are interested in flows described by multiple interacting vortices, as we will see in the next section 2.3.

Proceeding with the derivation of the Euler equation in vorticity form, suppose $\mathbf{f}$ is a conservative force, which we can write in terms of the gradient of a scalar field φ,

$$\mathbf{f} = -\nabla\varphi. \tag{2.36}$$

Taking the curl of the Euler equation (2.33) and substituting equation (2.36), we have:

$$\rho\frac{\partial}{\partial t}\left[\varepsilon_{ijk}\frac{\partial v_k}{\partial x_j}\right] + \rho\varepsilon_{ijk}\frac{\partial}{\partial x_j}\left[v_m\frac{\partial v_k}{\partial x_m}\right] = -\rho\varepsilon_{ijk}\frac{\partial^2\varphi}{\partial x_j x_k} - \varepsilon_{ijk}\frac{\partial^2 p}{\partial x_j x_k}. \tag{2.37}$$

Assuming both p and φ are C^2 functions, the right-hand side (RHS) of equation (2.37) is zero, as we have the curls of gradients. The second term on the left-hand side (LHS) requires some manipulation. We start by separating the velocity gradient tensor into symmetric and antisymmetric parts:

$$\begin{aligned}\frac{\partial v_i}{\partial x_j} = \frac{1}{2}\left[\frac{\partial v_i}{\partial x_j} + \frac{\partial v_i}{\partial x_j} + \frac{\partial v_j}{\partial x_i} - \frac{\partial v_j}{\partial x_i}\right] &= \frac{1}{2}\left[\frac{\partial v_i}{\partial x_j} + \frac{\partial v_j}{\partial x_i}\right] + \frac{1}{2}\left[\frac{\partial v_i}{\partial x_j} - \frac{\partial v_j}{\partial x_i}\right] \\ &= S_{i,j} + \Omega_{i,j}.\end{aligned} \tag{2.38}$$

$S_{i,j}$ and $\Omega_{i,j}$ are the symmetric and the antisymmetric parts of the velocity gradient tensor, respectively. Once we have done this separation, we can calculate the vorticity of $\mathbf{v}$ as

$$\omega_i = \varepsilon_{ijk}\frac{\partial v_k}{\partial x_j} = \varepsilon_{ijk}\Omega_{k,j} = -\varepsilon_{ijk}\Omega_{j,k}. \tag{2.39}$$

We can multiply both sides of equation (2.39) by ε_{imn}, and use the $\varepsilon - \delta$ identity:

$$\varepsilon_{imn}\varepsilon_{ijk} = \delta_{m,j}\delta_{n,k} - \delta_{m,k}\delta_{n,j}, \tag{2.40}$$

so that we have:

$$\varepsilon_{imn}\omega_i = \Omega_{n,m} - \Omega_{m,n} = 2\Omega_{n,m}, \Rightarrow \tag{2.41}$$

$$\Omega_{i,j} = \frac{1}{2}\varepsilon_{kji}\omega_k = -\frac{1}{2}\varepsilon_{ijk}\omega_k. \tag{2.42}$$

The $\varepsilon - \delta$ identity (2.40) can be proven by explicitly writing all terms for every possible value of each index. $\varepsilon_{imn}\varepsilon_{ijk}$ can only be nonzero if the four indices m, n, j, k have values different from i, and if $m \neq n$ and $j \neq k$. Now we have only two possibilities for matching indices: if $m = j$ and $n = k$, then ε_{imn} and ε_{ijk} will have the same sign. But if $m = k$ and $n = j$, the terms will have opposite signs. Summing these two possibilities, we obtain the RHS of equation (2.40).

Going back to the second term of the LHS of the curl of the Euler equation (2.37) and substituting equations (2.38) and (2.42):

$$v_m\frac{\partial v_k}{\partial x_m} = v_m\left(S_{k,m} + \Omega_{k,m}\right) = \frac{1}{2}v_m\left(\frac{\partial v_k}{\partial x_m} + \frac{\partial v_m}{\partial x_k}\right) - \frac{1}{2}v_m\varepsilon_{kmi}\omega_i. \tag{2.43}$$

Moving the first term in parenthesis on the RHS to the LHS and multiplying by 2:

$$v_m\frac{\partial v_k}{\partial x_m} = v_m\frac{\partial v_m}{\partial x_k} - \varepsilon_{kmi}v_m\omega_i. \tag{2.44}$$

Note that we can write

$$v_m\frac{\partial v_m}{\partial x_k} = \frac{1}{2}\frac{\partial}{\partial x_k}\left(v_m v_m\right). \tag{2.45}$$

Substituting equations (2.44) and (2.45) in the second term of the LHS of the curl of the Euler equation (2.37), we have:

$$\begin{aligned}\varepsilon_{ijk}\frac{\partial}{\partial x_j}\left[v_m\frac{\partial v_k}{\partial x_m}\right] &= \varepsilon_{ijk}\frac{\partial}{\partial x_j}\left[\frac{1}{2}\frac{\partial}{\partial x_k}\left(v_m v_m\right) - \varepsilon_{kmn}v_m\omega_n\right] \\ &= \frac{1}{2}\varepsilon_{ijk}\frac{\partial^2\left(v_m v_m\right)}{\partial x_j \partial x_k} - \varepsilon_{kij}\varepsilon_{kmn}\frac{\partial}{\partial x_j}\left(v_m\omega_n\right). \end{aligned} \tag{2.46}$$

The first term on the RHS is null as it is the curl of a gradient. Using the $\varepsilon - \delta$ identity:

$$\begin{aligned}\varepsilon_{ijk}\frac{\partial}{\partial x_j}\left[v_m\frac{\partial v_k}{\partial x_m}\right] &= -\left(\delta_{i,m}\delta_{j,n} - \delta_{i,n}\delta_{j,m}\right)\frac{\partial}{\partial x_j}\left(v_m\omega_n\right) \\ &= -v_i\frac{\partial\omega_j}{\partial x_j} + v_j\frac{\partial\omega_i}{\partial x_j} - \omega_j\frac{\partial v_i}{\partial x_j} + \omega_i\frac{\partial v_j}{\partial x_j}. \end{aligned} \tag{2.47}$$

On the RHS of equation (2.47), the last term is null because we are considering an incompressible flow. The first term is also zero because we can write it as

$$v_i\frac{\partial\omega_j}{\partial x_j} = v_i\varepsilon_{jkm}\frac{\partial^2 v_m}{\partial v_k \partial v_j} = 0, \tag{2.48}$$

as the derivative is symmetric to permutations in j and k. We are left with:

$$\varepsilon_{ijk}\frac{\partial}{\partial x_j}\left[v_m\frac{\partial v_k}{\partial x_m}\right] = v_j\frac{\partial\omega_i}{\partial x_j} - \omega_j\frac{\partial v_i}{\partial x_j}. \tag{2.49}$$

Substituting equation (2.49) for the second term on the LHS of the curl of the Euler equation (2.37), remembering that its RHS is null, we have the Euler equation for vorticity transport:

$$\frac{\partial\omega_i}{\partial t} + v_j\frac{\partial\omega_i}{\partial x_j} = \omega_j\frac{\partial v_i}{\partial x_j}. \tag{2.50}$$

On the LHS of the vorticity transport equation (2.50), we have the terms of a convection equation. On the RHS we have terms related to vortex stretching

(if $i = j$) and tilting (if $i \neq j$), due to the velocity field $\mathbf{v}$. However, in this work, we will only consider two-dimensional flows. Our system is confined to the $x_3 = 0$ plane, so we can only have vorticity in the $\hat{\mathbf{e}}_3$ direction, with $\omega_1 = \omega_2 = 0$. Moreover, there is no variation of the velocity field with respect to x_3, so the RHS of (2.50) turns out to be zero. Therefore, the Euler equation for the vorticity is:

$$\frac{\mathrm{d}\boldsymbol{\omega}}{\mathrm{d}t} = \frac{\partial \boldsymbol{\omega}}{\partial t} + \mathbf{v} \cdot \nabla \boldsymbol{\omega} = 0. \tag{2.51}$$

This is a pure convection equation, so it is clear that the vorticity field $\boldsymbol{\omega}$ moves through space dragged by the velocity field $\mathbf{v}$. In the case of a viscous flow, the viscous stress terms introduce an additional diffusion of the vorticity, with a diffusion coefficient given by the fluid viscosity.

2.3 Point-Vortex Flow

Now that we have derived the necessary fluid dynamics equations, we introduce the point-vortex flows, which we will use throughout this work. We can do it in many different ways. For instance, [1] introduces the point-vortex flow as a solution to the inviscid Burger's equation, which is equivalent to the Euler equation, neglecting force and pressure terms.

For our first presentation of the point-vortex flow, we will first introduce the concept of stream function, which we can use for a quick definition of the point-vortex flow.

A stream function $\psi(x_1, x_2, t)$ describes a two-dimensional incompressible flow, for which the velocity field is given by:

$$v_1 = \frac{\partial \psi}{\partial x_2}, \quad v_2 = -\frac{\partial \psi}{\partial x_1}. \tag{2.52}$$

This definition automatically satisfies the incompressibility condition:

$$\nabla \cdot \mathbf{v} = \frac{\partial v_1}{\partial x_1} + \frac{\partial v_2}{\partial x_2} = \frac{\partial}{\partial x_1}\frac{\partial \psi}{\partial x_2} - \frac{\partial}{\partial x_2}\frac{\partial \psi}{\partial x_1} = 0. \tag{2.53}$$

We can interpret the stream function also as a vector potential $\boldsymbol{\psi} = (0, 0, \psi)$, so that $\mathbf{v} = \nabla \times \boldsymbol{\psi}$. Notice that the stream function follows a Poisson equation where

the vorticity acts as the source. Taking the Laplacian – or the divergence of the gradient – of the stream function, we have:

$$\nabla^2\psi = \frac{\partial^2\psi}{\partial x_i \partial x_i} = \frac{\partial^2\psi}{\partial x_1 \partial x_1} + \frac{\partial^2\psi}{\partial x_2 \partial x_2} = -\frac{\partial v_2}{\partial x_1} + \frac{\partial v_1}{\partial x_2} = -\omega_3. \tag{2.54}$$

Back to the point-vortex flow, it can be defined by the stream function

$$\psi = -\frac{\Gamma}{4\pi}\ln\Big((x_1 - x_{1,c})^2 + (x_2 - x_{2,c})^2\Big), \tag{2.55}$$

so we have the flow

$$v_1 = \frac{\partial\psi}{\partial x_2} = -\frac{\Gamma}{2\pi}\cdot\frac{x_2 - x_{2,c}}{(x_1 - x_{1,c})^2 + (x_2 - x_{2,c})^2}; \tag{2.56}$$

$$v_2 = -\frac{\partial\psi}{\partial x_1} = \frac{\Gamma}{2\pi}\cdot\frac{x_1 - x_{1,c}}{(x_1 - x_{1,c})^2 + (x_2 - x_{2,c})^2}, \tag{2.57}$$

Equations (2.56) and (2.57) describe a vortex around the point $(x_{1,c}, x_{2,c})$, with the orbiting velocity decaying with the inverse of the distance from the center. It is easier to see the rotating behavior by changing to polar coordinates and setting $(x_{1,c}, x_{2,c}) = (0,0)$. Substituting $(x_1, x_2) = (r\cos\theta, r\sin\theta)$ and differentiating with respect to time, we obtain:

$$v_r = \frac{\mathrm{d}r}{\mathrm{d}t} = 0; \quad v_\theta = r\frac{\mathrm{d}\theta}{\mathrm{d}t} = \frac{\Gamma}{2\pi r}, \tag{2.58}$$

that is, we have no radial velocity, and the orbital velocity, perpendicular to the radius, decays with the inverse of the distance r. The sign of Γ sets the spinning direction of the vortex, counterclockwise if positive, and clockwise if negative. Calculating the vorticity of the point-vortex centered at the origin, omitting the index 3 from now on:

$$\omega = \frac{\partial v_2}{\partial x_1} - \frac{\partial v_1}{\partial x_2} = \frac{\Gamma}{2\pi r^4}\left[r^2 - 2x_1^2 + r^2 - 2x_2^2\right] = 0, \tag{2.59}$$

as long as $(x_1, x_2) \neq (0,0)$. In the origin, we have a vorticity singularity. We can

see this if we write the stream function in polar coordinates:

$$\psi = -\frac{\Gamma}{4\pi}\ln\left(r^2\right) = -\Gamma\frac{1}{2\pi}\ln r, \tag{2.60}$$

which is exactly $-\Gamma$ multiplied by the Green function of the 2D Laplacian operator, $G(r) = (2\pi)^{-1}\ln r$. So, making the connection with the equation for the Laplacian of the stream function and the vorticity (2.54), we have

$$\nabla^2\psi = -\omega_3 = -\Gamma\nabla^2 G = -\Gamma\delta(\mathbf{x})\,. \tag{2.61}$$

Therefore, the vorticity of the point-vortex flow is

$$\omega = \Gamma\delta(\mathbf{x})\,. \tag{2.62}$$

Now, we can define a flow by setting N point-vortices through the domain, so that we have:

$$\psi = -\frac{1}{4\pi}\sum_{n=1}^{N}\Gamma_n \ln\left[(x_1 - x_{1,n})^2 + (x_2 - x_{2,n})^2\right], \tag{2.63}$$

$$v_1 = -\frac{1}{2\pi}\sum_{n=1}^{N}\frac{\Gamma_n\,(x_2 - x_{2,n})}{(x_1 - x_{1,n})^2 + (x_2 - x_{2,n})^2}; \tag{2.64}$$

$$v_2 = \frac{1}{2\pi}\sum_{n=1}^{N}\frac{\Gamma_n\,(x_1 - x_{1,n})}{(x_1 - x_{1,n})^2 + (x_2 - x_{2,n})^2}. \tag{2.65}$$

Our vorticity field will be defined by a sum of N singularities, each corresponding to a different point-vortex:

$$\omega = \sum_{n=1}^{N}\Gamma_n\delta(\mathbf{x} - \mathbf{x}_n)\,. \tag{2.66}$$

From the 2D vorticity transport equation (2.51), we know that these singularities, and their corresponding vortices, should be advected by the velocity field $\mathbf{v}$. So

we can write the equations for the movement of the vortices, knowing each vortex should not be affected by its own velocity field. The m-th vortex moves according to:

$$\frac{\mathrm{d}x_{1,m}}{\mathrm{d}t} = -\frac{1}{2\pi}\sum_{n=1}^{N}\frac{\Gamma_n\left(x_{2,m}-x_{2,n}\right)}{\left(x_{1,m}-x_{1,n}\right)^2+\left(x_{2,m}-x_{2,n}\right)^2}; \tag{2.67}$$

$$\frac{\mathrm{d}x_{2,m}}{\mathrm{d}t} = \frac{1}{2\pi}\sum_{n=1}^{N}\frac{\Gamma_n\left(x_{1,m}-x_{1,n}\right)}{\left(x_{1,m}-x_{1,n}\right)^2+\left(x_{2,m}-x_{2,n}\right)^2}. \tag{2.68}$$

The point-vortex flow can also be obtained using the Biot-Savart law, departing from the definition of the vorticity (2.35), $\boldsymbol{\omega} = \nabla \times \mathbf{v}$:

$$\mathbf{v}(\mathbf{x},t) = \frac{1}{4\pi}\int_V \mathrm{d}\mathbf{x}'\,\frac{\boldsymbol{\omega}(\mathbf{x}',t)\times(\mathbf{x}-\mathbf{x}')}{(\mathbf{x}-\mathbf{x}')^3}. \tag{2.69}$$

Considering we only have vorticity in the $\hat{\mathbf{e}}_3$ direction, and that it depends only on x_1 and x_2, it is quite straight forward to integrate over x_3', considering our volume to be the whole 3D space, $V = \mathbb{R}^3$:

$$\mathbf{v}(x_1,x_2,t) = \frac{1}{2\pi}\int_{-\infty}^{\infty}\int_{-\infty}^{\infty}\mathrm{d}x_1'\mathrm{d}x_2'\,\omega_3(x_1',x_2',t)\,\frac{(x_1-x_1')\,\hat{\mathbf{e}}_2-(y_2-y_2')\,\hat{\mathbf{e}}_1}{\left(x_1-x_1'\right)^2+\left(x_2-x_2'\right)^2}. \tag{2.70}$$

Then, the velocity field is given by:

$$v_1 = -\frac{1}{2\pi}\int \mathrm{d}x_1'\mathrm{d}x_2'\,\frac{\omega_3(x_1',x_2',t)\,(x_2-x_2')}{\left(x_1-x_1'\right)^2+\left(x_2-x_2'\right)^2}; \tag{2.71}$$

$$v_2 = \frac{1}{2\pi}\int \mathrm{d}x_1'\mathrm{d}x_2'\,\frac{\omega_3(x_1',x_2',t)\,(x_1-x_1')}{\left(x_1-x_1'\right)^2+\left(x_2-x_2'\right)^2}, \tag{2.72}$$

so we have a vortex sheet, with vorticity varying through space. It is clear that the point-vortex flow is given by choosing a vorticity field defined by a sum of Dirac delta functions, each multiplied by a Γ_n factor.

The point-vortex flows will be used in Chapter 4 to generate chaotic flows

leading to complex spatial structures in our simulated microbial populations. The interactions between these flows and microbial behavior will be the focus of this work. To simulate these systems, we will consider domains with periodic boundary conditions. As the vortex velocity field has an infinite range ($\propto r^{-1}$), we will also need to consider the effect of an infinite number of images of the vortices over the boundaries of our square domain of sides L. This way, the field produced by a set of vortices will actually be given by:

$$\begin{aligned} v_1(\mathbf{x},t) &= -\frac{1}{2\pi}\sum_{j=1}^{N}\Gamma_j\sum_{n=-\infty}^{\infty}\sum_{m=-\infty}^{\infty}\frac{(x_2-x_{2,j}+Lm)}{(x_1-x_{1,j}+Ln)^2+(x_2-x_{2,j}+Lm)^2}; \\ v_2(\mathbf{x},t) &= \frac{1}{2\pi}\sum_{j=1}^{N}\Gamma_j\sum_{n=-\infty}^{\infty}\sum_{m=-\infty}^{\infty}\frac{(x_1-x_{1,j}+Ln)}{(x_1-x_{1,j}+Ln)^2+(x_2-x_{2,j}+Lm)^2}. \end{aligned} \tag{2.73}$$

Of course, as n or m increase, the terms become less and less significant, but we are going to simplify these sums so that we have only a single summation, with the magnitude of terms decreasing more quickly with their indices.

2.3.1 A Formula for Periodic Boundary Conditions

To simplify the analysis of the point-vortex flow in a domain with periodic boundary conditions, observe that we can describe a position through complex number $z = x_1 + ix_2$, and the same for the velocity field $u = v_1 + iv_2$. Using this notation, without considering periodic boundary conditions yet, we can write:

$$\begin{aligned} u &= \frac{1}{2\pi}\sum_{j=1}^{N}\frac{\Gamma_j\left(i\Delta x_{1,j}-\Delta x_{2,j}\right)}{\left(x_1-x_{1,j}\right)^2+\left(x_2-x_{2,j}\right)^2} \\ &= \frac{1}{2\pi i}\sum_{j=1}^{N}\frac{\Gamma_j\left(-\Delta x_{1,j}-i\Delta x_{2,j}\right)}{\left(\Delta x_{1,j}+i\Delta x_{2,j}\right)\left(\Delta x_{1,j}-i\Delta x_{2,j}\right)} \\ &= -\frac{1}{2\pi i}\sum_{j=1}^{N}\frac{\Gamma_j}{\Delta x_{1,j}-i\Delta x_{2,j}} \\ &= -\frac{1}{2\pi i}\sum_{j=1}^{N}\frac{\Gamma_j}{\overline{\Delta z_j}}. \end{aligned} \tag{2.74}$$

Taking the complex conjugate of (2.74):

$$\overline{u} = v_1 - iv_2 = \frac{1}{2\pi i}\sum_{j=1}^{N}\frac{\Gamma_j}{\Delta z_j}. \tag{2.75}$$

Now, adding the vortex images due to the PBC, we have:

$$\overline{u} = \frac{1}{2\pi i}\sum_{j=1}^{N}\sum_{n=-\infty}^{\infty}\sum_{m=-\infty}^{\infty}\frac{\Gamma_j}{\Delta z_j + L\,(n+im)}. \tag{2.76}$$

Considering only the summation over n, we can write:

$$\begin{aligned}
&\sum_{n=-\infty}^{\infty}\frac{1}{\Delta z_j + L\,(n+im)}\\
=&\frac{1}{\Delta z_j + iLm} + \sum_{n=1}^{\infty}\left[\frac{1}{\Delta z_j + iLm + Ln} + \frac{1}{\Delta z_j + iLm - Ln}\right]\\
=&\frac{1}{\Delta z_j + iLm} + \sum_{n=1}^{\infty} 2\frac{\Delta z_j + iLm}{\left(\Delta z_j + iLm\right)^2 + (Ln)^2}\\
=&\frac{1}{L}\sum_{n=-\infty}^{\infty}\frac{\Delta z_j/L + im}{\left(\Delta z_j/L + im\right)^2 + n^2}.
\end{aligned} \tag{2.77}$$

Now, we can use the result for the following expansion of the $\coth(\pi x)$ function:

$$\cot(\pi x) = \frac{1}{\pi}\sum_{n=-\infty}^{\infty}\frac{x}{x^2 - n^2}. \tag{2.78}$$

The interested reader can find the proof for this in Appendix A.1. Substituting this formula in equation (2.76):

$$\overline{u} = \frac{1}{2Li}\sum_{j=1}^{N}\Gamma_j\sum_{m=-\infty}^{\infty}\cot\left(\pi\frac{\Delta z_j}{L} + i\pi m\right). \tag{2.79}$$

This expression is useful for running simulations because it involves many fewer terms than equation (2.76). But we are still going to derive the expression for each velocity component.

For a complex variable $x = a + ib,\ a, b \in \mathbb{R}$, we can write the cotangent as:

$$\cot(a+ib) = \frac{\cot(a)\coth^2(b) - \cot(a)}{\cot^2(a) + \coth^2(b)} - i\frac{\coth(b)\cot^2(a) + \coth(b)}{\cot^2(a) + \coth^2(b)}, \tag{2.80}$$

remembering that $\cot(ix) = -i\coth(x)$. Looking only at the real part of the RHS of equation (2.80), we can write, using a few properties of (hyperbolic) trigonometric functions:

$$\begin{aligned}
\mathrm{Re}[\cot(a+ib)] &= \frac{\cot(a)\left[\coth^2(b) - 1\right]}{\cot^2(a) + \coth^2(b)} \\
&= \frac{\sin(a)\cos(a)\,\mathrm{csch}^2(b)}{\cos^2(a) + \coth^2(b)\sin^2(a)} \\
&= \frac{\sin(a)\cos(a)}{\cos^2(a)\sinh^2(b) + \cosh^2(b)\sin^2(a)} \\
&= \frac{\sin(2a)\ /2}{-\cos^2(a) + \cosh^2(b)} \\
&= \frac{\sin(2a)}{2\cosh^2(b) - 1 + 1 - 2\cos^2(a)} \\
&= \frac{\sin(2a)}{\cosh(2b) - \cos(2a)}.
\end{aligned} \tag{2.81}$$

Now, we can write the v_2, as in our case $a = \pi\Delta x_j/L$ and $b = \pi\left(\Delta y_j/L + m\right)$:

$$v_2(\mathbf{x}) = \frac{1}{2L}\sum_{j=1}^{N}\Gamma_j \sum_{m=-\infty}^{\infty} \frac{\sin\left(2\pi\Delta x_{1,j}/L\right)}{\cosh\left[2\pi\left(\Delta x_{2,j}/L + m\right)\right] - \cos\left(2\pi\Delta x_{1,j}/L\right)}. \tag{2.82}$$

We can do the same for the component v_1, and as our velocity components are symmetric with respect to coordinates x_1 and x_2, except for a minus sign, we have:

$$v_1(\mathbf{x}) = \frac{1}{2L}\sum_{j=1}^{N}\Gamma_j \sum_{m=-\infty}^{\infty} \frac{-\sin\left(2\pi\Delta x_{2,j}/L\right)}{\cosh\left[2\pi\left(\Delta x_{1,j}/L + m\right)\right] - \cos\left(2\pi\Delta x_{2,j}/L\right)}. \tag{2.83}$$

With the cosh term in the denominator, we can obtain a good approximation for the point-vortex flow in periodic domains using many fewer terms than would be

needed using equation (2.73).

Chapter 3

Spatial Master Equations and Approximations

Here we will present the necessary techniques for modeling spatial stochastic processes. The master equation (ME) is a very general object which can be used to describe a wide range of stochastic processes, through a differential equation for the time-evolution of the probability of a system being in each of its possible states. While analytical solutions for the ME can only be obtained in some limited scenarios, it is still a very useful tool as it allows a very clear and precise definition of stochastic processes. The ME also provides a clear connection to exact numerical simulations of stochastic processes through the Gillespie algorithm, which will also be introduced at the end of this chapter. Lastly, different approximations of the ME can be derived, which are useful for many applications.

We will introduce the master equation formalism and its mean-field approximation. Later, we will expand to spatial processes, where particles can move, and will also present the modeling of non-local interactions. For spatial processes, it is still simple to calculate mean-field approximations directly from the ME. For higher-order approximations, there are different techniques available, often relying on the rewrite of the ME as a field theory [29]. However, we will not get into higher-order approximations in this work.

3.1 Introduction to Master Equations

We start by describing a general stochastic process in an occupation number notation. Each state is characterized by a natural number n, the number of particles in the system. We first present a model with a scalar n, but it can be a vector $\mathbf{n}$, with each component describing the number of particles in each site of a lattice. There can even be multiple vectors, one for each species of particle.

The probability of the system being at state n at time t is denoted by $\mathrm{P}(n,t)$.

We also need to define the probabilities for transitions between different states. This can be done by defining the probability of transition per unit time – or the transition rate – from a state m to a state n as $\mathrm{T}(n,m)$. This means that the probability of this transition $m \to n$ happening during a Δt time interval is given by $T(n,m)\,\Delta t$.

Now, we can write the probability of the system is at a state n at a future time $t + \Delta t$ as

$$\begin{aligned}\mathrm{P}(n, t+\Delta t) = &\sum_{m \neq n} \mathrm{P}(m,t)\, T(n,m)\, \Delta t \\ &+ \mathrm{P}(n,t)\left[1 - \sum_{m \neq n} T(m,n)\, \Delta t\right] + \mathcal{O}\left(\Delta t^2\right). \end{aligned} \tag{3.1}$$

On the RHS of equation (3.1), the first term describes the scenario where the system occupies a state m different from n at time t, and goes through a transition to state n. The second term accounts for when the system is already in state n and suffers no transition (and of course, the sum over all transition probabilities should lead to 1). The last term considers the possibility that multiple reactions happen in the Δt time interval, which is possible, but it will necessarily scale with Δt at an order of at least two.

To obtain the master equation we will rearrange equation (3.1). Moving the first term inside brackets in the RHS to the LHS, dividing by Δt and taking the limit $\Delta t \to 0$, we obtain a differential equation:

$$\frac{\partial}{\partial t}\mathrm{P}(n,t) = \sum_{m \neq n} \left[\mathrm{T}(n,m)\,\mathrm{P}(m,t) - \mathrm{T}(m,n)\,\mathrm{P}(n,t)\right]. \tag{3.2}$$

The master equation can still be simplified by using the state shifting operator E, introduced in [52] as the step operator. It is defined to shift between states by a chosen quantity so that we have:

$$E_n^m\left[f(n)\right] = f\left(n+m\right). \tag{3.3}$$

The subscript n identifies the state parameter to be shifted, and the superscript m sets the amount by which to shift n. If there is a single parameter identifying the

state, the subscript can be omitted. Using this notation, we can write our master equation as:

$$\frac{\partial}{\partial t}\mathrm{P}(n,t) = \sum_{m\neq 0} (E_n^m - 1)[\mathrm{T}(n-m,n)\,\mathrm{P}(n,t)]\,, \tag{3.4}$$

which is easier to see if we also rewrite the master equation (3.2) as:

$$\frac{\partial}{\partial t}\mathrm{P}(n,t) = \sum_{m\neq 0} [\mathrm{T}(n,n+m)\,\mathrm{P}(n+m,t) - \mathrm{T}(n-m,n)\,\mathrm{P}(n,t)]\,. \tag{3.5}$$

Pay attention to the fact that an operator E^m appears together with a transition $n \to n-m$, and we must not forget this difference in sign between the transition and the state shifting operator.

Notice that we can also extend master equations to processes regarding systems with continuous state spaces, by describing states with a real variable x and a probability density $f(x,t)$, so that $f(x,t)\,\mathrm{d}x$ is the probability that the system occupies a state in the interval $(x, x+\mathrm{d}x)$. Also, we define the transition rate $\tau(x,x')$, such that $\tau(x,x')\mathrm{d}x\mathrm{d}t$ is the probability of the system transitioning to the interval $(x, x+\mathrm{d}x)$, between times t and $t+\mathrm{d}t$. With these new definitions, the ME for continuous state spaces can be written as

$$\frac{\partial}{\partial t} f\,(x,t) = \int \mathrm{d}x' \left[\tau\left(x,x'\right) f\left(x',t\right) - \tau\left(x',x\right) f\left(x,t\right)\right]. \tag{3.6}$$

In this work, we are interested in describing populations in space. Population size variables should have a discrete state space. However, position should be a continuous variable. Continuous state space master equations tend to be quite troublesome to deal with, so we will also discretize space. When necessary, we can recover the limit of continuous space. In the following subsection, we will present a very simple example of populational dynamics that can be described through a master equation. It will be useful to understand how one proceeds to analyze such a problem and also to introduce approximation methods.

3.1.1 The Birth-Death Model: A Simple Example

Here, we are going to apply the master equation formalism to a population where individuals can either reproduce asexually or die. If each individual has a birth rate b, we can have a transition $n \to n+1$ in n different ways, as each of the living individuals can reproduce. The transition probability corresponding to reproductions is

$$\mathrm{T}(n+1,n)\,\Delta t = n \cdot b\Delta t \cdot \left(1 - b\Delta t\right)^{n-1}, \tag{3.7}$$

where we have n possibilities for which a single individual reproduces with probability $b\Delta t$, while the other $n-1$ individuals don't reproduce, with probability $(1 - b\Delta t)$. As we take the limit $\Delta t \to 0$, only the first order term should survive, so we have:

$$\mathrm{T}(n+1,n) = bn. \tag{3.8}$$

In the same way, if the death rate is d, we have

$$\mathrm{T}(n-1,n) = dn. \tag{3.9}$$

Now we can write the master equation for the birth-death model:

$$\frac{\partial}{\partial t}\mathrm{P}(n,t) = b\,(n-1)\,\mathrm{P}(n-1,t) + d\,(n+1)\,\mathrm{P}(n+1,t) - (b+d)\,n\mathrm{P}(n,t)\,, \tag{3.10}$$

or, using the state shifting operator notation:

$$\frac{\partial}{\partial t}\mathrm{P}(n,t) = \left[b\left(E_n^{-1} - 1\right) + d\left(E_n^{+1} - 1\right)\right][n\mathrm{P}(n,t)] \tag{3.11}$$

Notice that n should be non-negative, which makes $n = 0$ what is called an absorbing state. See:

$$\frac{\partial}{\partial t}\mathrm{P}(0,t) = d\,\mathrm{P}(1,t)\,. \tag{3.12}$$

As $d > 0$, $\mathrm{P}(0,t)$ must be a monotonically non-decreasing function of time, i.e. it can only increase or stagnate, but never decrease.

For the birth-death model, we can obtain an analytical solution because the ME is linear in the state variable n in this case. This is quite a rare scenario, so we will present its solution, and use it to present the generating function. However, this will be our only example with an analytical solution.

The Generating Function

For a given probability mass (or density) function, we can define the generating function as:

$$\mathrm{G}(z,t) = \sum_{n=0}^{\infty} z^n \mathrm{P}(n,t)\,, \tag{3.13}$$

through which the probability of each state can be written as

$$\mathrm{P}(n,t) = \frac{\partial^n}{\partial z^n}\mathrm{G}(z,t)\bigg|_{z=0}\,. \tag{3.14}$$

Notice that if we do not take the constraint $z = 0$, we have an expression for the n-th derivative of the generating function:

$$\frac{\partial^n}{\partial z^n}\mathrm{G}(z,t) = \sum_{m=0}^{\infty} z^{m-n}[m\cdot(m-1)\cdot\cdots\cdot(m-n+1)]\mathrm{P}(m,t)\,. \tag{3.15}$$

Of course the summation could start from $m = n$, as every term for $m < n$ will be zero. This expression will be useful for substituting the characteristic function inside the master equation, in order to obtain a partial differential equation (PDE) for $\mathrm{G}(z,t)$, as we will do now.

If we multiply the birth-death process' master equation (3.11) by z^n and sum over n, we have, for the LHS:

$$\sum_{n=0}^{\infty} z^n \frac{\partial}{\partial t} \mathrm{P}(n,t) = \frac{\partial}{\partial t} \sum_{n=0}^{\infty} z^n \mathrm{P}(n,t) = \frac{\partial}{\partial t} \mathrm{G}(z,t)\,, \tag{3.16}$$

and for each term of the RHS:

$$\begin{aligned} b \sum_{n=0}^{N} z^n \,(n-1)\, \mathrm{P}(n-1,t) &= b \sum_{n=0}^{N} z^{n+1} n \mathrm{P}(n,t) = b z^2 \sum_{n=0}^{N} z^{n-1} n \mathrm{P}(n,t) \\ &= b z^2 \frac{\partial}{\partial z} \mathrm{G}(z,t)\,; \end{aligned} \tag{3.17}$$

$$d \sum_{n=0}^{N} z^n \,(n+1)\, \mathrm{P}(n+1,t) = d \sum_{n=0}^{N} z^{n-1} n \mathrm{P}(n,t) = d \frac{\partial}{\partial z} \mathrm{G}(z,t)\,; \tag{3.18}$$

$$(b+d) \sum_{n=0}^{N} z^n n \mathrm{P}(n,t) = (b+d)\, z \frac{\partial}{\partial z} \mathrm{G}(z,t)\,. \tag{3.19}$$

Therefore, we have the following PDE for the generating function:

$$\begin{aligned} \frac{\partial}{\partial t} \mathrm{G}(z,t) &= \left[b z^2 + d - (b+d)\, z \right] \frac{\partial}{\partial z} \mathrm{G}(z,t) \\ &= (z-1)\,(bz-d)\, \frac{\partial}{\partial z} \mathrm{G}(z,t)\,. \end{aligned} \tag{3.20}$$

This PDE can be solved using the characteristic method. If a variable s parametrizes a characteristic curve, we have:

$$\frac{\mathrm{d}G}{\mathrm{d}s} = \frac{\mathrm{d}z}{\mathrm{d}s} \frac{\partial G}{\partial z} + \frac{\mathrm{d}t}{\mathrm{d}s} \frac{\partial G}{\partial t} = 0. \tag{3.21}$$

If we substitute equation (3.20) in (3.21) and integrate over s, we obtain:

$$\int \mathrm{d}t + \int \frac{\mathrm{d}z}{(z-1)\,(bz-d)} = C, \tag{3.22}$$

where C is a constant. The integral over z can be solved through a partial fraction decomposition method:

$$t + \frac{1}{b-d} \ln \left| \frac{z-1}{bz-d} \right| = C \Rightarrow \left| \frac{z-1}{bz-d} \right| e^{(b-d)t} = e^{(b-d)C}. \tag{3.23}$$

$e^{(b-d)C}$ is still a constant, which we will set to a variable ζ to parametrize our characteristic curve:

$$\zeta = \left| \frac{z-1}{bz-d} \right| e^{(b-d)t}. \tag{3.24}$$

This expression can be inverted so that we can write z in terms of ζ:

$$z(t) = \frac{1 \pm d\zeta e^{-(b-d)t}}{1 \pm b\zeta e^{-(b-d)t}}, \tag{3.25}$$

where we have the positive sign from $\pm$ when $1 < z < d/b$ or $d/b < z < 1$, and the negative one when $z > \max(1, d/b)$ or $z < \min(1, d/b)$. To continue with an analytical solution, we need to choose an initial condition for the master equation, which will work as a boundary condition for the generating function's PDE. A reasonable initial condition would be that the population is equal to N at the initial time, that is $\mathrm{P}(n, 0) = \delta_{n,N}$. In this case, the PDE's boundary condition is:

$$\mathrm{G}(z, 0) = z(0)^N. \tag{3.26}$$

As we have already found $z(t)$ in equation (3.25) and the solution is constant along these characteristic curves, we can write our full solution for the characteristic function:

$$\mathrm{G}(z, t) = \left[\frac{1 \pm d\zeta}{1 \pm b\zeta} \right]^N = \left[\frac{|bz-d| \pm d\,|z-1|\, e^{(b-d)t}}{|bz-d| \pm b\,|z-1|\, e^{(b-d)t}} \right]^N. \tag{3.27}$$

Once the generating function is obtained, the problem is solved, as it is now possible to derive the expression for each $\mathrm{P}(n, t)\ \forall\, n, t$. It would still be time-

consuming, even for states with small n, but it is possible. An interesting result we can obtain is the probability of extinction $\mathrm{P}(0,t)$:

$$\mathrm{P}(0,t) = \mathrm{G}(0,t) = \left[\frac{d - e^{(b-d)t}}{d - be^{(b-d)t}}\right]^N . \tag{3.28}$$

If $b < d$, it is clear that the population should eventually go extinct, and we can show that by calculating the limit $\mathrm{P}(0, t \to \infty) = 1$. If $b > d$, we still have a nonzero probability of extinction. It will never reach 1, and we can see that it decreases with the N-th power of the ratio d/b, for N individuals in the initial condition:

$$\lim_{t\to\infty} \mathrm{P}(0,t) = \left(\frac{d}{b}\right)^N , \quad \text{if } b > d, \tag{3.29}$$

so it quickly becomes negligible as the initial condition N increases.

3.2 Mean-Field Approximation

Interestingly, if $b = d$, we should also have a certain extinction in the limit $t \to \infty$, independent of initial population N, as, in this case, the process is symmetric regarding transitions $n \to n+1$ and $n \to n-1$, but $n = 0$ is an absorbing state. To investigate the dynamics of $\mathrm{P}(0,t)$ in the case $b = d$, one would need to write the master equation for $b = d$ and derive the generating function PDE following the steps from equations (3.20) to (3.27).

In case we cannot derive analytical solutions for the master equation, we can still try to analyze some approximations before moving to numerical simulations. These approximations consist in obtaining expressions for some statistical moments. If we are interested only in the mean population size, for instance, we can obtain it from the master equation. The mean population size can be calculated directly from its definition:

$$\langle n(t) \rangle = \sum_n n\mathrm{P}(n,t) . \tag{3.30}$$

For a generic master equation (3.4), we can multiply it by n and sum over all

possible states:

$$\begin{aligned}\frac{\mathrm{d}}{\mathrm{d}t}\langle n(t)\rangle &= \sum_n n\frac{\partial}{\partial t}\mathrm{P}(n,t)\\ &= \sum_n n\sum_{m\neq 0}(E_n^m-1)[\mathrm{T}(n-m,n)\,\mathrm{P}(n,t)]\\ &= \sum_{m\neq 0}\sum_n n\mathrm{T}(n,n+m)\,\mathrm{P}(n+m,t)-\sum_{m\neq 0}\sum_n n\mathrm{T}(n-m,n)\,\mathrm{P}(n,t)\\ &= \sum_{m\neq 0}\sum_n (n-m)\,\mathrm{T}(n-m,n)\,\mathrm{P}(n,t)-\sum_{m\neq 0}\sum_n n\mathrm{T}(n-m,n)\,\mathrm{P}(n,t)\,,\end{aligned} \tag{3.31}$$

where we substituted $n \to n+m$ in the first summation to rewrite it in terms of $\mathrm{P}(n,t)$. Finally, summing terms in the last line of (3.31), we obtain the mean-field approximation:

$$\frac{\mathrm{d}}{\mathrm{d}t}\langle n(t)\rangle = \sum_{m\neq 0}\sum_n (-m)\,\mathrm{T}(n-m,n)\,\mathrm{P}(n,t) = -\sum_{m\neq 0}\langle m\mathrm{T}(n-m,n)\rangle\,. \tag{3.32}$$

For the birth-death model, presented in equation (3.11), the mean population is given by:

$$\frac{\mathrm{d}}{\mathrm{d}t}\langle n(t)\rangle = (b-d)\langle n(t)\rangle\,. \tag{3.33}$$

We know the solution of equation (3.33) is an exponential:

$$n(t) = n_0 e^{(b-d)t}, \tag{3.34}$$

for an initial condition $n\,(t=0) = n_0$. If $b < d$, the population decays towards extinction, but if $b > d$, it will grow to infinity. As this approximation is deterministic, we no longer have the possibility of extinction for $b > d$, compared to the solution of the master equation (3.29). This is one example of the limitations of this deterministic mean-field approximation.

Another part of the mean-field approximation is to also discard correlations by approximating higher-order moments by the corresponding product of first

moments:

$$\left\langle \prod_{i=1}^{N} x_i \right\rangle = \prod_{i=1}^{N} \langle x_i \rangle \,. \tag{3.35}$$

For the birth-death model, we did not have to do that, but it will be important for more complex models.

3.3 Populations Moving Through Space

Considering the spatial distribution of a system makes the mathematical description of their stochastic dynamics more complicated. In this section, we will present in detail how to tackle this problem.

As it was already mentioned, we will discuss only master equations in discrete space, or in a lattice, and we will take the continuous limit (lattice spacing $\to 0$) when necessary, usually after a mean-field approximation.

Consider a population of particles moving through space. For now, let's ignore demographic effects because these can be treated separately from movement and thus will lead to separate terms in the master equation. Therefore, we will treat movement alone, and then add it to the demographic master equation. Let's start with a set of particles moving through a one-dimensional lattice, with a lattice constant Δx, so that each site is indexed by its position $x_i = i\Delta x,\ (i = 0, 1, 2, \dots)$. We can consider at first that we have an infinite number of sites. The state of the system will be described by a vector $\mathbf{n}$ with the number of particles at each site, $n_i = \#$ particles at x_i.

We will consider only reactions of movement to nearest neighbors. In one dimension, there are only two possible reactions for the particles at each site. For the i-th site, a particle can move either to the left or to the right:

$$(n_i, n_{i+1}) \xrightarrow{h_i^R n_i} (n_i - 1, n_{i+1} + 1)\,; \tag{3.36}$$

$$(n_i, n_{i-1}) \xrightarrow{h_i^L n_i} (n_i - 1, n_{i-1} + 1)\,, \tag{3.37}$$

where h_i^R and h_i^L are respectively the rates of movement to the right and to the left.

Notice that these can depend on the position x_i of the particle, and also on time, $h_i = h_i(t)$, but we will omit the time dependence for now, for a more compact notation. The master equation corresponding to this microscopic process is:

$$\begin{aligned}\frac{\partial}{\partial t}\mathrm{P}(\mathbf{n},t) = &\sum_i \left(E_i^{+1}E_{i+1}^{-1} - 1\right)\left[h_i^R n_i \mathrm{P}(\mathbf{n},t)\right] \\ &+ \sum_i \left(E_i^{+1}E_{i-1}^{-1} - 1\right)\left[h_i^L n_i \mathrm{P}(\mathbf{n},t)\right].\end{aligned} \tag{3.38}$$

Here, the subscript of the state shifting operator denotes the site of the lattice, or the component of n, on which it acts. Expanding equation (3.38):

$$\begin{aligned}\frac{\partial}{\partial t}\mathrm{P}(\mathbf{n},t) = &\sum_i h_i^R\,(n_i+1)\,\mathrm{P}(\mathbf{n}+\mathbf{e}_i-\mathbf{e}_{i+1},t) \\ &+ \sum_i h_i^L\,(n_i+1)\,\mathrm{P}(\mathbf{n}+\mathbf{e}_i-\mathbf{e}_{i-1},t) \\ &- \sum_i \left(h_i^L + h_i^R\right) n_i \mathrm{P}(\mathbf{n},t),\end{aligned} \tag{3.39}$$

where $\mathbf{e}_i$ is the unitary vector in direction i, i.e. a vector with all entries being zero, except for the i-th component, which is equal to one. Now, we calculate the mean-field approximation. Let's look at the first line. Multiplying the equation by n_j and summing over all possible states $\mathbf{n}$, we have:

$$\begin{aligned}&\sum_{i,\mathbf{n}} h_i^R\,(n_i+1)\,n_j\mathrm{P}(\mathbf{n}+\mathbf{e}_i-\mathbf{e}_{i+1},t) \\ =&\sum_{i\notin\{j,j-1\}}\sum_{\mathbf{n}} h_i^R\,(n_i+1)\,n_j\mathrm{P}(\mathbf{n}+\mathbf{e}_i-\mathbf{e}_{i+1},t) \\ &+\sum_{\mathbf{n}} h_j^R\,(n_j+1)\,n_j\mathrm{P}(\mathbf{n}+\mathbf{e}_j-\mathbf{e}_{j+1},t) \\ &+\sum_{\mathbf{n}} h_{j-1}^R\,(n_{j-1}+1)\,n_j\mathrm{P}(\mathbf{n}+\mathbf{e}_{j-1}-\mathbf{e}_j,t),\end{aligned} \tag{3.40}$$

where we simply separated terms where $i \notin \{j, j-1\}$ from the summation, as for these terms there will be a difference when manipulating dummy indices $\mathbf{n}$:

$$
\begin{aligned}
&\sum_{i,\mathbf{n}} h_i^R \left(n_i+1\right) n_j \mathrm{P}(\mathbf{n}+\mathbf{e}_i-\mathbf{e}_{i+1},t) \\
&= \sum_{i\notin\{j,j-1\}} \sum_{\mathbf{n}} h_i^R n_i n_j \mathrm{P}(\mathbf{n},t) + \sum_{\mathbf{n}} h_j^R n_j \left(n_j-1\right) \mathrm{P}(\mathbf{n},t) \\
&\quad + \sum_{\mathbf{n}} h_{j-1}^R n_{j-1} \left(n_j+1\right) \mathrm{P}(\mathbf{n},t) \\
&= \sum_{i,\mathbf{n}} h_i^R n_i n_j \mathrm{P}(\mathbf{n},t) + \sum_{\mathbf{n}} \left[h_{j-1}^R n_{j-1} - h_j^R n_j\right] \mathrm{P}(\mathbf{n},t)\,. \qquad (3.41)
\end{aligned}
$$

We do the same for the second line of the master equation (3.39). Substituting the results back in (3.39), we are left only with terms at sites $j-1$, j and $j+1$, and we can write:

$$
\frac{\partial}{\partial t}\left\langle n_j(t)\right\rangle = \left\langle h_{j-1}^R n_{j-1}(t) + h_{j+1}^L n_{j+1}(t) - \left(h_j^R + h_j^L\right) n_j(t)\right\rangle . \qquad (3.42)
$$

Now, we can take the continuous limit, by substituting $n_j(t) \to \Delta x \rho(x,t) \Rightarrow n_{j\pm1}(t) \to \Delta x \rho(x \pm \Delta x)$, and $h_{j\pm1} \to h(x \pm \Delta x)$. Expanding spatial functions and keeping terms up to order $(\Delta x)^2$, we obtain:

$$
\begin{aligned}
\frac{\partial}{\partial t}\rho(x,t) = \Delta x \frac{\partial}{\partial x}&\left[\rho(x,t)\left(h^L(x,t) - h^R(x,t)\right)\right] \\
&+ \frac{(\Delta x)^2}{2}\frac{\partial^2}{\partial x^2}\left[\rho(x,t)\left(h^L(x,t) + h^R(x,t)\right)\right]. \qquad (3.43)
\end{aligned}
$$

Defining both the drift $v(x,t) = \Delta x \left(h^R(x,t) - h^L(x,t)\right)$ and the diffusion coefficient $D(x,t) = (\Delta x)^2/2 \cdot \left(h^L(x,t) + h^R(x,t)\right)$, we obtain:

$$
\frac{\partial}{\partial t}\rho(x,t) = -\frac{\partial}{\partial x}\left[v(x,t)\,\rho(x,t)\right] + \frac{\partial^2}{\partial x^2}\left[D(x,t)\,\rho(x,t)\right]. \qquad (3.44)
$$

It is very easy to generalize this to more dimensions, obtaining:

$$
\frac{\partial}{\partial t}\rho(\mathbf{x},t) = -\sum_i \frac{\partial}{\partial x_i}\left[v_i(x,t)\,\rho(x,t)\right] + \sum_{i,j}\frac{\partial^2}{\partial x_i x_j}\left[D_{i,j}(x,t)\,\rho(x,t)\right]. \qquad (3.45)
$$

Equation (3.45) is a very important result for obtaining mean-field approximations for populations moving in space. For the present work, we will only consider incompressible flows, $\nabla \cdot \mathbf{v}(\mathbf{x}, t) = 0$ (see Chapter 2). Also, we will be considering diffusion constant through space and time, $D_{i,j}(x, t) = D\delta_{i,j}$, so that we can write:

$$\frac{\partial}{\partial t}\rho(\mathbf{x}, t) = -\mathbf{v}(\mathbf{x}, t) \cdot \nabla\rho(x, t) + D\nabla^2\rho(\mathbf{x}, t)\,, \tag{3.46}$$

a usual advection-diffusion equation with constant diffusion. As these movement terms would be additive to the reaction ones in a master equation with demography, it is also sufficient to add the associated terms in the mean-field. That is, for a birth-death process of a population in space, under an incompressible velocity field $\mathbf{v}(\mathbf{x}, t)$ and diffusing with a coefficient D, the mean-field approximation for the spatiotemporal dynamics of the population density field is

$$\frac{\partial}{\partial t}\rho(\mathbf{x}, t) = -\mathbf{v}(\mathbf{x}, t) \cdot \nabla\rho(x, t) + D\nabla^2\rho(\mathbf{x}, t) + (b - d)\,\rho(\mathbf{x}, t)\,. \tag{3.47}$$

3.4 Non-local Interactions

Many ecological systems present individuals that interact at finite ranges, which can lead to self-organization. Examples include interactions between plants competing for water [36, 45], birds organizing into flocks [6], predators searching for their prey [10], among others. Of major interest to us, microbes can also interact over long distances through the production of different molecules that diffuse through space and reach other individuals [8, 18, 53, 55].

In this section, we are going to present non-local interactions, where biological reactions can depend on interactions between individuals that are spatially separated. Here, we describe a general framework for modeling non-local interactions, without assuming any specific details of the actual interaction mechanism.

In this work, we will only consider non-local demographic interactions, that is, non-local interactions affecting reproduction or death rates, but not affecting movement. It is possible, however, to also model movement with a non-local dependence on the number of neighbors of an individual [35, 38, 39].

Consider a system where the only process of interest is a demographic non-local interaction associated with the transition $\mathbf{n} \to \mathbf{n} + m\mathbf{e}_i$ in the number of

individuals, for any site i. We can write a master equation for this scenario:

$$\frac{\partial}{\partial t}\mathrm{P}(\mathbf{n},t) = \sum_i \left(E_i^{-m} - 1\right)\left[\sum_j G_{i,j} f_m\left(n_i, n_j\right)\mathrm{P}(\mathbf{n},t)\right], \tag{3.48}$$

where we only consider transitions $\mathbf{n} \to \mathbf{n} + m\mathbf{e}_i$, for any i. $f_m\left(n_i, n_j\right)$ is the contribution of the non-local interaction between sites i and j for the transition happening at site i. $G_{i,j}$ is the so-called interaction kernel. It is the weight given to this interaction between sites i and j, which usually depends on the distance between the two sites, defining the range of interaction. Notice that this redefinition of the transition rates means that we are considering a process where the interaction rate is not only $f_m\left(n_i, n_j\right)$, but $G_{i,j} f_m\left(n_i, n_j\right)$.

There is not much we can do with such a non-local interaction term except for looking at its effect in the mean-field approximation. However, even this approximation can be quite tricky depending on the form of the transition probability terms $f_m\left(n_i, n_j\right)$. Therefore, we will now focus on a simple non-local competition term, to be added to our birth-death model.

A non-local competition term can be defined with $m = -1$, because the competition will lead to the death of one of the competing individuals. Also, we make $f_{-1}\left(n_i, n_j\right) = c n_i\left(n_j - \delta_{i,j}\right)$, where c is the competition rate. The Kronecker delta appears because an individual cannot compete with himself, so we subtract one individual if $j = i$. For this scenario, where the rate of death in site i due to competition with site j is $c G_{i,j} n_i\left(n_j - \delta_{i,j}\right)$, we can calculate the mean-field term, without worrying about the form of the kernel G for now:

$$\begin{aligned}
\frac{\partial}{\partial t}\left\langle n_j(t)\right\rangle &= \sum_{\mathbf{n}} n_j \sum_i \left(E_i^{+1} - 1\right)\left[\sum_k G_{i,k} c n_i\left(n_k - \delta_{i,k}\right)\mathrm{P}(\mathbf{n},t)\right] \\
&= \sum_{i,k} c G_{i,k} \sum_{\mathbf{n}} \left(n_i + 1\right) n_j n_k \mathrm{P}(\mathbf{n} + \mathbf{e}_i, t) + \\
&\quad - \sum_{i,k} c G_{i,k} \sum_{\mathbf{n}} n_i n_j \left(n_k - \delta_{i,k}\right)\mathrm{P}(\mathbf{n},t)\,.
\end{aligned} \tag{3.49}$$

We can write the first term on the RHS of equation (3.49) as:

$$\sum_{i,k} cG_{i,k} \sum_{\mathbf{n}} (n_i + 1)\, n_j n_k \mathrm{P}(\mathbf{n} + \mathbf{e}_i, t) =$$
$$= \sum_{\mathbf{n}} \sum_{k \neq i} c \left[\sum_{i \neq j} G_{i,k} n_i n_j n_k + G_{j,k} n_j \left(n_j - 1\right) n_k \right] \mathrm{P}(\mathbf{n}, t) +$$
$$+ \sum_{\mathbf{n}} c \left[\sum_{i \neq j} G_{i,i} n_i \left(n_i - 1\right) n_j + c G_{j,j} n_j \left(n_j - 1\right)^2 \right] \mathrm{P}(\mathbf{n}, t)\,. \tag{3.50}$$

Expanding the square in the last term of equation (3.50) and joining terms appropriately, we obtain

$$\sum_{\mathbf{n}} \sum_{i,k} cG_{i,k} n_i n_j n_k \mathrm{P}(\mathbf{n}, t) - \sum_{\mathbf{n}} c \left(\sum_{k \neq j} G_{j,k} n_j n_k + G_{j,j} n_j^2 \right) \mathrm{P}(\mathbf{n}, t) +$$
$$- \sum_{\mathbf{n}} c \left(\sum_{i \neq j} G_{i,i} n_i n_j + G_{j,j} n_j^2 \right) \mathrm{P}(\mathbf{n}, t) + cG_{j,j} n_j, \tag{3.51}$$

which can finally be simplified to

$$\sum_{\mathbf{n}} \sum_{i,k} cG_{i,k} n_i n_j \left(n_k - \delta_{i,k}\right) \mathrm{P}(\mathbf{n}, t) - \sum_{\mathbf{n}} \sum_{k} cG_{j,k} n_j \left(n_k - \delta_{j,k}\right) \mathrm{P}(\mathbf{n}, t)\,. \tag{3.52}$$

Thus, the mean-field approximation for the non-local competition can be written as

$$\frac{\partial}{\partial t} \left\langle n_j(t) \right\rangle = -c \left\langle \sum_{k} G_{j,k} n_j(t) \left(n_k(t) - \delta_{j,k}\right) \right\rangle$$
$$\approx -c \sum_{k} G_{j,k} \left\langle n_j(t) \right\rangle \left\langle n_k(t) \right\rangle + cG_{j,j} \left\langle n_j(t) \right\rangle, \tag{3.53}$$

where we consider the number of particles on different sites to be uncorrelated, as part of the mean-field approximation. Now, again taking the continuous limit, $n_j(t) \to \rho(\mathbf{x}, t)\, \Delta\mathbf{x}$ and $\Delta\mathbf{x} \to 0$, also redefining the interaction kernel over a continuous space, $G_{j,k} \to G(\mathbf{x}, \mathbf{x}')$:

$$\frac{\partial}{\partial t}\rho(\mathbf{x},t) = cG(\mathbf{x},\mathbf{x})\,\rho(\mathbf{x},t) - c\rho(\mathbf{x},t)\int \mathrm{d}\mathbf{x}' G\left(\mathbf{x},\mathbf{x}'\right)\rho\left(\mathbf{x}',t\right). \tag{3.54}$$

We can couple this result with the birth, death and movement terms to build a spatial logistic model with non-local competition:

$$\begin{aligned}\frac{\partial}{\partial t}\rho(\mathbf{x},t) =& D\nabla^2\rho(\mathbf{x},t) - \mathbf{v}(\mathbf{x},t)\cdot\nabla\rho(\mathbf{x},t) + \left[b-d+cG(\mathbf{x},\mathbf{x})\right]\rho(\mathbf{x},t)\\ &- c\rho(\mathbf{x},t)\int \mathrm{d}\mathbf{x}' G\left(\mathbf{x},\mathbf{x}'\right)\rho\left(\mathbf{x}',t\right).\end{aligned} \tag{3.55}$$

If we consider only local competition, the continuous-space mean-field becomes

$$\frac{\partial}{\partial t}\rho(\mathbf{x},t) = D\nabla^2\rho(\mathbf{x},t) - \mathbf{v}(\mathbf{x},t)\cdot\nabla\rho(\mathbf{x},t) + (b-d+c)\,\rho(\mathbf{x},t) - c\rho(\mathbf{x},t)^2. \tag{3.56}$$

Notice that directly substituting $G(\mathbf{x},\mathbf{x}') = \delta(\mathbf{x}-\mathbf{x}')$ in equation (3.55) would lead to a divergence in the term $cG(\mathbf{x},\mathbf{x})\,\rho(\mathbf{x},t)$, but we do not have this problem if we go back to discrete space and substitute $G_{i,j} = \delta_{i,j}$ before taking the continuous limit.

From now on, we will focus on the non-local competition scenario. Non-local competition provides a better connection to systems with a finite number of particles in continuous space, which we want to numerically simulate, as there will have to be defined a finite interaction radius. The interaction radius can be made small, to approach a local competition scenario, but a large competition radius (relative to other parameters of the model) can lead to pattern formation, as it will be shown next.

3.5 Linear Stability Analysis

Now, we are going to analyze how different terms derived above (movement in section 3.3 and non-local competition in section 3.4) affect the linear stability of equilibrium points of the logistic model with non-local competition (3.55).

Equation (3.55) would be hard to solve analytically, but we can still calculate the stability of its equilibria. First, we will look into the effect of non-local competition and its capability to form patterns. Afterward, we look into the role of advection

and show that incompressible flows in closed systems do not change the stability of equilibrium points, but can alter the geometry of formed patterns.

3.5.1 Non-local Competition

In principle, this calculation can be done regardless of the functional expression of the kernel $G(\mathbf{x}, \mathbf{x}')$. However, we are already going to choose the form for the interaction kernel G that we will be working with throughout this text. It will be defined depending only on the distance between positions, $G(\mathbf{x}, \mathbf{x}') = G(\mathbf{x} - \mathbf{x}')$, with

$$G(\mathbf{x}) = \begin{cases} \left(\pi R^2\right)^{-1}, & \text{if } |\mathbf{x}| \leq R; \\ 0, & \text{else.} \end{cases} \tag{3.57}$$

That is, we choose a kernel with a finite interaction range, and constant interaction strength inside this range, reminding that we are considering a two-dimensional scenario, according to the focus of this dissertation. Notice that the kernel (3.57) integrates to one. In this subsection, we are going to ignore the advective term, $\mathbf{v} = 0$, as we will look into it afterward.

We start by obtaining the spatially uniform equilibrium solutions of equation (3.55), $\rho(\mathbf{x}, t) = \rho(t) \ \forall \ \mathbf{x}$. Substituting this in equation (3.55), and discarding advection, we have:

$$\begin{aligned} \frac{\partial}{\partial t}\rho(t) =& D\nabla^2\rho(t) + \left[b - d + cG(\mathbf{x}, \mathbf{x})\right]\rho(t) - c\rho(t)^2 \int \mathrm{d}\mathbf{x}' G\left(\mathbf{x}, \mathbf{x}'\right) \\ =& \left[b - d + \frac{c}{\pi R^2}\right]\rho(t) - c\rho(t)^2 . \end{aligned} \tag{3.58}$$

The equilibrium solution of equation (3.58) is obtained by looking into the scenario where $\rho(t)$ converges to a constant value, $\rho(t) = \rho_0$, so that

$$\frac{\partial}{\partial t}\rho_0 = 0 = \left(b - d + \frac{c}{\pi R^2}\right)\rho_0 - c\rho_0^2. \tag{3.59}$$

Equation (3.59) has two solutions:

$$\rho_0 = 0 \text{ or } \rho_0 = \frac{b-d}{c} + \frac{1}{\pi R^2}. \tag{3.60}$$

The extra $1/(\pi R^2)$ term might be unexpected, but it is important to remember that with the chosen kernel, the competition rate is $c/(\pi R^2)$, for individuals separated by a distance smaller than R. So as the competition radius R decreases, even though the competition increases, competitive interactions become rarer, as individuals have to be closer to compete, leading to a divergence of the population as $R \to 0$.

Therefore, if we decouple the competition rate and its radius, by setting the competition kernel

$$G(\mathbf{x}) = \begin{cases} 1, & \text{if } |\mathbf{x}| \leq R; \\ 0, & \text{else,} \end{cases} \tag{3.61}$$

then the homogeneous solution should obey:

$$\frac{\partial}{\partial t}\rho_0 = 0 = (b - d + c)\,\rho_0 - c\pi R^2 \rho_0^2, \tag{3.62}$$

so that

$$\rho_0 = 0 \text{ or } \rho_0 = \frac{b-d+c}{c\pi R^2}, \tag{3.63}$$

and now all terms are divided by the competition radius. The change from a normalized kernel (3.57) to a unnormalized one (3.61) may look like a simple rescaling of the kernel, only changing competition rates. However, by rescaling the kernel proportionally to the competition radius, it decouples the interaction radius from the competition rate. Therefore, the effect of varying the radius R is not the same.

For equation (3.60), taking $R \to 0$ necessarily drives the system to a divergence of the population. However, for equation (3.62), the value of ρ_0 in the limit $R \to 0$ will depend on the value of $b - d + c$. Moving on, we will use the unnormalized kernel (3.61), $G(\mathbf{x}) = 1, |\mathbf{x}| \leq R$, so that the competition rate is independent of the

radius, which is hopefully more intuitive. Of course, this choice will only matter when we are interested in how results change when varying the interaction radius R.

To look at the stability of the homogeneous equilibrium points (3.63), we look at the evolution of a perturbation to the equilibrium state. Suppose $\rho = \rho_0 + \eta$, $\eta \ll 1$. In this case, we have:

$$\frac{\partial}{\partial t}(\rho_0 + \eta) = f(\rho_0 + \eta) = f(\rho_0) + \eta \frac{\mathrm{d}}{\mathrm{d}\rho} f(\rho)\Big|_{\rho_0}, \tag{3.64}$$

with $f(\rho) = (b - d + c)\rho - c\pi R^2 \rho^2$ for the birth-death model with non-local competition. Because ρ_0 is an equilibrium point system (equation (3.59)), $f(\rho_0) = 0$. Therefore, we must have:

$$\frac{\partial}{\partial t}\eta = \eta \frac{\mathrm{d}}{\mathrm{d}\rho} f(\rho)\Big|_{\rho_0}. \tag{3.65}$$

Equation (3.65) implies that the perturbation η will have grow exponentially at rate

$$\frac{\mathrm{d}}{\mathrm{d}\rho} f(\rho)\Big|_{\rho_0} = b - d + c - 2c\pi R^2 \rho_0. \tag{3.66}$$

Therefore, the equilibrium point will be stable if the growth rate is negative so that the perturbation decays with time. For $\rho_0 = 0$, it will be stable if $b - d + c < 0$. For the nontrivial fixed point:

$$\frac{\mathrm{d}}{\mathrm{d}\rho} f(\rho)\Big|_{\rho_0} = -(b - d + c), \tag{3.67}$$

which means one of the fixed points will be stable and the other unstable. We just did a linear stability analysis of the equilibrium point, not considering spatial effects yet.

Now, let's look at the behavior of a space-inhomogeneous perturbation If $\rho(\mathbf{x}, t) = \rho_0 + \varepsilon\psi(\mathbf{x}, t)$, $\varepsilon \ll 1$, we have:

$$\begin{aligned}\varepsilon\frac{\partial}{\partial t}\psi(\mathbf{x},t) =& \varepsilon D\nabla^2\psi(\mathbf{x},t) + (b-d+c)(\rho_0+\varepsilon\psi(\mathbf{x},t)) + \\ & - c\left(\rho_0+\varepsilon\psi(\mathbf{x},t)\right)\int \mathrm{d}\mathbf{x}' G\left(\left|\mathbf{x}-\mathbf{x}'\right|\right)\left(\rho_0+\varepsilon\psi\left(\mathbf{x}',t\right)\right). \end{aligned} \tag{3.68}$$

Keeping only terms up to first order in ε, and remembering the equilibrium condition $(b-d+c)\,\rho_0 - c\pi R^2\rho_0^2 = 0$:

$$\begin{aligned}\frac{\partial}{\partial t}\psi(\mathbf{x},t) =& D\nabla^2\psi(\mathbf{x},t) + (b-d+c)\,\psi(\mathbf{x},t) + \\ & - c\pi R^2\rho_0\psi(\mathbf{x},t) - c\rho_0\int \mathrm{d}\mathbf{x}' G\left(\left|\mathbf{x}-\mathbf{x}'\right|\right)\psi\left(\mathbf{x}',t\right). \end{aligned} \tag{3.69}$$

A simple way to analyze the evolution of the inhomogeneous perturbation is to look at a Fourier mode perturbation, also assuming exponential growth [40]:

$$\psi(\mathbf{x},t) = \exp(\lambda(\boldsymbol{\omega})t + i\,\boldsymbol{\omega}\cdot\mathbf{x}), \tag{3.70}$$

so that we can write:

$$\begin{aligned}\lambda(\boldsymbol{\omega})\,\psi(\mathbf{x},t) =& - D\omega^2\psi(\mathbf{x},t) + \left(b-d+c-c\pi R^2\rho_0\right)\psi(\mathbf{x},t) + \\ & - c\rho_0 e^{\lambda(\boldsymbol{\omega})t}\int \mathrm{d}\mathbf{x}' G\left(\left|\mathbf{x}-\mathbf{x}'\right|\right)\exp\left(i\,\boldsymbol{\omega}\cdot\mathbf{x}'\right). \end{aligned} \tag{3.71}$$

For the kernel constant inside a radius R, the last term, given by the kernel's Fourier transform can be calculated in terms of a Bessel function of the first kind:

$$\int \mathrm{d}\mathbf{x}' G\left(\left|\mathbf{x}-\mathbf{x}'\right|\right)\exp\left(i\,\boldsymbol{\omega}\cdot\mathbf{x}'\right) = 2\pi R\frac{J_1(R\,|\boldsymbol{\omega}|)}{|\boldsymbol{\omega}|}\exp(i\,\boldsymbol{\omega}\cdot\mathbf{x}). \tag{3.72}$$

Substituting equation (3.72) in (3.71), we have:

$$\lambda(\boldsymbol{\omega}) = -D\omega^2 + \left(b-d+c-c\pi R^2\rho_0\right) - 2\pi R c\rho_0\frac{J_1(R\,|\boldsymbol{\omega}|)}{|\boldsymbol{\omega}|}. \tag{3.73}$$

If $\lambda(\boldsymbol{\omega}) > 0$ for some $\boldsymbol{\omega}$, then the associated Fourier mode of a spatially

inhomogeneous perturbation will grow and eventually lead to the formation of patterns with the corresponding wavelength. For the equilibrium point $\rho_0 = 0$, we have:

$$\lambda(\boldsymbol{\omega}) = -D\omega^2 + b - d + c, \tag{3.74}$$

so that, if $b - d + c > 0$, we will have $\lambda(\mathbf{0}) > 0$. Note that $\boldsymbol{\omega} = \mathbf{0}$ corresponds to an infinite wavelength, covering the whole domain of the system so that we do not have pattern formation. Instead, the system diverges from the $\rho_0 = 0$ fixed point everywhere. This behavior was expected from the previous analysis, where we saw that the trivial fixed point was unstable to homogeneous perturbations if $b - d + c > 0$.

Now, for the other fixed point, we can have more interesting behaviors as

$$\lambda(\boldsymbol{\omega}) = -D\omega^2 - 2\,(b - d + c)\,\frac{J_1(R\,|\boldsymbol{\omega}|)}{R\,|\boldsymbol{\omega}|}. \tag{3.75}$$

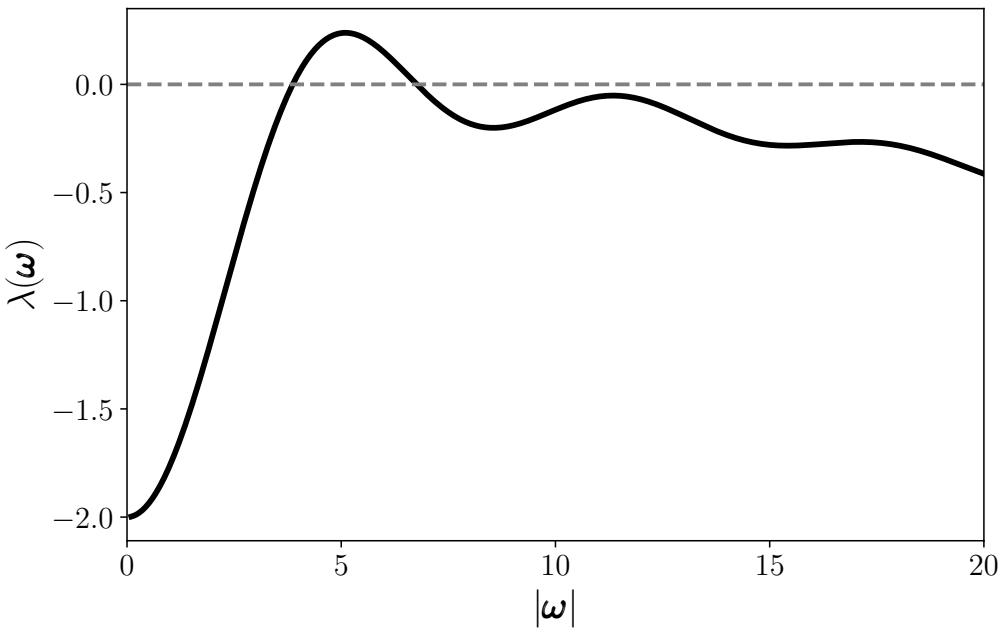

Figure 3.1: Perturbation growth rate $\lambda(\boldsymbol{\omega})$, according to equation (3.75), associated with the birth-death model with non-local competition

The Bessel function $J_1(R\,|\boldsymbol{\omega}|)$ has an oscillating behavior, so that $\lambda(\boldsymbol{\omega})$ might be positive for an intermediate wavenumber. For instance, in Figure 3.1, we can see

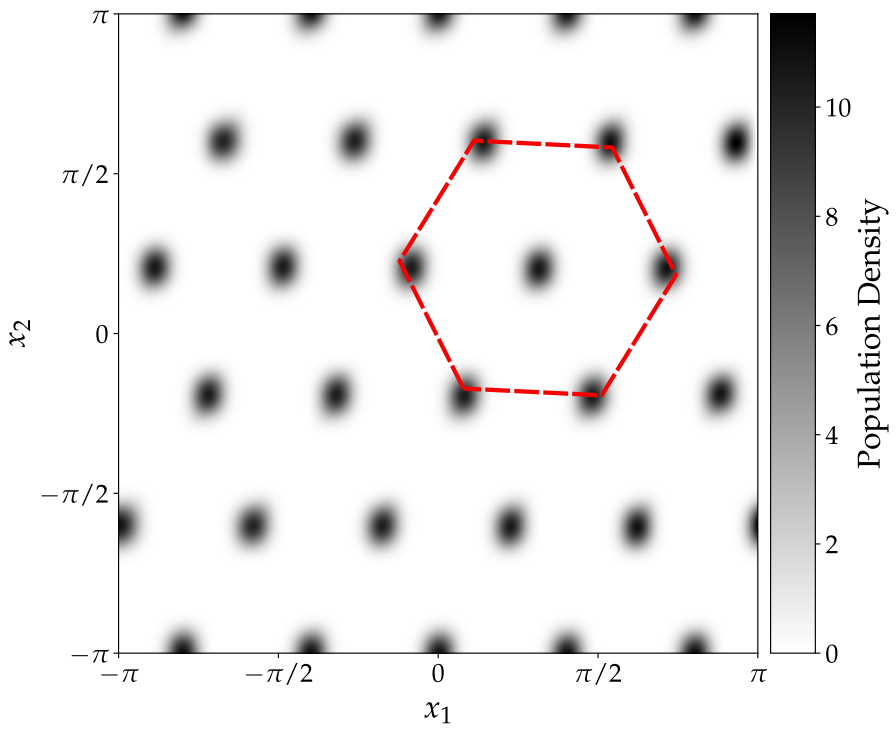

Figure 3.2: Formed pattern associated with perturbation exponents in Figure 3.1.

how the perturbation growth rate $\lambda(\boldsymbol{\omega})$ varies with the wavenumber vector. In this case, choosing $b - d = 1,\ c = 1,\ D = 10^{-3}$ and $R = 1$, we can see $\lambda(\boldsymbol{\omega}) > 0$ for some values of $|\boldsymbol{\omega}|$, leading to the formation of the pattern observed in Figure 3.2. Notice the hexagonal symmetry of the pattern. It appears slightly tilted because the system is isotropic and there is no preferential orientation for the pattern. This orientation depends only on the system's initial condition.

3.5.2 Incompressible Advection

Now, we will look into the effect of advection in the stability of equilibrium points of advection-reaction-diffusion equations such as the spatial birth-death model with non-local competition in equation (3.55).

Consider a general advection-reaction-diffusion equation for a scalar field $u(\mathbf{x}, t)$ in a n-dimensional space, with an incompressible advective flow $\mathbf{v}(\mathbf{x}, t)$ and constant diffusion D, and a local reaction field $f(u(\mathbf{x}, t))$:

$$\frac{\partial}{\partial t}u(\mathbf{x}, t) = -\mathbf{v}(\mathbf{x}, t) \cdot \nabla u(\mathbf{x}, t) + D\nabla^2 u(\mathbf{x}, t) + f(u(\mathbf{x}, t)) \,. \tag{3.76}$$

At first, it may seem like we could try to analyze equation (3.76) in the same way we did for the non-local competition in the last section. First, we obtain the equation for a small perturbation $\varepsilon\psi(\mathbf{x},t)$ $(\varepsilon \ll 1)$ around a spatially uniform equilibrium solution $u(\mathbf{x},t) = u_0$ of equation (3.76):

$$\frac{\partial}{\partial t}\psi(\mathbf{x},t) = -\mathbf{v}(\mathbf{x},t)\cdot\nabla\psi(\mathbf{x},t) + D\nabla^2\psi(\mathbf{x},t) + f'(u_0)\,\psi(\mathbf{x},t)\,. \tag{3.77}$$

However, when advection is involved, this analysis becomes much more complicated. Substituting the perturbation $\psi(\mathbf{x},t)$ for a Fourier mode with exponential growth in equation (3.77) is not enough, because the velocity field $\mathbf{v}$ still depends on the position $\mathbf{x}$. One could try taking the Fourier transform of equation (3.77), but the advection term would become a convolution between the Fourier transforms of the fields $\mathbf{v}$ and ψ, which is also very complex to analyze.

One alternative is to do the linear stability analysis through the energy method [50]. We define the so-called energy E of perturbation ψ as:

$$E = \frac{1}{2}\left\|\psi\right\|^2 = \frac{1}{2}\int_0^L \mathrm{d}x^n\,\psi^2. \tag{3.78}$$

We now look at the time variation of E. If it increases with time, u_0 is an unstable equilibrium, and if E decreases with time, u_0 is stable. The time derivative of E is

$$\begin{aligned}\frac{\mathrm{d}E}{\mathrm{d}t} &= \frac{1}{2}\int \mathrm{d}x^n\,\frac{\partial\psi^2}{\partial t} = \int \mathrm{d}x^n\,\psi\frac{\partial\psi}{\partial t}\\ &= \int \mathrm{d}x^n\,\psi\left(-\mathbf{v}\cdot\nabla\psi + D\nabla^2\psi + f'(u_0)\,\psi\right).\end{aligned} \tag{3.79}$$

Now we need to determine the contribution of each term on the rightmost integral to the time derivative of the energy. This is usually hard, and one needs to recur to different integral inequalities to prove either the stability or the instability of an equilibrium state. Our focus here is on the effect of the advection term. In the case of a domain with periodic boundary conditions, we can integrate by parts to obtain:

$$\int \mathrm{d}x^n\,\psi\,\mathbf{v}\cdot\nabla\psi = -\int \mathrm{d}x^n\psi\nabla\cdot(\psi\,\mathbf{v}) = -\int \mathrm{d}x^n\left(\psi^2\nabla\cdot\mathbf{v} + \psi\,\mathbf{v}\cdot\nabla\psi\right), \tag{3.80}$$

where the first term of the integration by parts is null due to the periodic boundary conditions of the system. Remembering that $\nabla \cdot \mathbf{v} = 0$, the first term in parentheses on the RHS of equation (3.80) is canceled. We are left with an equality of two terms of the same magnitude and opposite sign so that the term must be null:

$$\int \mathrm{d}x^n \, \psi \, \mathbf{v} \cdot \nabla \psi - \int \mathrm{d}x^n \psi \, \mathbf{v} \cdot \nabla \psi = 0. \tag{3.81}$$

Equation (3.81) implies that the advection term does not affect the time evolution of the energy of the perturbation in the linear stability analysis. We would obtain the same result for a system closed by walls so that $\mathbf{v} = 0$ in the boundaries of the domain. The velocity field will simply advect the perturbation field, conserving its total value summed over the domain, without making the perturbation stronger or weaker overall. Notice that this also means that the perturbation will locally change as it is advected by the flow, and this advection could interact with other pattern formation mechanisms and lead to novel behavior.

Also, remember that the lack of effect of the flow on the stability of the system depends on the flow being incompressible and the system being closed – either by walls or by periodic boundary conditions. For different boundary conditions, we cannot guarantee that the flow entering or leaving the system will not disrupt the stability of an equilibrium point. Also, compressible flows can produce spatial inhomogeneities on their own [5], independent of demographic mechanisms of pattern formation.

We will briefly analyze the effect of a simple shear flow on the spot pattern observed in Figure 3.2, to build some intuition about the effect of external flows. Consider a horizontal shear flow $\mathbf{v}(\mathbf{x}, t) = (\gamma \sin(x_2), 0)^{\mathrm{T}}$. The horizontal shear along the vertical profile will be given by

$$\frac{\partial v_1}{\partial x_2} = \gamma \cos(x_2), \tag{3.82}$$

which peaks in magnitude at $x \in \{-\pi, 0, \pi\}$, and is null at $x_2 \in \{-\pi/2, \pi/2\}$. Setting $\gamma = 1$, we observe the formation of stripes in regions of stronger shear and stretched spots in regions of low shear (Figure 3.3). Increasing the velocity (and shear) of the flow, we see in Figure 3.4 that we no longer have the formation of spots at the regions of low shear for $\gamma = 10$. The shear varies too quickly within the width of a spot, being large enough to stretch spots until connecting them,

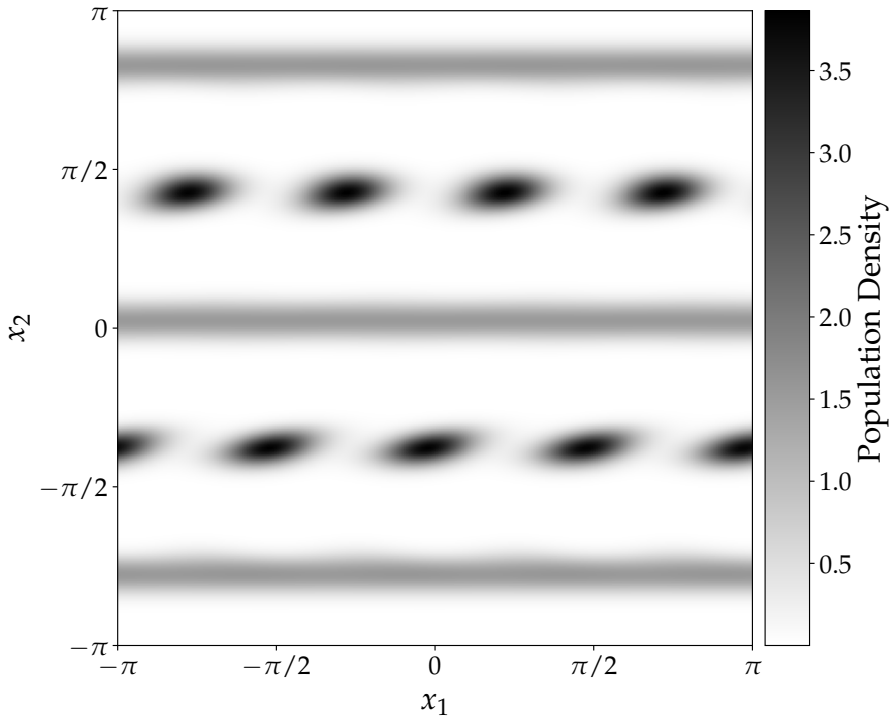

Figure 3.3: Formed pattern due to non-local competition, under a horizontal flow with sinusoidal profile: $v_1 = \gamma \sin(x_2)$, $\gamma = 1$.

forming stripes.

The patterns presented here and in the last subsection were obtained through numerical simulations using a pseudospectral algorithm [19] for implementation diffusion and local and non-local reaction terms, together with a semi-lagrangian scheme [48] for the implementation of advection.

3.6 Numerical Simulations: The Gillespie Algorithm

As we saw above, most problems involving master equations are not possible to solve analytically. For analytical methods, we resorted to mean-field approximations, but these ignore all stochastic fluctuations, which may be of great significance for certain phenomena. It is possible to derive approximations for higher moments of the process, which provide some insight into the effect of stochasticity, but these approximations are especially hard to derive for spatial processes due to the treatment of spatial correlations, even more so for non-local interactions. In this work, we rely on numerical simulations to explore the stochastic nature of complex master equations.

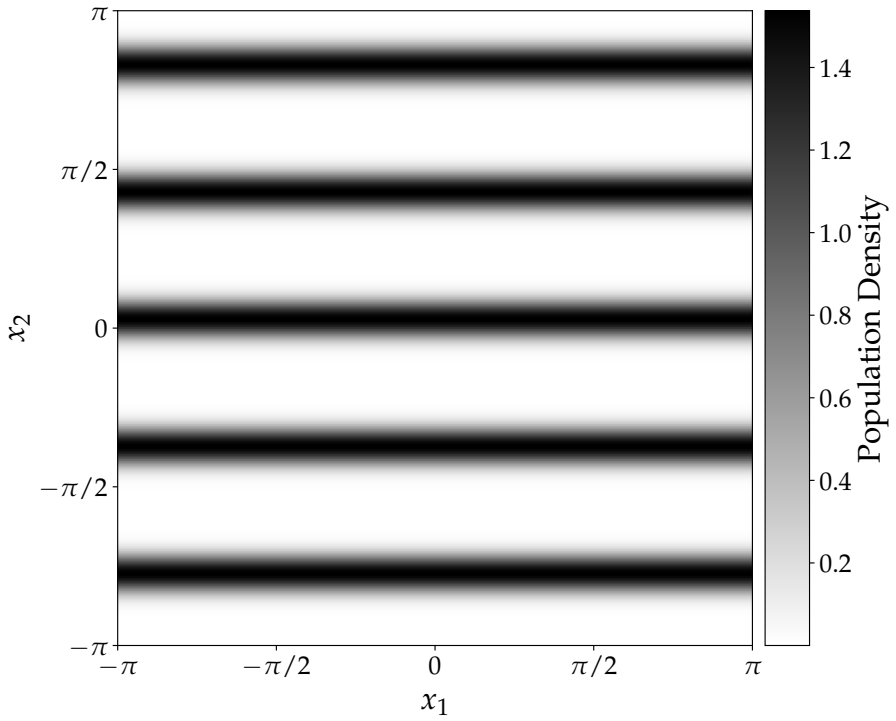

Figure 3.4: Formed pattern due to non-local competition, under a horizontal flow with sinusoidal profile: $v_1 = \gamma \sin(x_2)$, $\gamma = 10$.

In this section, we are going to present the Stochastic Simulation Algorithm (SSA), better known as the Gillespie Algorithm [23], a very efficient algorithm for the exact simulation of stochastic processes described by master equations. In what follows, we are going to derive here the algorithm as it was done in the original paper by Gillespie.

Let $\mathrm{P}(n, t, m, t+\tau)\,\Delta\tau$ be the probability that, given the system is in state n at time t, the next reaction will be a transition between states $n \to m$, happening at a time in the interval $(t+\tau, t+\tau+\Delta\tau)$. Remember that we defined the probability of a transition $n \to m$ happening in a time interval Δt as $\mathrm{T}(m, n)\,\Delta t$.

Now, if we define $\mathrm{P}_0(n, t, t+\tau)$ to be the probability that no reaction happens in the interval $(t, t+\tau)$, given the system is at state n at time t, we must have that

$$\mathrm{P}(n, t, m, t+\tau) = \mathrm{P}_0(n, t, t+\tau)\,\mathrm{T}(m, n)\,\Delta\tau. \tag{3.83}$$

Also, we can derive an expression for P_0, by noticing that

$$\mathrm{P}_0(n,t,t+\tau+\Delta\tau) = \mathrm{P}_0(n,t,t+\tau)\left[1-\sum_m \mathrm{T}(m,n)\,\Delta\tau\right]. \tag{3.84}$$

Manipulating this expression and taking the limit $\Delta\tau \to 0$, we obtain a differential equation

$$\frac{\mathrm{d}}{\mathrm{d}\tau}\mathrm{P}_0(n,t,t+\tau) = -\sum_m \mathrm{T}(m,n)\,\mathrm{P}_0(n,t,t+\tau)\,, \tag{3.85}$$

with solution

$$\mathrm{P}_0(n,t,t+\tau) = \left(\sum_m \mathrm{T}(m,n)\right)\exp\left[-\sum_m \mathrm{T}(m,n)\,\tau\right], \tag{3.86}$$

if we impose the normalization of the probability distribution. We concluded that the interval between reactions has an exponential distribution, with its coefficient depending on the sum of all the transition rates that take the system away from its current state n.

More so, substituting the last result in equation (3.83), we have

$$\mathrm{P}(n,t,m,t+\tau) = \mathrm{T}(m,n)\left(\sum_{m'}\mathrm{T}(m',n)\right)\exp\left[-\sum_{m'}\mathrm{T}(m',n)\,(\tau-t)\right]. \tag{3.87}$$

Therefore, given a system at state n at time t, and given the next reaction is happening at time $t+\tau$, the relative probability of reaction $n \to m$ being this next reaction, to happen at time $t+\tau$ is

$$\frac{\mathrm{T}(m,n)}{\sum_{m'}\mathrm{T}(m',n)}. \tag{3.88}$$

With these results, we can implement the stochastic dynamics corresponding to a given master equation, by accordingly sampling at each time the next reaction to happen, and how long it will take until it happens. A pseudocode implementing the SSA is presented in Algorithm 1.

Algorithm 1 The Stochastic Simulation Algorithm

1: $t \leftarrow t_0$ ▷ Set initial time and state
2: $n \leftarrow n_0$
3: **while** $t \leq t_{\text{end}}$ **do**
4: $\quad \mathrm{T}_{\text{sum}} \leftarrow \sum_m \mathrm{T}(m,n)$
5: $\quad r_1 \sim \mathcal{U}(0,1)$
6: $\quad \tau \leftarrow -\ln(r_1)/\mathrm{T}_{\text{sum}}$ ▷ Sample exp. distribution with mean T_{sum}
7: $\quad t \leftarrow t + \tau$
8: $\quad r_2 \sim \mathcal{U}(0,1)$
9: $\quad m \leftarrow \text{argmin}\left(\mathrm{T}_{\text{sum}}^{-1} \sum_{k=m_1}^{p} \mathrm{T}(k,n) > r_2\,,\ p \in \{m_i, i = 1,2,\ldots,N\} \right)$
10: $\quad n \leftarrow m$ ▷ Sample reaction with relative transition probabilities
11: **end while**

The SSA is quite straightforward to implement after deriving the results presented above, maybe except for lines 6 and 9. On line 6, we are sampling the time interval until the next reaction, according to equation (3.86). To do this sampling, we need to generate a random variable with an exponential distribution, which is done using the change of variable from a uniform to an exponential distribution (Appendix A.2). On line 9, we are sampling the next reaction to happen according to the relative probabilities (3.88). We order the states m_i so that the difference between consecutive terms inside the argmin function is exactly the relative probability of transition. The argmin function samples a reaction according to these relative probabilities, based on the sampled value of the random variable r_2.

For the work to be presented in the following, however, we still have to consider that individuals move through space while reacting stochastically. This would not be a problem if it was not for the non-local interactions such as the competition presented in the last section. As the non-local competition depends on the distance between individuals, the reaction rates vary over time and need to be constantly updated. To handle this, we can use the methods presented in reference [54], as our problem of non-local interactions can easily be translated into a time-varying network where nodes correspond to individuals, and we define edges based on the distance between individuals.

In summary, the algorithm, presented as the Temporal Gillespie Algorithm in [54], consists on defining a timescale $\Lambda\Delta t$ associated with changes in the network, in our case because of the movement of particles due to advection and Brownian motion. Then, when sampling the time until the next reaction τ, if it is larger than

$\Lambda\Delta t$, we update the network (particles' positions) as many times as needed, until reaching the reaction time. The time interval τ will never be a perfect multiple of $\Lambda\Delta t$, so once a reaction happens, there will still be some time left until the end of the current interval between network update, a fraction $\xi\Lambda\Delta t$, $\xi < 1$. A simple solution here would be to update the network by the left time interval $\xi\Lambda\Delta t$, which is also the more precise choice, and is what we implement in this work.

Chapter 4

Demographic Public Good Games Under Flows

In this chapter, we are going to analyze the problem of two microbial strains interacting in space under environmental flows. We consider that one strain produces a public good (PG) and shares it with the rest of the population, at a cost to its reproduction rate. The other strain does not produce such PG, but it benefits from the production of the first strain. We are going to consider a system in which public goods lead to an increased reproduction rate of its consumers. In this sense, we can refer to the PG producers as cooperators and to non-producers as defectors [51].

In the context of microbial ecology, public goods can consist of any type of molecule that is produced by microbes and (at least partially) released in the environment [51, 58]. In this work, we consider a scenario of consumable PGs, as considered in [4], different from other works in the literature that focus on non-consumable ones [8, 12, 53].

Siderophores are one example of public good that can be consumable [31]. These are molecules produced by microbes when iron is scarce in the environment in an absorbable form [14, 26, 31]. Siderophores bind to iron and make it soluble, allowing microbes to fulfill their iron needs. Siderophores may be consumed once absorbed together with iron. Conversely, examples of non-consumable public goods are enzymes, which are used to catalyze reactions. Enzymes are very stable and thus can be reused several times [13]. Siderophores can also be recycled in some cases [31], which would make them non-consumable PGs.

In this work, we are interested in studying how the dynamical spatial structure generated by environmental flows can affect the outcome of the competition between a PG producer and a non-producer strain. More specifically, we want to understand if the environmental flow can be an external mechanism that works to avoid the collapse of the two-strain community due to a tragedy of the commons.

First introduced by Hardin in 1968 [24] in a sociological context and quickly popularized into the realms of eco-evolutionary theory [43, 47, 51, 58], the tragedy of the commons concerns a scenario where individuals of a community, moved by self-interest, over-exploit a public resource until they exhaust this resource completely. This is the reason why pure cooperative behaviors are not considered evolutionarily stable, because non-cooperating mutants can exploit cooperators.

By pure cooperative behaviors, we mean cooperative behaviors without any other associated behavior that may make cooperation evolutionarily stable. Several mechanisms can evolve in ecological communities that avoid a tragedy of the commons [22, 25, 43, 57]. However, our focus, in this work, is not in these biological mechanisms. Instead, we wish to understand if evolutionarily stable cooperation can be achieved through external, abiotic mechanisms, which remain underappreciated [27, 59]. In other words, we wish to understand if there are physical environments that are more prone to the establishment of cooperative species. Aqueous media with complex flows are interesting physical environments to investigate, especially considering the evolution of early life in water [32].

In section 4.1, we will derive the master equation for the microbial public-good game as described above, as well as its corresponding mean-field approximation. In section 4.2, we look at the linear stability of equilibrium points of the mean-field approximation in the absence of environmental flows, concerning both spatially homogeneous and inhomogeneous perturbations. For spatially inhomogeneous perturbations, we show the possibility of pattern formation, which can enhance the survival of producers and even allow for the coexistence of producers and non-producers.

In section 4.3, we present numerical simulations of the stochastic system in the presence of environmental flows. We show that external flows can allow the coexistence of producers and non-producers, and explain the intuition behind this result.

4.1 The Spatial PG Game in the Master Equation

In our model, both producer and non-producer strains will follow dynamics similar to the logistic growth described in chapter 3. However, because we are now considering two different strains and hence two subpopulations, a focal individual from one strain will not only compete with their conspecifics as in the logistic model but also with heterospecifics.

To model our two-strain system, we will not describe public good molecules being produced and flowing through space explicitly. Instead, we are going to model this interaction through a spatially non-local implementation of the public good game, commonly used in economic theory [21], as observed in Figure 4.1.

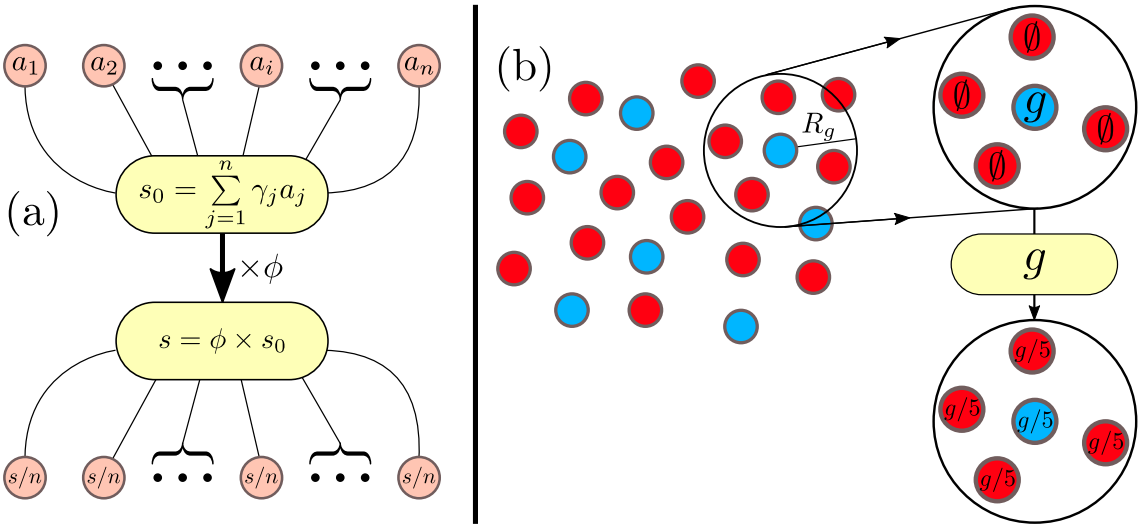

Figure 4.1: **(a)** Standard public goods game, often used in economic theory. **(b)** Implementation of the spatial public goods game in a population of cooperators (blue) and defectors (red).

The public good game consists of n agents, each endowed with an amount a_i of resources at first. Each agent can contribute a proportion γ_i of their resources to a shared pool. The resources in the shared pool can be multiplied by a factor ϕ to increase its value. The final amount of resources, after multiplied, is equally shared among players (Figure 4.1, panel **(a)**). Players also get to keep the resources they did not put in the shared pool, which can describe some level of privatization of the public good. For our microbial public good game, every producer will share all of its production, and the non-producers will have nothing to share. This assumption facilitates the implementation of a spatial PG game because it means we need to keep track only of the neighborhoods of cooperators to fully describe the dynamics of the game.

To implement the public good game in a spatially structured population, we set a PG game radius R_g, so that every individual plays the game with all of its neighbors within a distance smaller than R_g. As non-producers have zero contribution to the public-good pool, the game implementation reduces to evenly splitting the benefit of PG production of a producer individual among all of their neighbors, as drawn in Figure 4.1, panel **(b)**. Also, producers will have

a smaller growth rate than non-producers, due to the cost of PG production. Most importantly, we have the PG now being produced by cooperators and consumed by both strains. We will now get into the mathematical details of the implementation of this spatial PG game into our model.

We will consider a system of two strains moving through space undergoing birth, death and competition reactions, and playing the PG game described above. Except for the PG game, the other reactions have already been mathematically described in Chapter 3. Therefore, we only discuss here the implementation of the spatial PG game in the master equation. To this end, we will write a master equation where the only reaction is the spatial PG game.

We can include the spatial PG game in the master equation for the system as a non-local interaction term, in the same way we did for the non-local competition. If **A** is the vector for the number of cooperators, and **B** for the number of defectors, we can write:

$$\begin{aligned}\frac{\partial}{\partial t}\mathrm{P}(\mathbf{A},\mathbf{B},t) = &\sum_i \left(E_{A,i}^{-1}-1\right)\left[A_i \sum_j G_{i,j} f_j(\mathbf{A},\mathbf{B})\,\mathrm{P}(\mathbf{A},\mathbf{B},t)\right] + \\ &+\sum_i \left(E_{B,i}^{-1}-1\right)\left[B_i \sum_j G_{i,j} f_j(\mathbf{A},\mathbf{B})\,\mathrm{P}(\mathbf{A},\mathbf{B},t)\right],\end{aligned} \tag{4.1}$$

The master equation (4.1) is defined over a discrete lattice with sites indicated by subindices i or j. $E_{A,i}$ and $E_{B,i}$ are both state shifting operators (equation (3.3)), acting respectively on particles of species A and B, at site i. $G_{i,j} f_j(\mathbf{A},\mathbf{B})$ is the reproductive benefit for an individual at site i, due to public goods produced by all cooperators at a site j. We consider the kernel G to depend only on the distance between sites, so it must be symmetric, $G_{i,j} = G_{j,i}$. All the production of a cooperator is shared among the cooperator and its neighbors, according to the PG distribution kernel $G_{i,j}$. To implement this specific choice of PG sharing, we mathematically define the PG benefit function $f_j(\mathbf{A},\mathbf{B})$ to be

$$f_j(\mathbf{A},\mathbf{B}) = \frac{g A_j}{\sum_k G_{j,k}\,(A_k + B_k)}. \tag{4.2}$$

In equation (4.2), the numerator gA_j means that the reproductive benefit for an individual at site i is proportional to the number of producers in the neighbor

site j. g is the proportionality factor, with units of reproduction rate per number of producer individuals. The denominator enforces the sharing of the reproductive benefits due to PG production at site j among all neighbor sites k. This sharing is proportional to the value of the kernel $G_{j,k}$ at each of these neighbor sites k. This form of f_j can be understood as a consequence of a model with explicit PG molecules, considering the PG to have relatively fast dynamics. This consideration of fast dynamics is a common technique for simplifying models [3, 9, 11], as shown in Appendix B,.

The total reproductive benefit provided by producers at a site j can be calculated by summing the benefit that individuals at site j provide to every individual in the community, summing over all sites i with the respective weights through the kernel $G_{i,j}$, and dividing by the number of individuals at site j:

$$\sum_i (A_i + B_i)\, G_{i,j} f_j(\mathbf{A}, \mathbf{B})\,. \tag{4.3}$$

Substituting the PG benefit function (4.2) in (4.4), we can write:

$$\sum_i (A_i + B_i)\, G_{i,j} f_j(\mathbf{A}, \mathbf{B}) = g A_j \frac{\sum_i G_{i,j}\,(A_i + B_i)}{\sum_k G_{j,k}\,(A_k + B_k)} = g A_j, \tag{4.4}$$

where the numerator and denominator balanced each other out because we are considering symmetric kernels, $G_{j,i} = G_{i,j}$. Dividing equation (4.4) by the number of cooperators at site j, A_j, we conclude that each producer provides a total reproductive benefit at a constant rate g. This constant rate of reproductive benefit can be understood as a consequence of the constant rates of production and consumption of public goods, as seen in Appendix B. The reproductive benefit g is shared with other individuals according to the distribution set by the kernel G. If there are many individuals surrounding a producer, the benefit share of each neighbor will be very small. If the PG distribution kernel has a finite range and a producer is alone inside this range, it will keep the totality of the benefit to itself.

Taking the mean-field approximation of master equation (4.1) for both **A** and **B**, we obtain:

$$\frac{\mathrm{d}}{\mathrm{d}t}A_i(t) = A_i(t)\sum_j G_{i,j}\frac{gA_j(t)}{\sum_k G_{j,k}\left(A_k + B_k\right)}; \tag{4.5}$$

$$\frac{\mathrm{d}}{\mathrm{d}t}B_i(t) = B_i(t)\sum_j G_{i,j}\frac{gA_j(t)}{\sum_k G_{j,k}\left(A_k + B_k\right)}. \tag{4.6}$$

Now, taking the limit of continuous space, we have:

$$\frac{\mathrm{d}}{\mathrm{d}t}A(\mathbf{x},t) = gA(\mathbf{x},t)\int \mathrm{d}\mathbf{x}'\left[\frac{G(\mathbf{x}-\mathbf{x}')\,A(\mathbf{x}',t)}{\int \mathrm{d}\mathbf{x}''\,G\left(\mathbf{x}'-\mathbf{x}''\right)\left[A\left(\mathbf{x}'',t\right)+B\left(\mathbf{x}'',t\right)\right]}\right]; \tag{4.7}$$

$$\frac{\mathrm{d}}{\mathrm{d}t}B(\mathbf{x},t) = gB(\mathbf{x},t)\int \mathrm{d}\mathbf{x}'\left[\frac{G(\mathbf{x}-\mathbf{x}')\,A(\mathbf{x}',t)}{\int \mathrm{d}\mathbf{x}''\,G\left(\mathbf{x}'-\mathbf{x}''\right)\left[A\left(\mathbf{x}'',t\right)+B\left(\mathbf{x}'',t\right)\right]}\right]. \tag{4.8}$$

4.1.1 The Full Master Equation for the Two-Strain System

We can then define the full two-strain system completely through the reactions for each site i of a 2D lattice:

Birth (with PG benefit):

$$A_i \xrightarrow{b_i - k} A_i + A_i, \quad B_i \xrightarrow{b_i} B_i + B_i, \tag{4.9}$$
$$b_i = b + \sum_j G^g_{i,j}\frac{gA_j}{\sum_k G^g_{j,k}\left(A_k + B_k\right)};$$

Death (itrinsic and due to competition):

$$A_i \xrightarrow{d_i} \emptyset, \quad B_i \xrightarrow{d_i} \emptyset, \tag{4.10}$$
$$d_i = d + c\sum_j G^c_{i,j}\left(A_j + B_j\right),$$

where we distinguish between the kernels associated with the non-local com-

petition and the PG game by a superindex – G^c is the kernel for the non-local competition and G^g is the one for the spatial PG game. Besides the demographic reactions (4.9) and (4.10), we also have movement via Brownian motion and advection by an external velocity field.

We will not write the master equation associated with these reactions because it is quite long and will not be used. Still, it is straightforward to derive the mean-field approximation according to equation (3.32). Also, we have already derived mean-field expressions for demographic reactions (birth, death and competition) and movement in Chapter 3, and just derived the term for the PG game in equations (4.7) and (4.8).

Adding together all terms associated with demography and movement, we can write the mean-field approximation for the two-strain system in the limit of continuous space:

$$\begin{aligned}\frac{\partial}{\partial t}A(\mathbf{x},t) = {} & D\nabla^2 A(\mathbf{x},t) - \mathbf{v}(\mathbf{x},t)\cdot\nabla A(\mathbf{x},t) + (b-k-d+c)\,A(\mathbf{x},t) + \\ & + gA(\mathbf{x},t)\int \mathrm{d}\mathbf{x}'\left[\frac{G_g(\mathbf{x}-\mathbf{x}')\,A(\mathbf{x}',t)}{\int \mathrm{d}\mathbf{x}''\,G_g(\mathbf{x}'-\mathbf{x}'')\left[A(\mathbf{x}'',t)+B(\mathbf{x}'',t)\right]}\right] + \\ & - cA(\mathbf{x},t)\int \mathrm{d}\mathbf{x}'\,G_c(\mathbf{x}-\mathbf{x}')\left[A(\mathbf{x}',t)+B(\mathbf{x}',t)\right]; \end{aligned} \tag{4.11}$$

$$\begin{aligned}\frac{\partial}{\partial t}B(\mathbf{x},t) = {} & D\nabla^2 B(\mathbf{x},t) - \mathbf{v}(\mathbf{x},t)\cdot\nabla A(\mathbf{x},t) + (b-d+c)\,B(\mathbf{x},t) + \\ & + gB(\mathbf{x},t)\int \mathrm{d}\mathbf{x}'\left[\frac{G_g(\mathbf{x}-\mathbf{x}')\,A(\mathbf{x}',t)}{\int \mathrm{d}\mathbf{x}''\,G_g(\mathbf{x}'-\mathbf{x}'')\left[A(\mathbf{x}'',t)+B(\mathbf{x}'',t)\right]}\right] + \\ & - cB(\mathbf{x},t)\int \mathrm{d}\mathbf{x}'\,G_c(\mathbf{x}-\mathbf{x}')\left[A(\mathbf{x}',t)+B(\mathbf{x}',t)\right]. \end{aligned} \tag{4.12}$$

As shown before b and d are respectively the intrinsic birth and death rates. c is the competition rate, D is the diffusion rate, and $\mathbf{v}(\mathbf{x},t)$ is the external velocity field, which we will consider to be the point-vortex flow. g is the reproduction benefit due to PG consumption, and k is the PG production cost, which enters the master equation directly decreasing the birth rate of cooperators. G_c and G_g are

the non-local interaction kernels for the competition and the PG game, respectively. These kernels were redefined from the rates in discrete lattices (4.9) and (4.10) as $G^{\alpha}_{i,j} \to G_{\alpha}(\mathbf{x}-\mathbf{x}')$, for $\alpha \in \{c,g\}$. We will consider both kernels to be uniform inside finite ranges:

$$G_{\alpha}(\mathbf{x}) = \begin{cases} 1, & |\mathbf{x}| \leq R_{\alpha}, \\ 0, & \text{else.} \end{cases} \tag{4.13}$$

4.2 Linear Stability Analysis

Here, we are going to look into the equilibrium solutions of equations (4.11) and (4.12) and their stability against spatially homogeneous and inhomogeneous perturbations. We are going to ignore advection for now, as we already saw in section 3.5.2 that incompressible flows do not affect the stability of equilibrium points in domains with periodic boundary conditions.

First, we will derive spatially uniform equilibrium solutions for the system, $A(x,t) = A(t)\,, B(x,t) = B(t)$:

$$\frac{\partial}{\partial t}A(t) = \left(b - d + c - k + g\frac{A(t)}{A(t)+B(t)}\right)A(t) - \pi R_c^2 c A(t)[A(t)+B(t)] \tag{4.14}$$

$$\frac{\partial}{\partial t}B(t) = \left(b - d + c + g\frac{A(t)}{A(t)+B(t)}\right)B(t) - \pi R_c^2 c B(t)[A(t)+B(t)]\,. \tag{4.15}$$

The fixed points of this system are obtained by solving the equations

$$f_A(A,B) = \left(b - d + c - k + g\frac{A}{A+B}\right)A - \pi R_c^2 c A\,(A+B) = 0, \tag{4.16}$$

$$f_B(A,B) = \left(b - d + c + g\frac{A}{A+B}\right)B - \pi R_c^2 c B\,(A+B) = 0. \tag{4.17}$$

The first solution is the trivial one, $(A,B) = (0,0)$. Even though the denominator of the PG term may diverge for the trivial solution, when we take the limit of abundances going to zero, we have:

$$\lim_{A,B\to 0} \frac{A^2}{A+B} = \lim_{A,B\to 0} \frac{AB}{A+B} = 0. \tag{4.18}$$

Alternatively, we can obtain this limit by considering that the public good has a very small degradation rate $\sigma \ll 1$, so that the denominator becomes $A + B + \sigma$, and we can take $A = B = 0$ without divergences, and then we can discard σ.

If A and B are both different from zero, the existence of solutions for equations (4.16) and (4.17) requires that $k = 0$, which is not a realistic parameterization for our system. Thus, the PG dynamics we propose does not have any stationary state in which both strains coexist. Setting either A or B to zero, we obtain other two possible fixed points:

$$(A, B) = (0, K_B), \quad K_B = \frac{b - d + c}{\pi R_c^2 c} \quad \text{or} \tag{4.19}$$

$$(A, B) = (K_A, 0), \quad K_A = \frac{b - d + c + g - k}{\pi R_c^2 c}. \tag{4.20}$$

4.2.1 Stability Under Spatially Uniform Perturbations

Now, let's look at the stability of each solution, which we will calculate through the Jacobian of the system evaluated at each equilibrium point (A_0, B_0):

$$J(A_0, B_0) = \begin{bmatrix} \frac{\partial f_A}{\partial A} & \frac{\partial f_A}{\partial B} \\ \frac{\partial f_B}{\partial A} & \frac{\partial f_B}{\partial B} \end{bmatrix}_{(A_0, B_0)}, \tag{4.21}$$

with

$$\frac{\partial f_A}{\partial A} = b - d + c - k + g\frac{A\,(A+2B)}{(A+B)^2} - \pi R_c^2 c\,(2A+B)\,; \tag{4.22}$$

$$\frac{\partial f_A}{\partial B} = -g\frac{A^2}{(A+B)^2} - \pi R_c^2 c A; \tag{4.23}$$

$$\frac{\partial f_B}{\partial A} = g\frac{B^2}{(A+B)^2} - \pi R_c^2 c B; \tag{4.24}$$

$$\frac{\partial f_B}{\partial B} = b - d + c + g\frac{A^2}{(A+B)^2} - \pi R_c^2 c\,(A+2B)\,. \tag{4.25}$$

For the trivial fixed point, we have

$$J(0,0) = \begin{bmatrix} b-d+c-k & 0 \\ 0 & b-d+c \end{bmatrix}. \tag{4.26}$$

The point $(0,0)$ is stable if both eigenvalues are negative. Because $k > 0$, $b - d + c - k < b - d + c$. Therefore, $(0,0)$ is a stable fixed point if $b + c < d$. Notice that the stability of this fixed point does not depend on the benefit of PG g. This result implies that extinction cannot be avoided by simply producing PGs that provide a higher reproduction benefit for the population because the PG benefits are shared with every other individual in the community. At first, both strains may grow, but once the defector-to-cooperator ratio is large enough, there will not be enough producers to sustain the whole community. Due to the production cost k, cooperators decrease in abundance faster than defectors.

For the fixed point of survival of defectors only, we have eigenvalues $d - b - c$ and $-k$, so this fixed point is stable if $b > d$. Finally, the stability of the survival of cooperators will depend on the presence/absence of defectors. For this fixed point, we have the following pairs of eigenvalues and eigenvectors:

$$k : \left(\frac{-b-c+d-2g+k}{b+c-d+g}, 1\right)^{\mathrm{T}}; \qquad -b-c+d-g+k : (1,0)^{\mathrm{T}}, \tag{4.27}$$

where the eigenvectors are oriented in the space of abundances (A, B). If we have a perturbation that only varies the number of cooperators, this fixed point will

be stable if $b - d + g - k > 0$. However, in the case of a perturbation introducing defectors, its component aligned with the first eigenvector will grow with exponent $k > 0$. So the fixed point of producer survival is unstable to the invasion of defectors.

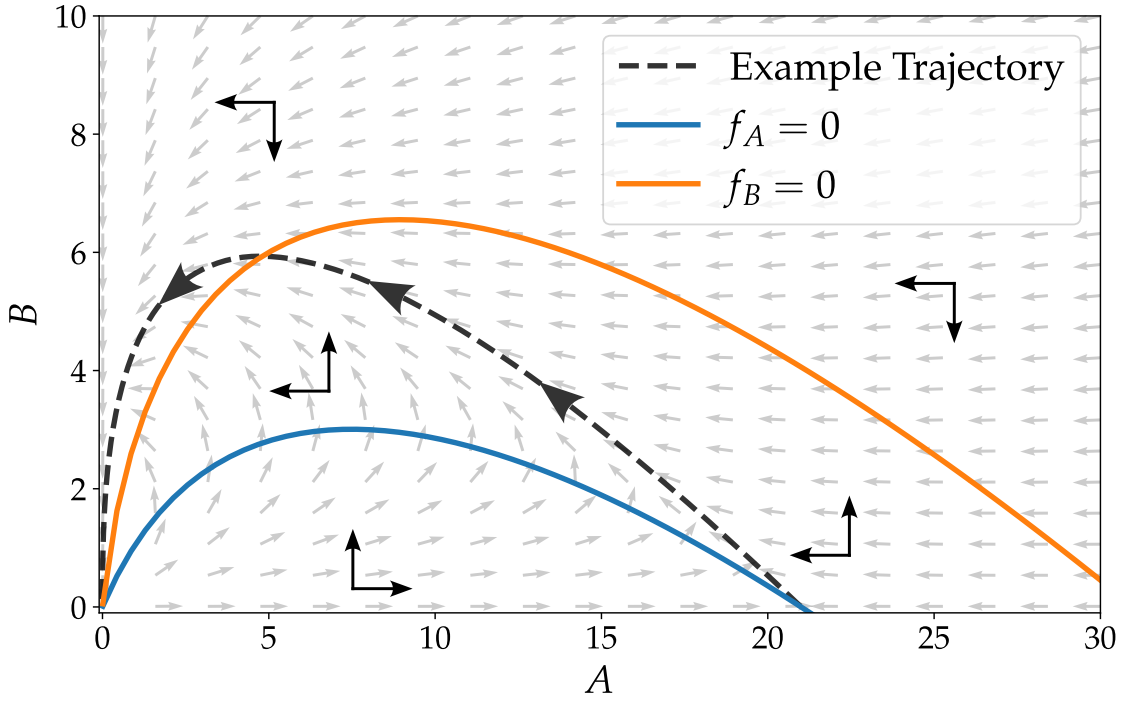

Figure 4.2: Nullclines for the two-strain system. In blue, we have the nullcline for $A = 0$; in orange, the one for $B = 0$. The dashed black line shows a trajectory leaving from close to the fixed point of survival of cooperators, with a small initial fraction of defectors, showing the instability of this fixed point.

In Figure 4.2, we can see the nullclines for the two-strain system for parameters $b = 0.8, d = 1.0, k = 0.3, g = 1.1, c = 0.03$, curves along which the time derivatives of either A or B are null. We plot the field (f_A, f_B) in the background, and pairs of horizontal and vertical arrows indicating the direction of the components of this field, that switch as we cross the nullclines. Crossing the nullcline $f_A = 0$ changes the value of f_A, and the same for f_B. We also plot an example trajectory leaving from $(A, B) = (K_A, 0.01)$, showing the instability of the fixed point $(K_A, 0)$ to the presence of defectors.

4.2.2 Stability Under Spatially Non-Uniform Perturbations

To analyze the effect of spatially inhomogeneous perturbations, we substitute $A(\mathbf{x},t) = A_0 + \varepsilon\phi(\mathbf{x},t)$ and $B(\mathbf{x},t) = B_0 + \varepsilon\psi(\mathbf{x},t)$, $\varepsilon \ll 1$, where (A_0, B_0) is one of the three uniform fixed points of the system. Substituting these perturbations in (4.11) and (4.12) and truncating the resulting equations at first order in ε, we can describe the short-term evolution of perturbations ϕ and ψ.

This is straightforward to do for local terms, and we already showed how to deal with the non-local competition term in subsection 3.5.1. However, we have a problem with the public good game term, as it involves ε terms in the denominator. One possible solution is to multiply the sum in the denominator by the appropriate difference to get a difference of squares and discard the term proportional to ε^2:

$$
\begin{aligned}
&\frac{G_g(\mathbf{x}-\mathbf{x}')\,A(\mathbf{x}',t)}{\int \mathrm{d}\mathbf{x}''\, G_g(\mathbf{x}'-\mathbf{x}'')\left[A(\mathbf{x}'',t)+B(\mathbf{x}'',t)\right]} = \\
&= \frac{G_g(\mathbf{x}-\mathbf{x}')\,(A_0+\varepsilon\phi(\mathbf{x}',t))}{A_0+B_0+\varepsilon\int \mathrm{d}\mathbf{x}''\, G_g(\mathbf{x}'-\mathbf{x}'')\left[\phi(\mathbf{x}'',t)+\psi(\mathbf{x}'',t)\right]} \\
&= \frac{G_g(\mathbf{x}-\mathbf{x}')(A_0+\varepsilon\phi(\mathbf{x}',t))\left[A_0+B_0-\varepsilon\int \mathrm{d}\mathbf{x}''\, G_g(\mathbf{x}'-\mathbf{x}'')\left[\phi(\mathbf{x}'',t)+\psi(\mathbf{x}'',t)\right]\right]}{(A_0+B_0)^2-\varepsilon^2\left[\int \mathrm{d}\mathbf{x}''\, G_g(\mathbf{x}'-\mathbf{x}'')\left[\phi(\mathbf{x}'',t)+\psi(\mathbf{x}'',t)\right]\right]^2} \\
&\approx \frac{G_g(\mathbf{x}-\mathbf{x}')\,(A_0+\varepsilon\phi(\mathbf{x}',t))}{A_0+B_0} + \\
&-\varepsilon\frac{G_g(\mathbf{x}-\mathbf{x}')\,A_0}{(A_0+B_0)^2}\int \mathrm{d}\mathbf{x}''\, G_g(\mathbf{x}'-\mathbf{x}'')\left[\phi(\mathbf{x}'',t)+\psi(\mathbf{x}'',t)\right], \qquad (4.28)
\end{aligned}
$$

where we already discarded terms of order ε^2. Integrating equation (4.28) over $\mathbf{x}'$, multiplying by $gA(\mathbf{x},t)$, and again discarding terms proportional to ε^2, we obtain the term of the linearized equation for the dynamics of the perturbation corresponding to the PG game:

$$gA(\mathbf{x},t)\int d\mathbf{x}'\left[\frac{G_g(\mathbf{x}-\mathbf{x}')\,A(\mathbf{x}',t)}{\int d\mathbf{x}''\,G_g(\mathbf{x}'-\mathbf{x}'')\left[A(\mathbf{x}'',t)+B(\mathbf{x}'',t)\right]}\right]=$$
$$=\frac{gA_0}{A_0+B_0}\left(A_0+\varepsilon\phi(\mathbf{x},t)\right)+\frac{gA_0}{A_0+B_0}\varepsilon\int d\mathbf{x}'\,G_g(\mathbf{x}-\mathbf{x}')\,\phi(\mathbf{x}',t)+$$
$$-\frac{gA_0^2}{(A_0+B_0)^2}\varepsilon\int d\mathbf{x}'\int d\mathbf{x}''\,G_g(\mathbf{x}-\mathbf{x}')\,G_g(\mathbf{x}'-\mathbf{x}'')\left[\phi(\mathbf{x}'',t)+\psi(\mathbf{x}'',t)\right]. \tag{4.29}$$

The competition term can be analyzed following the same steps described in section 3.5.1, now with both intra- and interstrain competition:

$$cA(\mathbf{x},t)\int d\mathbf{x}'\,G_c(\mathbf{x}-\mathbf{x}')\left[A(\mathbf{x}',t)+B(\mathbf{x}',t)\right]=$$
$$=c\left(A+\varepsilon\phi(\mathbf{x},t)\right)\int d\mathbf{x}'\,G_c(\mathbf{x}-\mathbf{x}')\left[A+B+\varepsilon\left(\phi(\mathbf{x}',t)+\psi(\mathbf{x}',t)\right)\right]=$$
$$=c\left(A+B\right)\left(A+\varepsilon\phi(\mathbf{x},t)\right)+cA\varepsilon\int d\mathbf{x}'\,G_c(\mathbf{x}-\mathbf{x}')\left(\phi(\mathbf{x}',t)+\psi(\mathbf{x}',t)\right). \tag{4.30}$$

We can do the same calculations for the PG and competition terms in equation (4.12) for the time evolution of B.

Consider a single wavenumber component of the spatial perturbation, $\boldsymbol{\omega}$. The equations for the perturbation ϕ and ψ are linear in the perturbations because we are considering a short-term expansion. Therefore, the solution for these perturbations should grow (or decay) exponentially with time, so we can write

$$\phi(\mathbf{x},t)=\exp\left(\lambda_\phi(\omega)\,t+i\boldsymbol{\omega}\cdot\mathbf{x}\right);\ \psi(\mathbf{x},t)=\exp\left(\lambda_\psi(\omega)\,t+i\boldsymbol{\omega}\cdot\mathbf{x}\right). \tag{4.31}$$

The integration of the perturbations with the non-local kernels gives the Bessel functions we have already seen in Chapter 3:

$$\int \mathrm{d}\mathbf{x}' G(\mathbf{x}-\mathbf{x}')\,\phi(\mathbf{x},t) = \exp\left(\lambda_\phi(k)\,t\right) \int_{\mathbf{x}-R_i}^{\mathbf{x}+R_i} \mathrm{d}\mathbf{x}' \exp\left(i\boldsymbol{\omega}\cdot\mathbf{x}'\right)$$
$$= 2\pi R_i \frac{J_1(R_i\,|\boldsymbol{\omega}|)}{|\boldsymbol{\omega}|} \exp\left(\lambda_\phi(\omega)\,t + i\boldsymbol{\omega}\cdot\mathbf{x}\right), \tag{4.32}$$

and the same can be done for ψ. Notice that the double integral in the PG game term will lead to squaring the term multiplying the exponential in equation (4.32).

Now, we take the space-dependent mean-field equations (4.11) and (4.12) and substitute the perturbed equilibrium solutions, $A(\mathbf{x},t) = A_0 + \varepsilon\phi(\mathbf{x},t)$ and $B(\mathbf{x},t) = B_0 + \varepsilon\psi(\mathbf{x},t)$, together with the manipulations (4.29) and (4.30), and the integration of the non-local interaction kernels (4.32). The terms independent of ε will cancel out, as we consider (A_0, B_0) to be an equilibrium point. Collecting terms proportional to ε, we have the equations for the dynamics of the perturbations:

$$\begin{aligned}\lambda_\phi(\omega)\,\phi(\mathbf{x},t) = &- D\omega^2\phi(\mathbf{x},t) + \left[b - d + c - k + g\frac{A_0}{A_0+B_0} - \pi R_c^2 c\,(A_0+B_0)\right]\phi(\mathbf{x},t)\\ &- 2\pi R_c c A_0 \frac{J_1(R_c\,|\boldsymbol{\omega}|)}{|\boldsymbol{\omega}|}\left[\phi(\mathbf{x},t)+\psi(\mathbf{x},t)\right]\\ &+ 2\pi R_g \frac{gA_0}{A_0+B_0}\frac{J_1\left(R_g\,|\boldsymbol{\omega}|\right)}{|\boldsymbol{\omega}|}\phi(\mathbf{x},t)\\ &- 4\pi^2 R_g^2 \frac{gA_0^2}{(A_0+B_0)^2}\frac{J_1\left(R_g\,|\boldsymbol{\omega}|\right)^2}{|\boldsymbol{\omega}|^2}\left[\phi(\mathbf{x},t)+\psi(\mathbf{x},t)\right];\end{aligned} \tag{4.33}$$

$$\begin{aligned}\lambda_\psi(\omega)\,\psi(\mathbf{x},t) = &- D\omega^2\psi(\mathbf{x},t) + \left[b - d + c + g\frac{A_0}{A_0+B_0} - \pi R_c^2 c\,(A_0+B_0)\right]\psi(\mathbf{x},t)\\ &- 2\pi R_c c B_0 \frac{J_1(R_c\,|\boldsymbol{\omega}|)}{\omega R_c}\left[\phi(\mathbf{x},t)+\psi(\mathbf{x},t)\right]\\ &+ 2\pi R_g \frac{gB_0}{A_0+B_0}\frac{J_1\left(R_g\,|\boldsymbol{\omega}|\right)}{|\boldsymbol{\omega}|}\phi(\mathbf{x},t)\\ &- 4\pi^2 R_g^2 \frac{gA_0B_0}{(A_0+B_0)^2}\frac{J_1\left(R_g\,|\boldsymbol{\omega}|\right)^2}{|\boldsymbol{\omega}|^2}\left[\phi(\mathbf{x},t)+\psi(\mathbf{x},t)\right].\end{aligned} \tag{4.34}$$

For the trivial equilibrium $(A_0, B_0) = (0,0)$, both $\lambda_\phi(\omega)$ and $\lambda_\psi(\omega)$ will be negative for any $\boldsymbol{\omega}$, provided that $b - d + c < 0$. Therefore, this equilibrium point is stable also against spatially non-uniform perturbations. However, as we will

discuss next, the two other fixed points (survival of cooperators or survival of defectors) can present pattern formation, given the appropriate choice of parameters for the system. In the survival-of-defectors fixed point, non-uniform population distributions will form only if $b > d$. Otherwise, defectors will go extinct, as expected from the absence of public goods in this fixed point.

Cooperators can grow to form patterns in the absence of defectors if $b - k - d + c + g > 0$. The condition for pattern formation may be derived by calculating the eigenvalues of a perturbation $(\phi(\mathbf{x}, t), \psi(\mathbf{x}, t))^{\mathrm{T}}$, according to equations (4.33) and (4.34). For the survival-of-cooperators fixed point, one of the eigenvalues will be k. The eigenvector associated with the eigenvalue k has a component associated with the growth of defectors, as already discussed in the analysis of uniform perturbations, equation (4.27). We are interested in the other eigenvalue, which for the Fourier-mode perturbation becomes:

$$\lambda(\boldsymbol{\omega}) = -D\omega^2 - \frac{2\pi c R_c J_1(R_c |\boldsymbol{\omega}|)}{|\boldsymbol{\omega}|} + \frac{2\pi g R_g J_1(R_g |\boldsymbol{\omega}|)}{|\boldsymbol{\omega}|} - \frac{4\pi^2 g R_g^2 J_1(R_g |\boldsymbol{\omega}|)^2}{|\boldsymbol{\omega}|^2}. \tag{4.35}$$

In the absence of defectors, cooperators can form patterns if $\lambda(\boldsymbol{\omega}) > 0$. The cooperator density will organize itself in spots, similarly to the case of single-species under logistic growth with non-local competition (Figure 3.2). It is interesting to notice that after cooperators form such a pattern, the population becomes much more robust to the invasion by defectors. This result is in agreement with Uppal and Vural (2018) [53], where they simulate a very similar system and show that pattern formation makes a population of cooperators more resistant to invasions by cheating mutations. As defector mutants invade an isolated aggregate of cooperators, they will exploit cooperators to extinction in that aggregate, but will not manage to spread to other aggregates due to the non-local competition with neighbor aggregates. As a result, these aggregates invaded by defectors lose access to public goods and go extinct. Uppal and Vural (2018) [53] also show that environmental flows with shear can enhance the survival of cooperators by accelerating the splitting of aggregates. Increasing the number of separate groups of cooperators, there are many left groups to outlast the groups that die due to cheating mutations.

4.3 Stable Coexistence in Stochastic Simulations

The analysis conducted in the section 4.2 showed that our model does not allow the coexistence of the two strains, at least in the mean-field approximation. Also, the derivation of the fixed points of the system and their stability will be useful in analyzing the effect of flows, which we will consider through numerical simulations.

Here, we are going to look into how the behavior of the system depends on the public good's production cost k and benefit g, while also varying the velocity of the environmental flow. As explained in section 3.6, we conduct this numerical analysis using the hybrid Gillespie algorithm [54]. This method exactly simulates the master equation for the dynamics defined by demographic reactions (4.9) and (4.10). Between reactions, we also update the positions of particles according to their Brownian motion and the advection by the external flow, which here we model as a point-vortex flow, described in Chapter 2.

As we are interested in a scenario where the public goods are essential for the survival of the community, we parameterize the model setting $b - d < 0$ and $b - d + g - k > 0$. We set both the competition and the PG game to have the same interaction radii, $R_g = R_c$. The values of each parameter we keep fixed are displayed in Table 4.1. Notice that we do not fix the value of the competition rate c. Instead, we fix the carrying capacity of cooperators at the equilibrium point of their survival. That is, we fix

$$K = \frac{b - k - d + c + g}{c}. \tag{4.36}$$

K can be understood as the carrying capacity inside a circle of radius R_c, so that the carrying capacity of the whole domain is $KL^2/\left(\pi R_c^2\right)$, where L is the length of the sides of the square domain we use for the numerical simulations. Fixing K instead of c, we have better control of the maximum number of particles expected in numerical simulations, which is important to keep reasonable computational times. Controlling the expected population size is especially important in our model because the dynamics we are considering requires the calculation of the pairwise distances between particles, to implement both the competition and the PG game reactions.

As shown in Table 4.1, we vary the PG production cost, from 0.1 to 0.7. We also

Parameter	**Value**	**Description**
L	1	Square domain's side length
D	10^{-4}	Diffusion coefficient
$R_c = R_g$	0.05	Interaction radii
b	0.8	Intrinsic birth rate
d	1.0	Intrinsic death rate
n_{PV}	5	Number of point-vortices
Γ	$\{0, 10^{-3}, 10^{-2}, \ldots, 10^{2}\}$	Strength of each point-vortex
k	$\{0.1, 0.2, \ldots, 0.7\}$	PG production cost
g	$\{k+0.2, k+0.3, \ldots, k+0.9\}$	PG benefit
c	$(b-k-d+c+g)/20$	Competition rate

Table 4.1: Values for parameters of the system used for simulations.

vary the PG benefit constant g from $k+0.2$ to $k+0.9$, as we are more interested in the effect of the difference between PG benefit and cost $g-k$ than in the effect of the absolute value of g. For each pair of parameters $(g, g-k)$, we run 20 simulations for each value of Γ, which sets the strength of each vortex in the point-vortex flow. The rotation direction of each vortex is randomly sampled, with equal probabilities for both directions. In all of our simulations, we start with a population of 1000 individuals, with 10% of defectors. We analyze the invasion dynamics of defectors as well as the possible effects of the environmental flow in determining the long-term dynamics of the community.

Figure 4.3 synthesizes the results of our simulations showing the frequency of extinction of cooperators, that is, the proportion of simulations in which cooperators go extinct. This is shown in the color scale from dark blue to yellow. For $\Gamma = 0.1$, cooperators never go extinct because we are working in a low-diffusion regime, and mixing is low for small values of Γ. If mixing is low, defectors cannot encounter cooperators often enough to exploit their PG production, which prevents cooperator extinctions. We do not show phase diagrams for

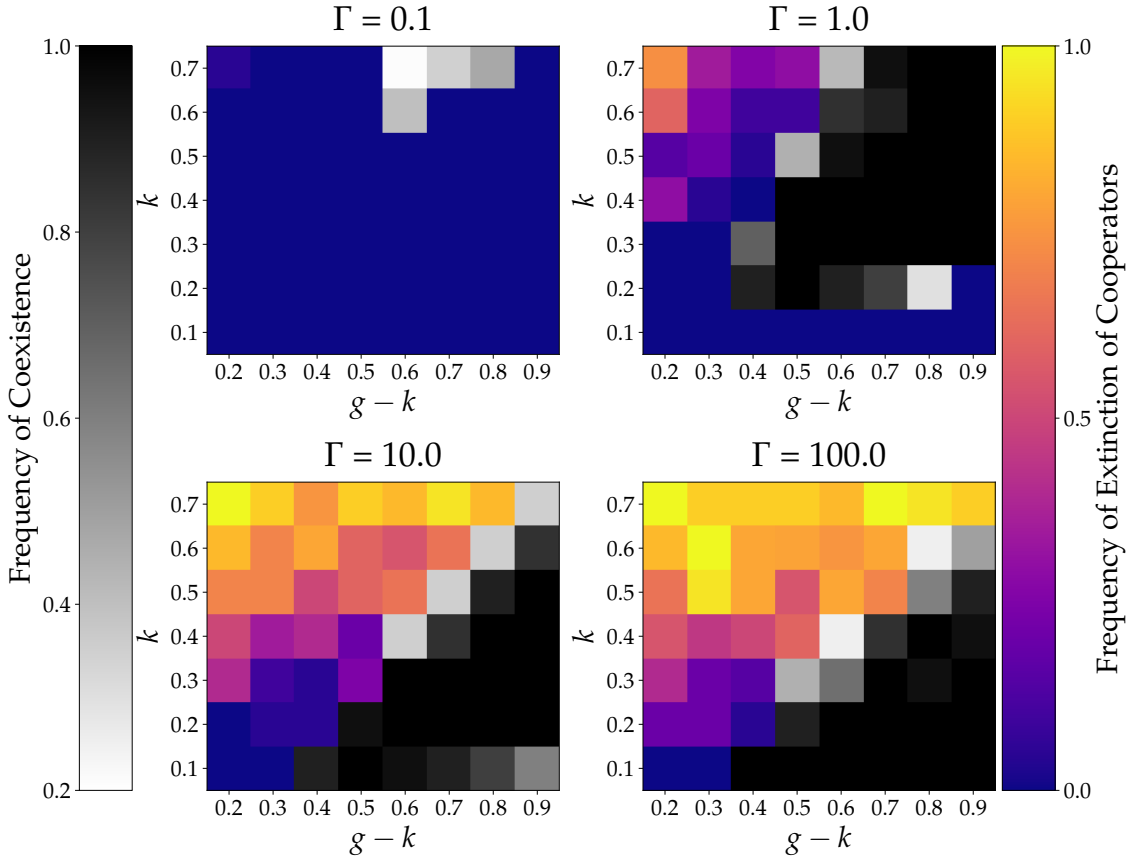

Figure 4.3: Frequency of different outcomes of simulations for multiple parameterizations of the two-strain system. The colors from blue to yellow denote the proportion of simulations that ended with the extinction of cooperators. If more than 20% (4/20) simulations presented coexistence at a given point, it is colored instead in a black and white scale, denoting the proportion of simulations presenting coexistence.

$\Gamma \in \{0, 10^{-3}, 10^{-2}\}$ as they would be dark blue everywhere, with no extinction of cooperators for any pair $(k, g-k)$.

Increasing the value of Γ to 1.0, the $(k, g-k)$ parameter space develops a region of cooperator extinction, associated with increased PG production cost k. More interestingly, there also appears a phase of stable coexistence of cooperators and defectors, represented in grayscale in Figure 4.3. For each point of the phase diagram, if more than 20% of the simulations (4 out of 20), we plot in such grayscale the proportion of simulations leading to the coexistence of the two strains. Coexistence is only possible if the environmental flow is fast enough, for the appropriate combination of small PG cost k and large benefit g.

Given the numerical character of this result, it is important to clarify what we

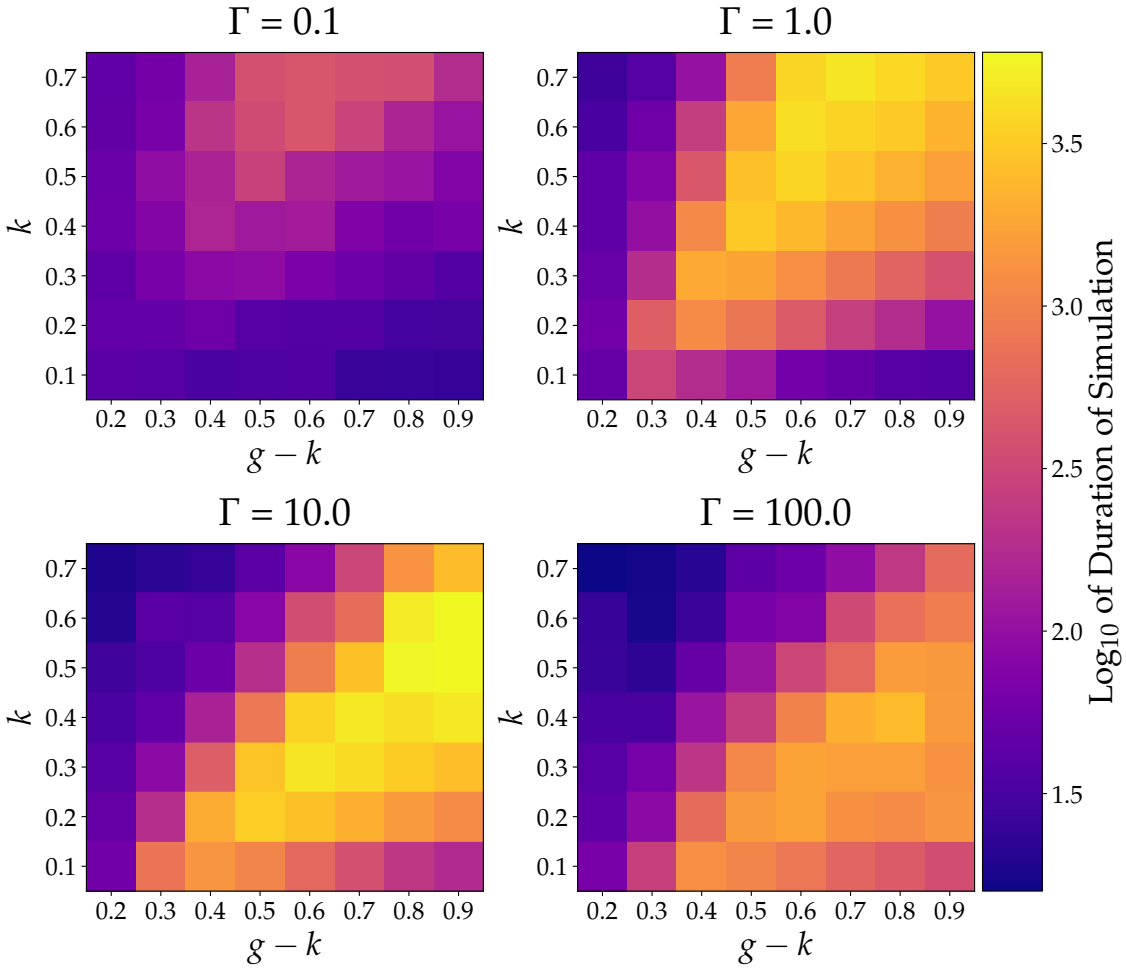

Figure 4.4: Duration of simulations, in simulation time.

define as coexistence, and how we conclude that it is stable. We run simulations with a fixed maximum execution time (wall-clock time) and only stop them earlier if one of the strains goes extinct. We consider that a simulation shows coexistence if it runs out of time before the extinction of either strain. This could be a bad proxy for stating that the system is in a coexistence phase if the maximum execution time was set too low, which could create artificial coexistence results. To discard this possibility, we measure the average simulation time of realizations across the parameter space. We find that those simulations we are relating to strain coexistence run several orders of magnitude longer than those associated with the dominance of one of the strains (Figure 4.4). This large difference in simulation times confirms that we have coexistence for a very long time, which is a good indicator of its stability.

Referring to this coexistence behavior as "stable" may be misleading, as there

can still be a very small probability of extinction for parameters in the coexistence phase. Regardless, it is safe to say that we identify a phase where the coexistence of the two strains is observed for much longer times than in other phases. Possibly, it would be ideal to refer to this phase as a quasi-stable coexistence, though it does not necessarily have the intended meaning. We carry on with the "stable" nomenclature, understanding that we mean a much prolonged coexistence scenario.

We can see some examples of the increased duration of the stochastic trajectories of the strain abundances in Figure 4.5. In the coexistence region of the parameter space, these trajectories are very different from those observed when one of the strains goes extinct. For $(k, g-k) = (0.3, 0.3)$, we can see that most trajectories end quickly, but a few persist for a longer time. This persistence is purely stochastic. When the community reaches low abundances, there often is an increased separation between strains, which leads to the extinction of defectors. But if the two strains meet, the defectors can again exploit cooperators which are starting to recover, leading to the observed oscillations. We observe similar oscillatory behavior in trajectories for $(k, g-k) = (0.6, 0.4)$, with many realizations ending quickly and a few showing oscillations before extinction. Increasing k, however, increases the probability that, due to the exploitation of PG production, cooperators go extinct before defectors.

Looking at trajectories associated with higher values of $g-k$, on the right side of Figure 4.5, we observe many more oscillations. These oscillations still depend on the stochastic nature of the system. Increasing the value of g also increases the magnitude of reproductive fluctuations, which enhances the probability of observing these abundance oscillations (see Figure 4.7 and the associated discussion in paragraphs below). For $(k, g-k) = (0.7, 0.7)$, despite the oscillations, there is no stable coexistence, with the majority of the trajectories leading to the extinction of cooperators. But for $(k, g-k) = (0.3, 0.8)$, the oscillations persist indefinitely, and we can observe coexistence for all the simulated trajectories.

The appearance of a coexistence phase associated with high-velocity flows can be associated with the formation of coherent structures in the chaotic flow, as it is argued by Krieger, Sinai and Nowak (2020) [32]. Another possibility is that the flow has a strong mixing effect, which could also be expected in a scenario of strong diffusion. It is important to remember that we are considering a chaotic external flow. Once the flow is fast enough, we can expect it to undo the spatial correlations created by biological reactions. That is, the fast chaotic is so fast flow

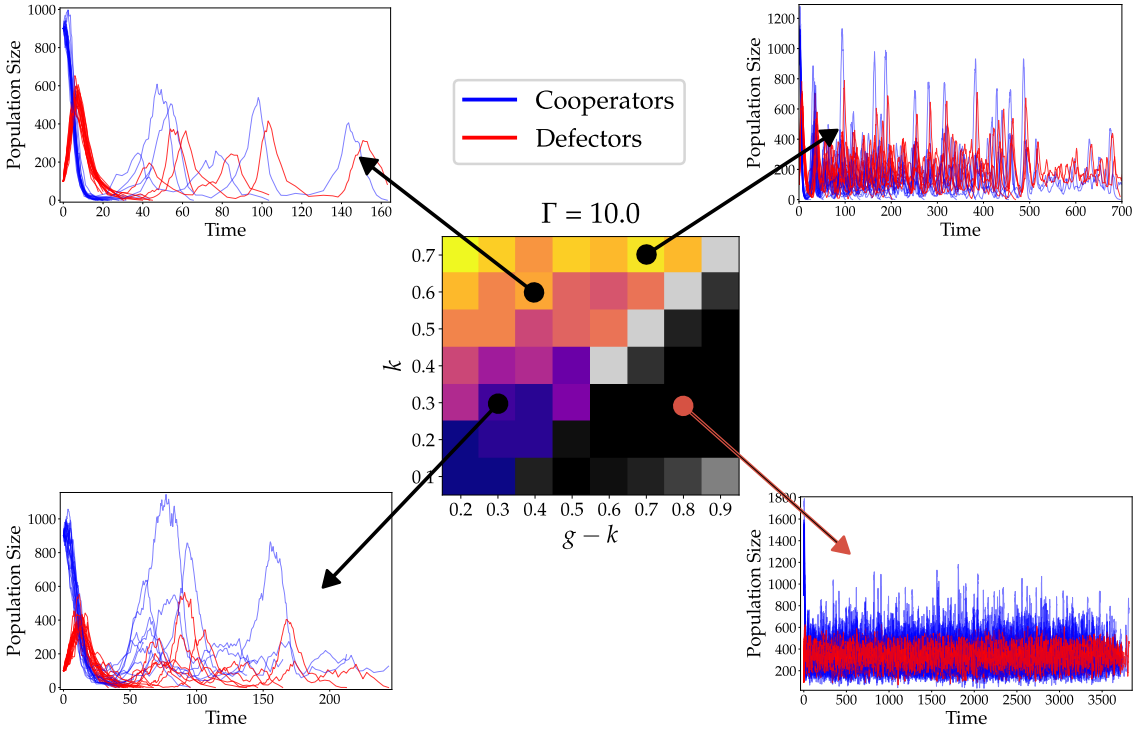

Figure 4.5: Examples of abundance trajectories for different parameterizations of the two-strain system, for vortex strength $\Gamma = 10.0$. Notice the different time scales in the x-axis of panels showing the dynamics of strain abundances.

that the composition of the neighborhoods of individuals at times of consecutive reactions is uncorrelated. To test if fast mixing is the explanation for the observed coexistence, we run simulations without the point-vortex flow, varying the value of the diffusion coefficient D.

In Figure 4.6, we plot the phase diagrams for the frequency of extinction and coexistence. This time, we do not include the external flow and only vary the diffusion coefficient associated with the Brownian motion of individuals. In this case, we should not expect strong diffusion to generate spatial structures. On the contrary, we expect it to drive the system to a well-mixed state. Regardless, we still observe the coexistence of the two strains as we increase mixing. This result provides a good indication that fast chaotic mixing breaks spatial correlations similarly to how strong diffusion does.

Notice that for fast diffusion we have a smaller region of coexistence than for fast environmental flows. This is an expected result because diffusion should take less time to break spatial correlations due to its random nature. The environmental flows, even if chaotic, are still deterministic. Therefore, the closer two individuals are, the longer it will take for them to be separated due only to the flow. And in our

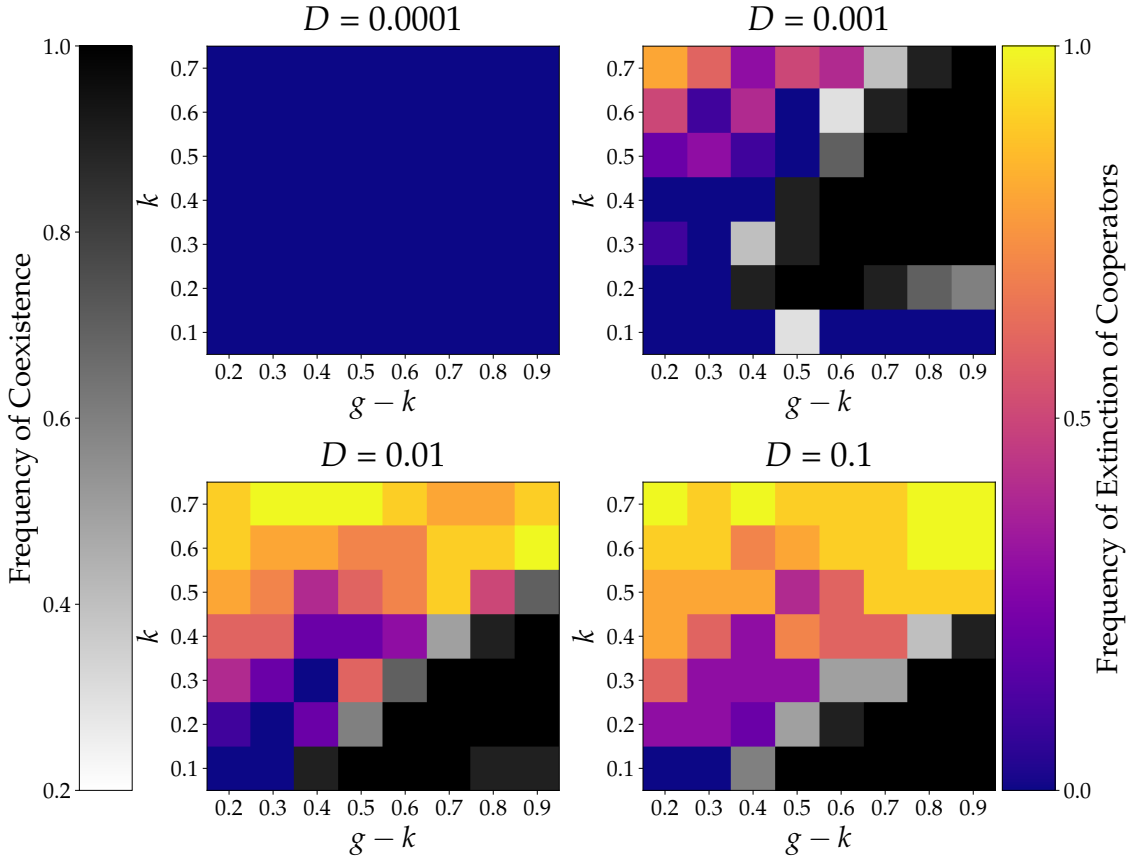

Figure 4.6: Frequency of different outcomes of simulations for multiple parameterizations of the two-strain system. The colors from blue to yellow denote the proportion of simulations that ended with the extinction of cooperators. If more than 20% (4/20) simulations presented coexistence at a given point, it is colored instead in a black and white scale, denoting the proportion of simulations presenting coexistence.

simulations, we place new individuals in the same position as their progenitors, so they will take longer to separate under fast deterministic flows than under fast diffusion.

We understand that chaotic mixing drives the population density of the system close to a well-mixed scenario. But it is important to remember that a uniform distribution of particles does not mean that every particle interacts with all the other particles at a given point in time. Even in the well-mixed limit, if we are still considering a discrete particle system, the behavior at each point in space will depend on the proportion of individuals of each strain in the local neighborhood, which fluctuates along the system.

It is possible to analytically consider the effect of local neighborhoods in the

well-mixed limit by taking into account the proportions of each strain to randomly compose the neighborhood of an individual. This can be understood as a pair approximation[20, 42, 37], in the limit of null pair correlation.

Coexistence in the high-diffusion limit was already observed in [4] working with a similar model. In this study, however, instead of a spatial PG game, the authors explicitly model PG molecules that are produced, diffuse through space and are consumed. They, moreover, show that the region of the parameter space associated with coexistence increases with the increasing speed of PG production and consumption. This consideration of fast PG production and consumption is the same that we made in the approximation used to define the PG game, shown in Appendix B.

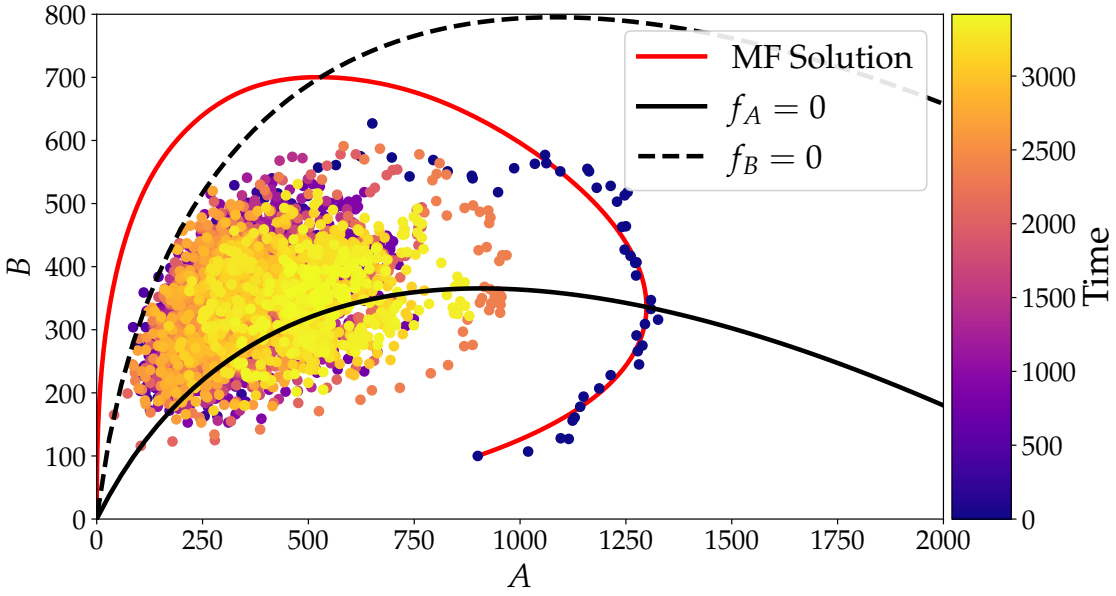

Figure 4.7: Stochastic trajectory in (A, B) phase space for $\Gamma = 10$, $(k, g-k) = (0.3, 1.1)$. Superimposed, we can see the nullclines and the spatially uniform trajectory for the same parameters.

In another work [3], the authors observe coexistence in a lattice model with local PG game interactions. They argue that the effect of diffusion between sites is equivalent to having local additive noise in each lattice site, which increases the probability of the system crossing the $f_A = 0$ nullcline (Figure 4.2). In our model, defined in continuous space, we can understand the local neighborhood of an individual as the equivalent to a single site in the lattice model of [3]. Indeed, if we plot one trajectory of the strain abundances in the (A, B) phase space, we can observe that it does cross the $f_A = 0$ nullcline (Figure 4.7).

Larger values of g make fluctuations stronger, which explains why higher values of $g - k$ increase the probability of crossing the nullcline in the direction of survival of cooperators. Also, increasing the cost k not only increases the defectors' reproductive advantage but also weakens fluctuations in the abundance of cooperators.

Most of the stochastic trajectory in Figure 4.7 appears above the nullcline, where $f_A < 0$ in the mean-field approximation, but the observed trajectory is a sum of the trajectories in each local neighborhood. If most of the local neighborhoods are in states above the nullcline in their respective scales and others are below, the sum over neighborhoods will appear above the nullcline, which indicates a move in the direction of extinction. However, there may still be local neighborhoods where cooperators are free from defectors and growing.

We observed that fast chaotic flows and diffusion have similar effects on the ecological dynamics of the two-strain system – the main difference we find is that external flows take longer to separate very close individuals, particularly a progenitor from its progeny [60]. However, if we are interested in looking for the effect of mixing generating coexistence in real-world systems, it should be easier to find this fast mixing associated with external flows than with the active movement of individuals. Active movement is often driven by environmental cues, which would lead to spatial correlations different from the ones expected from random diffusion [46, 49].

Chapter 5

Discussion and Perspectives

In this work, we developed a master equation model for two microbial strains sharing an environment that is constantly mixed by an external chaotic flow. One of the strains (cooperators) produces consumable public goods (PG). The other strain (defectors) does not contribute to the production but still benefits from the public goods. Because of the cost associated with producing public goods, defectors can have a reproductive advantage over cooperators when exploiting their production. We analyze how chaotic environmental flows affect the ecology of this two-strain system, through analytical mean-field approximations and stochastic numerical simulations.

First, we look into the spatially uniform mean-field approximation of the model, which ignores the effect of spatial variability. Ignoring spatial variability, we have three possible stationary states: extinction of both strains, cooperator-survival, or defector-survival. We do not observe the possibility of the coexistence of the two strains. If we consider a scenario where public goods are necessary for survival, the only stable stationary state of the system is extinction.

Second, we consider spatially non-uniform solutions to the mean-field approximation, which includes pattern formation with microorganisms organizing themselves in clusters. We still do not see stable coexistence of the two strains. However, these non-uniform distributions of population density enhance the survival of producers, as observed in similar models [53]. Defectors invading a population of cooperators organized in separate clusters may outgrow the specific cluster they invade, but these defectors are unlikely to spread to other clusters of cooperators, due to non-local competition. Uppal and Vural (2018) [53] also showed that environmental flows can further improve the chances of survival of cooperators as shear induces a faster splitting of cooperator clusters. Notice that, in this case, flow shear cannot be too strong, otherwise it would make the aggregation of cooperators impossible (see Figures 3.3 and 3.4).

Finally, we observe that chaotic environmental flows allow the coexistence of cooperator and defector strains in numerical simulations. These flows create

stable coexistence by changing the spatial correlations in the population density. The point-vortex flow generates transient spatial structures in the population. But, if these structures change much faster than microbes interact and reproduce, the only effect of the flow will be to weaken the correlation between population distributions at times of consecutive biological reactions. Fast chaotic flows force the neighborhoods of every individual to constantly change. With this change, the system will have some regions of space where defectors manage to exploit cooperators, locally moving towards a tragedy of the commons. There will also be other regions where defectors are rare, so cooperators can locally survive. These behaviors seem to balance one another to allow stable coexistence.

It may be possible to derive this coexistence phase as a fixed point of higher-order approximations of the model, such as pair approximations [20, 37, 42] or spatial moment dynamics approximations [7, 34]. These techniques allow one to reduce spatially explicit models to systems of ODEs, greatly improving analytical tractability, while still keeping track of spatial correlations. If one can show that stable coexistence is possible with these approximations in the limit of fast mixing, which breaks spatial correlations, it could confirm our current understanding of the mechanism for allowing coexistence through chaotic flows by breaking spatial correlations, at least in the timescale of biological processes. Notice that the break of spatial correlations does not mean that we can work with a mean-field approximation ignoring spatial variability (such as in equations (4.14) and (4.15), that we derived for the two-strain system). Even if the probability distribution for the position of each individual is uniform over space, the neighborhood of each cooperator (of defector) will be different, and this is taken into account by pair approximations and spatial moment dynamics approximations.

We also observed that increasing the intensity of the Brownian motion of individuals leads to similar results as changing the external chaotic flow. This is a good indication that the point-vortex flow allows for coexistence because it weakens the spatial pair correlations that are generated by microbial demographic reactions [60]. Based on the results for the strong-diffusion limit, we can expect that any flow with high enough shear — which implies fast mixing — should allow for coexistence in our model of public good dynamics. It would be interesting to analyze the case of a parabolic flow, for which the shear linearly decreases with the distance from the center of the channel. For such flow, we can expect to observe coexistence in the region of large enough shear. The stratification of the population along the gradient of shear can be important for understanding the possibility of

invasion across frontiers of strong shear.

Despite the equivalence of fast environmental flows and strong diffusion for our coexistence results, the flows are a more realistic mechanism than the high diffusion for fast mixing [32, 46]. Strong diffusion would require that individuals actively move at a high speed in random directions. While many plankton species are motile, their movement is aligned with chemical gradients, which can lead to accumulation at regions of high nutrient concentration [49], opposite to the expected effect of strong diffusion, that is associated with random movement. But fast enough external chaotic flows can be feasible, depending on the environment surrounding the community of interest, especially as turbulence operates in multiple spatial scales. While large-scale eddies can be associated with the frontier between ecological niches already separated at first, smaller eddies down the turbulence cascade will be associated with stronger mixing [17, 59]. The analysis of the parallel shear flow suggested in the last paragraph may also be useful for understanding interactions along high-shear filament separations associated with large fast eddies.

While we present interesting results for the role of chaotic environmental flows in the ecology of microbial public good games, there are some limitations if we are interested in making our model more similar to real systems. Our model implements public goods implicitly through a spatial public goods game. In reality, PG molecules are produced and diffuse through space. Behar, Brenner and Louzon (2014) [4] have shown that explicit public goods dynamics can lead to coexistence in scenarios of relatively fast PG dynamics, similar to the limit we considered when deriving the implementation of the spatial PG game (see Appendix B). The effect of flows in this two-strain system might change drastically when changing from the spatial PG game to explicit PG molecules because these molecules can be advected by the flow, extending the range of cooperation, which would also become spatially dependent under non-uniform flows. The effect of PG mixing needs to be further investigated. In the specific case of siderophores as public goods, it may also be relevant to consider the possibility of attachment to floating particles, which seems to significantly affect cooperation levels [14], though it can be hard to model this effect in the spatial distribution of individuals. It could also be important to understand how the interaction between external flows and active motion of microorganisms can affect the possibility of coexistence [46, 49, 59].

Based on our results for the coexistence of two strains allowed by fast mixing,

we can speculate on the effect of flows in richer communities. While the spatial separation of competing species can enhance their coexistence, environmental flows may force the mixing of these species, making coexistence harder. On the other hand, based on the present work, fast mixing can also improve the probability of coexistence by easing the effect of exploitative interactions on the exploited species. This can contribute to the explanation of the paradox of the plankton [28] through the spatially heterogeneous distribution of plankton species across the oceans, due to turbulent flows [30]. This problem could also be investigated through pair approximations for many species, which might lead to equations with multiple coexistence equilibrium solutions.

Lastly, stable coexistence has not been observed in models of non-consumable public goods [8, 12, 53]. However, the scenario of high dispersal with short-range interactions has not been thoroughly explored for these models. This consideration would be important for determining if coexistence is not possible in the case of non-consumable public goods, or if the range of parameters for coexistence is small, and has not been explored yet.

Appendix A

Proofs

A.1 Expansion of the Hyperbolic Cotangent

Here, we are going to prove the following expansion for the cotangent function:

$$\cot(\pi x) = \frac{x}{\pi} \sum_{n=-\infty}^{\infty} \frac{1}{x^2 - n^2}. \tag{A.1}$$

□ We can do so by writing the Fourier series for $\cos(tx)$, in the interval $(-\pi, \pi)$:

$$\begin{aligned} \cos(tx) &= a_0 + \sum_{n=1}^{\infty} a_n \cos(nx) + \sum_{n=1}^{\infty} b_n \sin(nx)\,, \\ a_0 &= \frac{1}{2\pi} \int_{-\pi}^{\pi} \mathrm{d}x \cos(tx)\,; \\ a_n &= \frac{1}{\pi} \int_{-\pi}^{\pi} \mathrm{d}x \cos(tx)\cos(nx)\,; \\ b_n &= \frac{1}{\pi} \int_{-\pi}^{\pi} \mathrm{d}x \cos(tx)\sin(nx)\,. \end{aligned} \tag{A.2}$$

$\cos(tx)$ is an even function, so $b_n = 0\ \forall n$. We can calculate:

$$a_0 = \frac{\sin(t\pi)}{t\pi}; \tag{A.3}$$

$$a_n = \frac{1}{\pi}\int_{-\pi}^{\pi} \mathrm{d}x \frac{\cos[(t-n)\,x] + \cos[(t+n)\,x]}{2}$$
$$= \frac{1}{\pi}\left\{\frac{\sin[(t-n)\,x]}{t-n} + \frac{\sin[(t+n)\,x]}{t+n}\right\}. \tag{A.4}$$

This can now be simplified if we set $x = \pi$:

$$a_n = \frac{1}{\pi\,(t^2-n^2)}\left\{(t+n)\sin(t\pi)\cos(n\pi) + (t-n)\sin(t\pi)\cos(n\pi)\right\}$$
$$= 2\frac{(-1)^n\, t\sin(t\pi)}{\pi\,(t^2-n^2)}, \tag{A.5}$$

so now we can write:

$$\cos(t\pi) = \frac{\sin(t\pi)}{t\pi} + 2\sum_{n=1}^{\infty}\frac{t\,(-1)^n}{\pi\,(t^2-n^2)}\sin(n\pi)$$
$$= \frac{\sin(t\pi)}{\pi}\sum_{n=-\infty}^{\infty}\frac{t}{t^2-n^2}. \tag{A.6}$$

Dividing by $\sin(t\pi)$, our derivation is finished:

$$\cot(t\pi) = \frac{t}{\pi}\sum_{n=-\infty}^{\infty}\frac{1}{t^2-n^2} \quad \blacksquare \tag{A.7}$$

A.2 Change of Variable from Uniform to Exponential Distribution

□ If we have a random variable $x \sim \mathcal{U}(0,1)$ another variable $y = f(x) = -\ln(x)/a,\ a > 0$, should have a distribution:

$$p(y) = \int_0^1 \mathrm{d}x\,\delta(y - f(x)) = \int_0^1 \mathrm{d}x\,\delta(y + \ln(x)/a)\,. \tag{A.8}$$

Substituting $x = \exp(au) \Rightarrow \mathrm{d}x = a\exp(au)\,\mathrm{d}u$:

$$p(y) = \int_{-\infty} \mathrm{d}u\, ae^{au}\delta(y+u) = a\exp(-ay)\,, \tag{A.9}$$

which is the PDF of an exponential distribution with coefficient a. ■

Appendix B

PG Explicit Model with Fast PG Dynamics

Here, we define a simple model with explicit PG molecules being produced and consumed. Then, we consider the limit of fast dynamics for these molecules, to obtain an approximation that motivates the model presented in Chapter 4. This consideration of fast variables is a common technique to reduce the number of equations of a system [9, 11, 36]. Here, we will ignore the spatial structure of the system for simplicity and will go straight to the mean-field approximation, which is straightforward to derive.

If A and B are respectively the concentrations of cooperators and defectors, and C is the concentration of PG molecules, we can write our model:

$$\frac{\mathrm{d}}{\mathrm{d}t}A = (b - k - d + hC)\,A - cA\,(A + B)\,; \tag{B.1}$$

$$\frac{\mathrm{d}}{\mathrm{d}t}B = (b - d + hC)\,B - cA\,(A + B)\,; \tag{B.2}$$

$$\frac{\mathrm{d}}{\mathrm{d}t}C = \gamma A - \delta\,(A + B)\,C, \tag{B.3}$$

where b is the intrinsic birth rate, d is the death rate, k is the PG production cost, c is the competition rate, γ is the PG production rate, δ is the PG consumption rate, and h is the reproductive benefit of PG to the reproduction rate, or fitness, of individuals.

If we consider that reactions involving PG production and consumption are much faster than other demographic events, C quickly converges to its equilibrium value, which we can take as its fixed value:

$$\frac{\mathrm{d}}{\mathrm{d}t}C = 0 \Rightarrow C = \frac{\gamma}{\delta}\frac{A}{A + B}. \tag{B.4}$$

If we define $g = h\gamma/\delta$ and substitute equation (B.4) in equations (B.1) and (B.2), we obtain the same equations as (4.14) and (4.15) for the mean-field uniform solution of the two-strains model with the PG game:

$$\frac{\mathrm{d}}{\mathrm{d}t}A = \left(b - k - d + g\frac{A}{A+B}\right)A - cA\left(A+B\right); \tag{B.5}$$

$$\frac{\mathrm{d}}{\mathrm{d}t}B = \left(b - d + g\frac{A}{A+B}\right)B - cA\left(A+B\right). \tag{B.6}$$

Bibliography

[1] Aref, H.: Integrable, Chaotic, and Turbulent Vortex Motion in Two-Dimensional Flows. Annual Review of Fluid Mechanics **15**(1), 345–389 (1983). doi:10.1146/annurev.fl.15.010183.002021

[2] Batchelor, G.K.: An Introduction to Fluid Dynamics. Cambridge University Press (1967)

[3] Behar, H., Brenner, N., Ariel, G., Louzoun, Y.: Fluctuations-induced coexistence in public goods dynamics. Physical Biology **13**(5), 056006 (2016). doi:10.1088/1478-3975/13/5/056006

[4] Behar, H., Brenner, N., Louzoun, Y.: Coexistence of productive and non-productive populations by fluctuation-driven spatio-temporal patterns. Theoretical Population Biology **96**, 20–29 (2014). doi:10.1016/j.tpb.2014.06.002

[5] Benzi, R., Jensen, M.H., Nelson, D.R., Perlekar, P., Pigolotti, S., Toschi, F.: Population dynamics in compressible flows. The European Physical Journal Special Topics **204**(1), 57–73 (2012). doi:10.1140/epjst/e2012-01552-0

[6] Bialek, W., Cavagna, A., Giardina, I., Mora, T., Silvestri, E., Viale, M., Walczak, A.M.: Statistical mechanics for natural flocks of birds. Proceedings of the National Academy of Sciences **109**(13), 4786–4791 (2012). doi:10.1073/pnas.1118633109

[7] Binny, R.N., Plank, M.J., James, A.: Spatial moment dynamics for collective cell movement incorporating a neighbour-dependent directional bias. Journal of The Royal Society Interface **12**(106), 20150228 (2015). doi:10.1098/rsif.2015.0228

[8] Borenstein, D.B., Meir, Y., Shaevitz, J.W., Wingreen, N.S.: Non-Local Interaction via Diffusible Resource Prevents Coexistence of Cooperators and Cheaters in a Lattice Model. PLOS ONE **8**(5), e63304 (2013). doi:10.1371/journal.pone.0063304

[9] Colombo, E.H., López, C., Hernández-García, E.: Pulsed Interaction Signals as a Route to Biological Pattern Formation. Physical Review Letters **130**(5), 058401 (2023). doi:10.1103/PhysRevLett.130.058401

[10] Colombo, E.H., Martínez-García, R., López, C., Hernández-García, E.: Spatial eco-evolutionary feedbacks mediate coexistence in prey-predator systems. Scientific Reports **9**(1), 18161 (2019). doi:10.1038/s41598-019-54510-6

[11] Constable, G.W.A., McKane, A.J.: Fast-mode elimination in stochastic metapopulation models. Physical Review E **89**(3), 032141 (2014). doi:10.1103/PhysRevE.89.032141

[12] Constable, G.W.A., Rogers, T., McKane, A.J., Tarnita, C.E.: Demographic noise can reverse the direction of deterministic selection. Proceedings of the National Academy of Sciences **113**(32), E4745–E4754 (2016). doi:10.1073/pnas.1603693113

[13] Cooper, G.M.: The Central Role of Enzymes as Biological Catalysts. In: The Cell: A Molecular Approach. 2nd Edition. Sinauer Associates (2000)

[14] Cordero, O.X., Ventouras, L.A., DeLong, E.F., Polz, M.F.: Public good dynamics drive evolution of iron acquisition strategies in natural bacterioplankton populations. Proceedings of the National Academy of Sciences **109**(49), 20059–20064 (2012). doi:10.1073/pnas.1213344109

[15] Crespi, B.J.: The evolution of social behavior in microorganisms. Trends in Ecology & Evolution **16**(4), 178–183 (2001). doi:10.1016/S0169-5347(01)02115-2

[16] Davidson, L.: TME226 Mechanics of fluids, Chalmers University of Technology. https://www.tfd.chalmers.se/~lada/MoF/ebook.html

[17] d'Ovidio, F., De Monte, S., Alvain, S., Dandonneau, Y., Lévy, M.: Fluid dynamical niches of phytoplankton types. Proceedings of the National Academy of Sciences **107**(43), 18366–18370 (2010). doi:10.1073/pnas.1004620107

[18] Driscoll, W.W., Pepper, J.W.: THEORY FOR THE EVOLUTION OF DIFFUSIBLE EXTERNAL GOODS. Evolution **64**(9), 2682–2687 (2010). doi:10.1111/j.1558-5646.2010.01002.x

[19] Dutykh, D.: A brief introduction to pseudo-spectral methods: Application to diffusion problems. pp. 167–209 (2019). doi:10.1007/978-3-030-31574-0_8

[20] Ellner, S.P.: Pair Approximation for Lattice Models with Multiple Interaction Scales. Journal of Theoretical Biology **210**(4), 435–447 (2001). doi:10.1006/jtbi.2001.2322

[21] Fehr, E., Gächter, S.: Cooperation and Punishment in Public Goods Experiments. American Economic Review **90**(4), 980–994 (2000). doi:10.1257/aer.90.4.980

[22] Foster, K.R., Shaulsky, G., Strassmann, J.E., Queller, D.C., Thompson, C.R.L.: Pleiotropy as a mechanism to stabilize cooperation. Nature **431**(7009), 693–696 (2004). doi:10.1038/nature02894

[23] Gillespie, D.T.: Exact stochastic simulation of coupled chemical reactions. The Journal of Physical Chemistry **81**(25), 2340–2361 (1977). doi:10.1021/j100540a008

[24] Hardin, G.: The Tragedy of the Commons. Science **162**(3859), 1243–1248 (1968). doi:10.1126/science.162.3859.1243

[25] Hauert, C., De Monte, S., Hofbauer, J., Sigmund, K.: Volunteering as Red Queen Mechanism for Cooperation in Public Goods Games. Science **296**(5570), 1129–1132 (2002). doi:10.1126/science.1070582

[26] Hider, R.C., Kong, X.: Chemistry and biology of siderophores. Natural Product Reports **27**(5), 637–657 (2010). doi:10.1039/B906679A

[27] Holyoak, M., Casagrandi, R., Nathan, R., Revilla, E., Spiegel, O.: Trends and missing parts in the study of movement ecology. Proceedings of the National Academy of Sciences **105**(49), 19060–19065 (2008). doi:10.1073/pnas.0800483105

[28] Hutchinson, G.E.: The Paradox of the Plankton. The American Naturalist **95**(882), 137–145 (1961)

[29] Kamenev, A.: Keldysh and DOI-Peliti Techniques for Out-of-Equilibrium Systems. In: I.V. Lerner, B.L. Althsuler, V.I. Fal'ko, T. Giamarchi (eds.) Strongly Correlated Fermions and Bosons in Low-Dimensional Disordered Systems,

NATO Science Series, pp. 313–340. Springer Netherlands, Dordrecht (2002). doi:10.1007/978-94-010-0530-2_13

[30] Károlyi, G., Péntek, Á., Scheuring, I., Tél, T., Toroczkai, Z.: Chaotic flow: The physics of species coexistence. Proceedings of the National Academy of Sciences **97**(25), 13661–13665 (2000). doi:10.1073/pnas.240242797

[31] Kramer, J., Özkaya, Ö., Kümmerli, R.: Bacterial siderophores in community and host interactions. Nature Reviews Microbiology **18**(3), 152–163 (2020). doi:10.1038/s41579-019-0284-4

[32] Krieger, M.S., Sinai, S., Nowak, M.A.: Turbulent coherent structures and early life below the Kolmogorov scale. Nature Communications **11**(1), 2192 (2020). doi:10.1038/s41467-020-15780-1

[33] Lamb, S.H.: Hydrodynamics. Courier Corporation (1945)

[34] Law, R., Dieckmann, U.: Moment Approximations of Individual-based Models. In: J.A.J. Metz, R. Law, U. Dieckmann (eds.) The Geometry of Ecological Interactions: Simplifying Spatial Complexity, Cambridge Studies in Adaptive Dynamics, pp. 252–270. Cambridge University Press, Cambridge (2000). doi:10.1017/CBO9780511525537.017

[35] López, C.: Macroscopic description of particle systems with nonlocal density-dependent diffusivity. Physical Review E **74**(1), 012102 (2006). doi:10.1103/PhysRevE.74.012102

[36] Martínez-García, R., Calabrese, J.M., Hernández-García, E., López, C.: Minimal mechanisms for vegetation patterns in semiarid regions. Philosophical Transactions of the Royal Society A: Mathematical, Physical and Engineering Sciences **372**(2027), 20140068 (2014). doi:10.1098/rsta.2014.0068

[37] Martinez-Garcia, R., López, C., Vazquez, F.: Species exclusion and coexistence in a noisy voter model with a competition-colonization tradeoff. Physical Review E **103**(3), 032406 (2021). doi:10.1103/PhysRevE.103.032406

[38] Martínez-García, R., Murgui, C., Hernández-García, E., López, C.: Pattern Formation in Populations with Density-Dependent Movement and Two Interaction Scales. PLOS ONE **10**(7), e0132261 (2015). doi:10.1371/journal.pone.0132261

[39] Mogilner, A., Edelstein-Keshet, L.: A non-local model for a swarm. Journal of Mathematical Biology **38**(6), 534–570 (1999). doi:10.1007/s002850050158

[40] Murray, J.D.: Mathematical Biology II: Spatial Models and Biomedical Applications. Springer Science & Business Media (2006)

[41] Nadell, C.D., Drescher, K., Foster, K.R.: Spatial structure, cooperation and competition in biofilms. Nature Reviews Microbiology **14**(9), 589–600 (2016). doi:10.1038/nrmicro.2016.84

[42] Peralta, A.F., Carro, A., Miguel, M.S., Toral, R.: Stochastic pair approximation treatment of the noisy voter model. New Journal of Physics **20**(10), 103045 (2018). doi:10.1088/1367-2630/aae7f5

[43] Rankin, D.J., Bargum, K., Kokko, H.: The tragedy of the commons in evolutionary biology. Trends in Ecology & Evolution **22**(12), 643–651 (2007). doi:10.1016/j.tree.2007.07.009

[44] Reddy, J.N.: An Introduction to Continuum Mechanics. Cambridge University Press (2013)

[45] Rietkerk, M., Boerlijst, M.C., van Langevelde, F., HilleRisLambers, R., de Koppel, J.v., Kumar, L., Prins, H.H.T., de Roos, A.M.: Self-Organization of Vegetation in Arid Ecosystems. The American Naturalist **160**(4), 524–530 (2002). doi:10.1086/342078

[46] Rusconi, R., Guasto, J.S., Stocker, R.: Bacterial transport suppressed by fluid shear. Nature Physics **10**(3), 212–217 (2014). doi:10.1038/nphys2883

[47] Smith, P., Schuster, M.: Public goods and cheating in microbes. Current Biology **29**(11), R442–R447 (2019). doi:10.1016/j.cub.2019.03.001

[48] Staniforth, A., Côté, J.: Semi-Lagrangian Integration Schemes for Atmospheric Models—A Review. Monthly Weather Review **119**(9), 2206–2223 (1991). doi:10.1175/1520-0493(1991)119<2206:SLISFA>2.0.CO;2

[49] Stocker, R., Seymour, J.R.: Ecology and Physics of Bacterial Chemotaxis in the Ocean. Microbiology and Molecular Biology Reviews **76**(4), 792–812 (2012). doi:10.1128/mmbr.00029-12

[50] Straughan, B.: The Energy Method, Stability, and Nonlinear Convection. Springer Science & Business Media (2013)

[51] Tarnita, C.E.: The ecology and evolution of social behavior in microbes. Journal of Experimental Biology **220**(1), 18–24 (2017). doi:10.1242/jeb.145631

[52] Toral, R., Colet, P.: Stochastic Numerical Methods: An Introduction for Students and Scientists. John Wiley & Sons (2014)

[53] Uppal, G., Vural, D.C.: Shearing in flow environment promotes evolution of social behavior in microbial populations. eLife **7**, e34862 (2018). doi:10.7554/eLife.34862

[54] Vestergaard, C.L., Génois, M.: Temporal Gillespie Algorithm: Fast Simulation of Contagion Processes on Time-Varying Networks. PLOS Computational Biology **11**(10), e1004579 (2015). doi:10.1371/journal.pcbi.1004579

[55] van Vliet, S., Hauert, C., Fridberg, K., Ackermann, M., Dal Co, A.: Global dynamics of microbial communities emerge from local interaction rules. PLOS Computational Biology **18**(3), e1009877 (2022). doi:10.1371/journal.pcbi.1009877

[56] West, S.A., Diggle, S.P., Buckling, A., Gardner, A., Griffin, A.S.: The Social Lives of Microbes. Annual Review of Ecology, Evolution, and Systematics **38**(1), 53–77 (2007). doi:10.1146/annurev.ecolsys.38.091206.095740

[57] West, S.A., Griffin, A.S., Gardner, A.: Evolutionary Explanations for Cooperation. Current Biology **17**(16), R661–R672 (2007). doi:10.1016/j.cub.2007.06.004

[58] West, S.A., Griffin, A.S., Gardner, A., Diggle, S.P.: Social evolution theory for microorganisms. Nature Reviews Microbiology **4**(8), 597–607 (2006). doi:10.1038/nrmicro1461

[59] Wheeler, J.D., Secchi, E., Rusconi, R., Stocker, R.: Not Just Going with the Flow: The Effects of Fluid Flow on Bacteria and Plankton. Annual Review of Cell and Developmental Biology **35**(1), 213–237 (2019). doi:10.1146/annurev-cellbio-100818-125119

[60] Young, W.R., Roberts, A.J., Stuhne, G.: Reproductive pair correlations and the clustering of organisms. Nature **412**(6844), 328–331 (2001). doi:10.1038/35085561